Symmetry violation in weak decays

Vos, Kimberley Keri

Symmetry violation in weak decays

This work is part of a research program funded in part by the Stichting voor Fundamenteel Onderzoek der Materie (FOM), which is financially supported by the Nederlandse Organisatie voor Wetenschappelijk Onderzoek (NWO).

ISBN: 978-90-367-8247-0 Printed version
ISBN: 978-90-367-8246-3 Electronic version

rijksuniversiteit
groningen

Symmetry violation in weak decays

Proefschrift

ter verkrijging van de graad van doctor aan de
Rijksuniversiteit Groningen
op gezag van de
rector magnificus prof. dr. E. Sterken
en volgens besluit van het College van Promoties.

De openbare verdediging zal plaatsvinden op

vrijdag 5 februari 2016 om 11.00 uur

door

Kimberley Keri Vos

geboren op 29 augustus 1988
te Odoorn

Promotores

Prof. dr. R.G.E. Timmermans
Prof. dr. H.W.E.M. Wilschut

Beoordelingscommissie

Prof. dr. B. D. Altschul
Prof. dr. D. Boer
Prof. dr. A. Young

Contents

Chapter 1

Introduction

Symmetries play a crucial role in our understanding of nature. Energy and momentum conservation, for example, follow from the invariance of the laws of physics under space-time translations. These translations together with Lorentz transformations, i.e. Lorentz boosts and rotations, form the Poincaré group, which describes the symmetries of 4-dimensional space-time. For relativistic theories, invariance under Lorentz transformations is generally assumed. The associated Lorentz symmetry ensures that all physical laws obey the principle of relativity, that is, the laws of physics are the same for all observers that move at constant velocity with respect to each other. The speed of light, predicted by Maxwell's equations, is then also the same for observers in different inertial reference frames. This relativity principle is the basis of Einstein's special and general relativity (GR). Special relativity and quantum mechanics form the underlying structure of the Standard Model of particle physics (SM). Lorentz symmetry is thus one of the fundaments of particle physics.

At the basis of the SM are also the discrete symmetries parity (P), which reverses the spatial coordinates $\vec{x} \to -\vec{x}$, charge-conjugation (C), which reverses particles and antiparticles, and time reversal (T), which reverses $t \to -t$. The combined discrete symmetry CPT is conserved in any relativistic local quantum field theory, and is therefore closely connected to Lorentz symmetry. In fact, CPT can only be broken if Lorentz symmetry is also broken. However, Lorentz violation does not necessarily imply CPT violation [1]. In this thesis, we study the possible violation of both Lorentz and discrete symmetries in the weak-interaction sector of the SM.

1.1 Symmetries of the weak interaction

Nature was believed to be symmetric under P, until the surprising discovery of parity violation in β decay in 1957 [2]. This implies that the weak interaction distinguishes between left- and right-handed fermions. This discovery can be considered as the starting point of the development of the SM. At present, the SM is the successful description of elementary particles and their interactions. It is based on $SU(3)_C \times SU(2)_L \times U(1)_Y$ gauge symmetry, which describes the strong interaction, the weak interaction, and the electromagnetic interaction. Only gravity is not included in the SM.

The discovery of parity violation and subsequent detailed studies of β decay led to

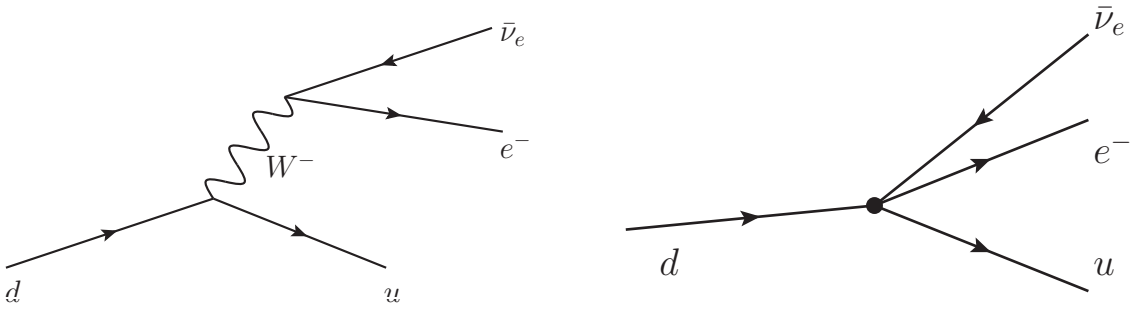

Figure 1.1: Diagram of β decay at the quark level in which a d quark transforms into a u quark, an electron, and an antineutrino. Figure (a) shows the description in the SM, via the exchange of the W boson. Figure (b) is the effective description in which the heavy W boson is "integrated out" at low energy, and only a four-fermion (point) interaction remains.

the establishment of the vector−axial-vector ($V - A$) structure of the weak interaction, involving only left-handed fermions. In the same year also C violation [3] was discovered and in 1964 also CP violation [4] was found in the weak interaction. In the SM, CP violation is equivalent to T violation, because CPT is conserved. Direct T violation was discovered much later [5].

The current description of the weak interaction could be affected if at some level an, as yet unknown, interaction contributes. The focus of this thesis is to study to which extent this can be excluded.

1.2 Beyond the Standard Model

The SM correctly describes a large number of experiments. Nevertheless, it leaves important observations unexplained. Intriguing is the large dominance of matter over antimatter in the universe, which cannot be understood within the SM. Actually, the SM only describes a small part of the universe, and leaves dark matter and dark energy unexplained. Furthermore, the discovery of neutrino oscillations implies that neutrinos have a mass, which is not incorporated in the SM. Other unanswered questions involve the number of families and the unification of gravity and the SM. To answer these questions new physics, i.e. physics beyond the SM (BSM), is needed. Because symmetries and symmetry violation play an important part in the SM, they could also help in unraveling the nature of this BSM physics.

Searches for BSM physics range from high-energy experiments, for example at the Large Hadron Collider (LHC), to low-energy high-precision experiments. High-energy experiments directly test various speculative theory proposals that predict new heavy particles. Complementary to these are low-energy experiments that search for deviations from the SM predictions in high-precision experiments, as we discuss below. Apart from the discovery of neutrino oscillations, the searches at both of these frontiers in particle

physics did not find any conclusive evidence for new physics until now.

For low-energy experiments, it is useful to consider the effect of new particles, without making any model-dependent assumptions on the nature of the BSM physics, by using effective field theory (EFT) techniques. This approach can be illustrated by considering β decay, depicted in Fig. 1.1. The W boson is heavy compared to the leptons and up and down quarks. At low energies (well below the W-boson mass), the interaction does not depend on the dynamics of the heavy W boson, and we can describe the interaction effectively by "integrating out" the W boson. It then reduces to the Fermi interaction, in which the four light fermions directly interact at the vertex. This effective description fails at high energies, where the dynamics of the W boson becomes important.

The SM can also be seen as an EFT which works well up to a certain energy scale (at least up to the W-boson mass). At low energies, we do not need to know the precise properties of the physics at high energies. This is similar to β decay, which we can describe at low energies without knowledge of the W boson. Another example is given in Fig. 1.2, in which a speculative heavy particle R couples to the d and u quark via a loop. At energies below the mass of R, we can "integrate out" R and we are left with an effective udW vertex. The contribution of R to this vertex is suppressed by its heavy mass squared. If we add this effective vertex to the SM vertex we incorporate the effects of particle R, and we can predict its effects on, for instance, β decay. High-precision measurements might therefore constrain the mass and the coupling of R.

EFT allows us to parametrize the effects of all possible high-energy physics in a model-independent way. The effects of new particles are suppressed by powers of their mass and can be included by adding additional interactions to the SM Lagrangian. Since the action,

$$S = \int d^4x \, \mathcal{L} \, , \tag{1.1}$$

is dimensionless in natural units ($\hbar = c = 1$), the Lagrangian density $\mathcal{L}$ can only contain terms with mass dimension 4. From this, the dimension of the different SM field operators can be determined. The SM contains only renormalizable operators of dimension 4 and lower. In an EFT, new interactions resulting from heavy, "integrated out", particles are described by gauge-invariant higher-dimensional operators, with mass dimension higher than 4. Such operators are expected to scale according to their dimension with coupling constants $c_i = (1/\Lambda)^{\delta-4} g_i$, where Λ is a high-energy scale, and g_i is a dimensionless coupling constant. If $\delta = 4$ the interaction is called "marginal", because the couplings are equally important at all energies. Interactions with $\delta < 4$ are called "relevant" and the effect of these terms grows with energy. These are the renormalizable operators of the SM. Higher-dimensional operators have $\delta > 4$ and are called "irrelevant", because they are less important at low energies. Schematically, the effective Lagrangian is parametrized by

$$\mathcal{L}^{(\text{eff})} = \mathcal{L}_{\text{SM}} + \frac{1}{\Lambda} c^{(5)} \mathcal{O}^5 + \frac{1}{\Lambda^2} \sum_i c_i^{(6)} \mathcal{O}_i^6 + \cdots \, . \tag{1.2}$$

where $c^{(5)}$ and $c_i^{(6)}$ are the dimensionless coupling constants and $\mathcal{O}_i^{5,6}$ are the dimension-5 and 6 operators, respectively. The dots represent operators of dimension 7 and higher, which are even more suppressed. In this thesis, we only consider higher-dimensional operators that obey the SM symmetry groups. That leaves, if one assumes Lorentz invariance,

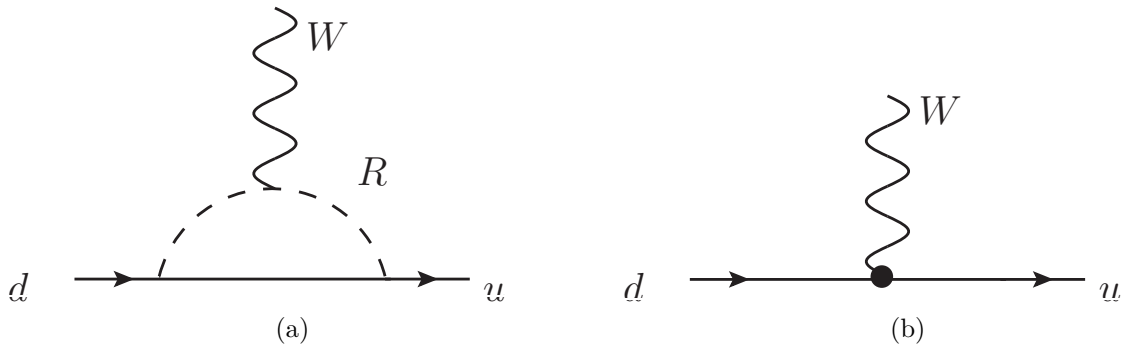

Figure 1.2: Example of a new heavy particle R that contributes to β decay via a loop (a) and its effective description (b) at low energies. The effective interaction is described by higher-dimensional operators that could generate different couplings than the SM $V - A$ couplings.

only one dimension-5 operator[1] This operator, which generates a Majorana mass for the neutrino [6], can be neglected for our study of β decay (Sec. 2.2.1). Therefore, we focus on dimension-6 operators in this thesis.

The discovery of parity violation in β decay established the $V - A$ structure of the SM. Other interactions, such as right-handed vector ($V + A$), scalar (S), or tensor (T) interactions, and additional $V-A$ interactions, might be generated by new heavy particles. At low energies, these interactions are described by dimension-6 operators that contribute to β decay and which are suppressed by Λ^2 [7, 8]. A scalar interaction, for example, is described by the dimension-6 operator $\mathcal{O}_6 = \bar{e}\nu_e \cdot \bar{u}d$, which contains four fermions which all have mass dimension 3/2. Low-energy, high-precision experiments therefore limit these exotic interactions. Traditionally, β-decay experiments were considered separately from, for example, high-energy collider experiments. In this thesis, we show that the EFT parametrization allows one to relate observables that at first sight appear to be unrelated. This sheds a new light on the complementarity of β-decay experiments and other measurments.

Of great importance is also the search for additional mechanisms of CP or equivalently T violation. The amount of CP violation within the SM is not enough to explain the dominance of matter over antimatter in the universe, and additional sources of CP violation might help to answer this outstanding question. We consider the searches for T violation in β decay and the searches for the electric dipole moments (EDMs) of particles, which violate both P and T. In the EFT parametrization, these searches are also linked, and in fact set bounds on the same dimension-6 interactions.

Besides the search for T violation and exotic interactions in β decay, this thesis also discusses the breaking of Lorentz symmetry. The motivation for such searches comes from theory proposals that attempt to unify the SM and GR. Such a unification would be necessary to precisely describe phenomena at extremely high energy scales, while for experiments on Earth, which take place at considerably lower energies, our current theories

[1]When we add a light right-handed neutrino, more dimension-5 operators exist. However, these can also be neglected for our study of β decay.

suffice. Models that describe this unification are, therefore, hard to test. Interestingly, however, some of these proposed models also predict that Lorentz symmetry is no longer exactly valid. At low energies, the energies that the SM covers, the effect of this breaking can also be described in an EFT. Therefore, Lorentz symmetry breaking could leave tiny imprints on low-energy experiments. It would give rise to unique signatures, because experiments would now depend on their absolute orientation in space or on the velocity of the particles involved. Of course, the validity of Lorentz symmetry has been tested for many years, but tests in the weak interaction are rather new. This thesis will discuss these tests in a number of weak decays.

1.3 Outline

Chapter 2 of this thesis discusses symmetry violations in neutron and nuclear β decay. It covers the most precise experiments in β decay and the current best limits on new scalar and tensor interactions (Sec. 2.2.1). These limits are then compared to limits from experiments at the LHC (Sec. 2.4.2) and to limits obtained from neutrino-mass measurements (Sec. 2.4.3). In Sec. 2.5, the search for T violation in β decay is compared to limits from EDMs. The study of Lorentz violation in β decay is discussed in Sec. 2.6. Finally, a roadmap for future β-decay studies is given, taking into account constraints from the LHC, the neutrino mass, and EDMs. In Chapter 3 the search for T violation in radiative β decay is discussed. Here we show that T-violating observables in radiative β decay probe the same new physics as EDM searches. Therefore, they are subject to the strong bounds already set by EDM measurements. The next two chapters focus on Lorentz-symmetry breaking in the weak interaction. Chapter 4 describes the possibilities to improve current bounds on Lorentz violation both in β decay (Sec. 4.1) and in orbital electron capture (Sec. 4.2), extending to weak decays in general. Chapter 5 more explicitly discusses the search for Lorentz violation in nonleptonic kaon decay and pion decay. In Sec. 5.1, we discuss the complications with QCD uncertainties when searching for Lorentz violation in nonleptonic decays. In pion decay it is possible to probe both Lorentz violation in the W-boson sector and in the muon sector (Sec. 5.2). These two sectors are relatively unexplored, and we show how future pion-decay experiments can improve the current bounds on Lorentz violation discussed in Sec. 2.6. Chapter 6 gives a summary of this thesis and some final remarks.

Chapter 2

Symmetry violations in nuclear and neutron β decay

This chapter reviews the role of β decay as a low-energy probe of physics beyond the Standard Model. Traditional searches for deviations from the Standard Model structure of the weak interaction in β decay are discussed in light of constraints from the Large Hadron Collider and the neutrino mass. Limits on the violation of time-reversal symmetry in β decay are compared to the strong constraints from electric dipole moments. Novel searches for Lorentz symmetry breaking in the weak interaction in β decay are also included, where the unique sensitivity of β decay to test Lorentz invariance is discussed. In the conclusion a possible roadmap for future β-decay experiments is presented.

2.1 Introduction

The study of nuclear and neutron β decay has played a major role in uncovering the structure of the weak interaction, and therefore in the development of the electroweak sector of the Standard Model (SM) of particle physics. The intensity and the variety of β emitters, combined with the high precision with which β-decay parameters can be measured, ensured that β decay remained important in searches for new physics beyond the SM (BSM). Novel techniques of laser cooling and atom trapping [9, 10] made it possible to detect the momentum of the recoiling nucleus, allowing for searches in unexplored observables that became available. New sources for slow neutrons enabled further progress in the study of neutron β-decay observables [11, 12, 13]. The motivation for these modern experiments is on the one hand to improve the accuracy of SM parameters, and, on the other hand, to search for physics BSM.

Searches for BSM physics in β decay look for deviations from the left-handed vector-axial-vector ("$V-A$") space-time structure of the weak interaction; see Refs. [14, 15] and references therein. High-precision β-decay experiments are sensitive to possible contributions of non-SM (or exotic) currents, in particular, right-handed vector, scalar, and tensor currents, that couple to hypothetical new, heavy particles. These exotic currents can also

Accepted for publication: K. K. Vos, H.W. Wilschut, and R.G.E. Timmermans, Rev. Mod. Phys. (2015).

give additional violations of the discrete symmetries parity (P), charge conjugation (C), and time-reversal invariance (T).

Traditionally, β decay has been viewed as complementary to the direct searches for new, heavy particles at high-energy colliders. However, with the availability of meson factories the emphasis of searching for new physics in precise measurements of semileptonic decay parameters has shifted from β decay. New physics has also been severely constrained by the emergence of the new field of neutrino oscillations and by the precise measurements of static observables such as the weak charges of quarks and electrons and the P- and T-odd electric dipole moments (EDMs) of particles, atoms, or molecules. Moreover, theoretical developments made it clear how various observables are interconnected, and therefore how the discovery potential of β-decay experiments compares to that of other fields.

Recently, another twist has been added to β decay as a promising precision laboratory to test the invariance of the weak interaction under Lorentz transformations, that is, boosts and rotations. The available evidence for the Lorentz invariance of the weak interaction is, in fact, surprisingly poor. The possibility to break Lorentz and the closely related CPT invariance [1] occurs in many proposals that attempt to unify the SM with general relativity, one of the central open issues in theoretical high-energy physics. During the last decade, the phenomenological consequences of such a breakdown of Lorentz symmetry have been charted [16], and recently such theoretical studies have been extended to β decay [17].

This chapter gives a broad overview of the searches for symmetry violations in nuclear and neutron β decay and discusses their significance compared to various other observables, both in precision measurements and in collider searches. In this way, it attempts to identify which β-decay studies are the most relevant to pursue. In Sec. 2.2 we first introduce the effective field theory (EFT) framework, which enables us to compare various experiments in a model-independent approach. We define the β-decay observables in Sec. 2.3.

In Sec. 2.4 we review the best bounds on exotic right-handed vector, scalar, and tensor couplings. We first address the most sensitive β-decay experiments, in which we also include limits from pion-decay experiments.

Second, we discuss how the neutrino mass and data from the Large Hadron Collider (LHC) experiments constrain BSM physics. We compare the bounds from these two sectors with the bounds from β-decay experiments. The violation of time-reversal invariance is discussed in Sec. 2.5. In β decay, T-violation manifests itself in nonzero imaginary parts of the couplings, which are probed by triple-correlation observables in β decay. We discuss how these bounds compare to those derived from the stringent upper limits on the values of EDMs.

In Sec. 2.6, we address the possibility that the weak interaction violates Lorentz symmetry, and in particular rotational invariance, in nuclear and neutron β decay. Such Lorentz violation (LV) would give rise to unique signals with no SM "background," which, even when extremely small, could be experimentally detectable. Nuclear and neutron β decay offer a unique sensitivity to some Lorentz-violating parameters, especially in the gauge and neutrino sector, which we discuss separately.

We conclude with a roadmap for the opportunities in future β-decay studies, in light of the obtained and foreseen bounds from other frontiers.

	F $\Delta J = 0$	GT $\Delta J = 0, \pm 1$	Mixed $\Delta J = 0$	First unique forbidden $\Delta J = \pm 2$	Section
	$\pi_i \pi_f = +1$			$\pi_i \pi_f = -1$	
SM parameter	V_{ud}	ρ	ρ, V_{ud}, λ		2.3
BSM T-even	$A_{L,R}$	$\alpha_{L,R}$	$\alpha_{L,R}$		2.4.1
BSM T-odd	-	Im α_L	Im A_L and Im α_L Im a_{LR}		2.5
LV	$\chi^{\mu\nu}_{r,s}$ -	$\chi^{\mu\nu}_{i,a}$ -	 a_{LV}	$\chi_{\mu\nu}$ -	2.6

Table 2.1: Classification of nuclear β decays and their characteristic use in the SM and in the search for BSM physics.

2.2 Formalism

Nuclear and neutron β decay are semileptonic processes, mediated by the W gauge boson of the electroweak interaction. This interaction is described by a spontaneously broken $SU(2)_L \times U(1)_Y$ gauge symmetry. Under $SU(2)_L$ symmetry, left-handed leptons transform as a doublet, while right-handed particles are $SU(2)_L$ singlets. This is denoted by

$$L_A = (\nu_A, l_A)_L \ , \quad R_A = (l_A)_R \ , \tag{2.1}$$

where A is the flavor index and the left- and right-handed fields are

$$\psi_L \equiv \frac{1}{2}(1 - \gamma_5)\psi \ , \quad \psi_R \equiv \frac{1}{2}(1 + \gamma_5)\psi \ . \tag{2.2}$$

The W boson interacts only with left-handed fermions (and right-handed antifermions), which reflects the maximal violation of parity (P) and charge-conjugation (C) in the weak interaction. In the minimal SM neutrinos are assumed to be massless, and right-handed neutrinos are absent. The role of the neutrino mass is discussed in Sec. 2.4.3.

The $\beta^-(\beta^+)$ decay transition $d \to u e^- \bar{\nu}_e$ ($u \to d e^+ \nu_e$) is, in the limit of infinite W-boson mass, described by the effective Lagrange density

$$\mathcal{L}_{\text{SM}} = \frac{G_F V_{ud}}{\sqrt{2}} \bar{e} \gamma_\mu (1 - \gamma_5) \nu_e \ \bar{u} \gamma^\mu (1 - \gamma_5) d + \text{H.c.} \ , \tag{2.3}$$

where G_F is the Fermi coupling constant, V_{ud} is the ud entry of the Cabibbo-Kobayashi-Maskawa (CKM) mixing matrix, and H.c. denotes the Hermitian conjugate. We work in natural units, $\hbar = c = 1$, and use $\gamma^5 \equiv i\gamma^0\gamma^1\gamma^2\gamma^3$ and $\epsilon^{0123} = -\epsilon_{0123} = 1$.

At the nucleon level, all possible quark bilinears and their associated form factors need to be inserted [18], such that

$$\begin{aligned} \langle p | \bar{u} \gamma_\mu d | n \rangle &= \bar{p} \left[g_V(q^2) \gamma_\mu + \frac{g_M(q^2)}{M} \sigma_{\mu\nu} q^\nu + \frac{\tilde{g}_S(q^2)}{2M} q_\mu \right] n \ , \\ \langle p | \bar{u} \gamma_\mu \gamma_5 d | n \rangle &= \bar{p} \left[g_A(q^2) \gamma_\mu \gamma_5 + \frac{\tilde{g}_T(q^2)}{2M} \sigma_{\mu\nu} q^\nu \gamma_5 + \frac{\tilde{g}_P(q^2)}{2M} q^\mu \gamma_5 \right] n \ , \end{aligned} \tag{2.4}$$

where $q = p_n - p_p$ is the momentum transfer and M is the nucleon mass. The vector form factor g_V and the axial-vector form factor g_A give the leading contributions to β decay, because the nuclei can be treated nonrelativistically. In the isospin limit, the induced form factor g_M, called weak magnetism, is given by $(\mu_p - \mu_n)/2$, i.e. the difference between the magnetic moments of the proton and the neutron. In the isospin limit the induced scalar form factor $\tilde{g}_S$ and tensor form factor $\tilde{g}_T$ vanish [18], and we can neglect them at present. The induced pseudoscalar form factor $\tilde{g}_P$ gets an additional suppression of q/M, because of the $\bar{p}\gamma_5 n$ structure. We comment on pseudoscalar couplings in Sec. 2.4.1.

The leading-order SM expression for neutron decay is

$$\mathcal{L}_{\rm SM} = \frac{G_F V_{ud}}{\sqrt{2}} g_V(q^2) \bar{e}\gamma_\mu(1-\gamma_5)\nu_e \bar{p}\gamma^\mu \left(1 - \frac{|g_A(q^2)|}{g_V}\gamma_5\right) n + \text{h.c.} \tag{2.5}$$

In the limit of $q^2 \to 0$, the vector charge is $g_V(0) = 1$, up to small corrections. This is dictated by the hypothesis of the conserved vector current (CVC). The axial-vector charge g_A is only partially conserved (PCAC). The best current value is derived from neutron β-decay experiments, $|g_A| = 1.2723(23)$ [19].

In nuclear β decay one can exploit the properties of the parent and daughter nucleus to select particular parts of the interaction. Pure Fermi (F) transitions probe the vector currents (γ^μ), while pure Gamow-Teller (GT) transitions probe the axial-vector currents ($\gamma_5\gamma^\mu$). Mixed transitions always require knowledge of the Fermi and Gamow-Teller transition matrix elements, $M_F \equiv \langle f|1|i\rangle$ and $M_{GT} \equiv \langle f|\vec{\sigma}|i\rangle$, respectively. The conditions for spin change (ΔJ) and parity change ($\pi_i\pi_f$) for Fermi and Gamow-Teller transitions are given in Table 2.1. This table also lists for which aspect in SM and BSM research these transitions are used. We have defined the Fermi-Gamow-Teller mixing ratio

$$\rho \equiv g_A M_{GT}/g_V M_F \ , \tag{2.6}$$

and

$$\lambda \equiv |g_A|/g_V \ . \tag{2.7}$$

It is desirable to reduce the uncertainties of nuclear structure and select the simplest isotopes. For Fermi transitions the superallowed $0^+ \to 0^+$ transitions are of the most interest. For mixed transitions, mirror nuclei are preferred. For general mirror nuclei ρ has to be measured, while neutron decay ($J^\pi = 1/2^+ \to J^\pi = 1/2^+$, $|M_F|^2 = 1$ and $|M_{GT}|^2 = 3$) allows for the determination of the value of λ [11, 12, 13]. An elaborate compilation of neutron-decay amplitudes is given in Ref. [20].

When searching for physics BSM, nuclei serve as "micro-laboratories" that can be judiciously chosen to look for certain manifestations of new physics. In this chapter, we address both the traditional searches for exotic couplings and the novel searches for Lorentz violation. In the latter, the possibility of angular-momentum violation needs to be considered, where the simplest of the forbidden decays, first-forbidden unique transitions, become relevant [21]. Both fields search for BSM physics generated by an unknown fundamental theory at a high-energy scale. To study the effect of new physics at low energies, we work in an EFT approach. Within this framework the effects of new physics at low energies are described in a model-independent way with an effective Lagrangian of the form

$$\mathcal{L}^{(\text{eff})} = \mathcal{L}_{\rm SM} + \mathcal{L}_{\rm BSM} \ . \tag{2.8}$$

The search for exotic couplings focuses on right-handed vector, scalar, and tensor couplings. These non-SM interactions can be included in the Lagrangian by adding higher-dimensional operators to $\mathcal{L}_{\text{BSM}}$. The effects of Lorentz violation can also be described in an EFT framework [16, 17]. We discuss both frameworks separately.

2.2.1 Exotic couplings

In EFT, deviations from the $V-A$ structure due to exotic couplings are generated by higher-dimensional operators, which are suppressed by the high-energy scale Λ and that obey the SM gauge symmetries. The effective Lagrangian is parametrized as

$$\mathcal{L}^{(\text{eff})} = \mathcal{L}_{\text{SM}} + \frac{1}{\Lambda^k}\mathcal{L}^{(4+k)} \ , \tag{2.9}$$

where

$$\mathcal{L}^{(4+k)} = \sum_i c_i \mathcal{O}_i^{(4+k)} \ , \tag{2.10}$$

and where c_i are dimensionless constants and $\mathcal{O}_i^{(4+k)}$ are dimension-$(4+k)$ operators. The complete SM only contains operators with mass dimension 4 or lower. For Lorentz-symmetric BSM physics, the lowest term we could add is $\mathcal{L}^{(5)}$. There is, however, only one dimension-5 operator, namely the operator that generates Majorana neutrino masses [6][1]. In searches for exotic couplings in β decay we can neglect this operator. We focus only on $\mathcal{L}^{(6)}$, as even higher-dimensional terms are suppressed by additional powers of the large scale Λ.

The $\mathcal{O}_i^{(6)}$ that contribute to semileptonic charged decays are listed in Refs. [8, 22]. At low energies these dimension-6 operators generate the original vector (C_V), axial-vector (C_A), scalar (C_S), pseudoscalar (C_P), and tensor (C_T) couplings [23]. At the quark level, the effective Lagrangian for β decay, with nonderivative four-fermion couplings, is[2]

$$\begin{aligned}\mathcal{L}^{(\text{eff})} \;=\; & \frac{4G_F V_{ud}}{\sqrt{2}} \sum_{\epsilon,\delta=L,R} \Big\{ a_{\epsilon\delta}\, \bar{e}\gamma^\mu \nu_e^\epsilon \cdot \bar{u}\gamma_\mu d_\delta \\ & + A_{\epsilon\delta}\, \bar{e}\nu_e^\epsilon \cdot \bar{u} d_\delta + \alpha_\epsilon\, \bar{e}\frac{\sigma^{\mu\nu}}{\sqrt{2}}\nu_e^\epsilon \cdot \bar{u}\frac{\sigma_{\mu\nu}}{\sqrt{2}} d_\epsilon \Big\} \ ,\end{aligned} \tag{2.11}$$

where we sum over the chirality (L, R) of the final states.

The coefficients represent

- $a_{\epsilon\delta}$: all possible V and A couplings[3].
- $A_{\epsilon\delta}$: exotic scalar and pseudoscalar couplings (where ϵ denotes the chirality of the neutrino and δ the chirality of the d quark).
- α_ϵ: exotic tensor couplings (where ϵ denotes the chirality of both the neutrino and the d quark).

[1] Adding a light singlet neutrino allows more dimension-5 operators. However, these can also be neglected for our study of β decay.

[2] We follow Ref. [24], except for a factor $G_F V_{ud}/\sqrt{2}$ that we have extracted.

[3] This includes the SM contribution and additional V and A couplings that are suppressed by Λ^2.

These coefficients are related to the couplings C_i and C_i' ($i = S, V, A, T, P$) of Ref. [23] by Eqs. (2.110) and (2.111) of Appendix 2.A. In the SM all couplings except $a_{LL} = 1$ are zero. For tensor couplings, only α_L and α_R occur, since $\sigma_{\mu\nu}\gamma_5 = (i/2)\epsilon_{\mu\nu\alpha\beta}\sigma^{\alpha\beta}$. The constants $a_{\epsilon\delta}$, $A_{\epsilon\delta}$, and α_ϵ can be related to c_i, by matching their values at the low-energy scale with standard EFT techniques. The chiral structure of the coefficients is expressed by the first and second indices, which denote the chirality of the neutrino and the d-quark, respectively. All couplings with first index R involve a right-handed neutrino. In the SM, right-handed neutrinos are absent, but they are present in many new-physics models. The role of the right-handed neutrino is discussed in Sec. 2.4.3. The new exotic couplings can be complex, representing the possibility of time-reversal (T) violation (Sec. 2.5). The introduction of left-handed and right-handed couplings leads to parity violation when the coefficients differ. In the absence of right-handed couplings, parity violation is maximal.

To describe β decay of the nucleon we define the hadronic matrix elements [24]

$$\langle p|\bar{u}\gamma_\mu d|n\rangle = g_V(q^2)\bar{p}\gamma_\mu n \ , \tag{2.12a}$$
$$\langle p|\bar{u}\gamma_\mu\gamma_5 d|n\rangle = g_A(q^2)\bar{p}\gamma_\mu\gamma_5 n \ , \tag{2.12b}$$
$$\langle p|\bar{u}d|n\rangle = g_S(q^2)\bar{p}n \ , \tag{2.12c}$$
$$\langle p|\bar{u}\gamma_5 d|n\rangle = g_P(q^2)\bar{p}\gamma_5 n \ , \tag{2.12d}$$
$$\langle p|\bar{u}\sigma_{\mu\nu} d|n\rangle = g_T(q^2)\bar{p}\sigma_{\mu\nu} n \ , \tag{2.12e}$$

modifying the effective Lagrangian in Eq. (2.11) accordingly. As before, the vector charge is $g_V \equiv g_V(0) = 1$. The other couplings g_A, g_S, g_P, and g_T can be calculated theoretically by using lattice QCD. Estimates for g_A on the lattice are currently not competitive with the experimental value $|g_A(0)| = 1.2723(23)$ determined from neutron β decay [19]. The scalar, pseudoscalar, and tensor constants, g_S, g_P, and g_T, are determined theoretically. They are further discussed in Sec. 2.4.

Searches for exotic coupling also include searches for right-handed $V + A$ currents. Such currents are predicted for instance by left-right (LR) models, which add an $SU(2)_R$ gauge symmetry to the SM. This extends the SM with an additional gauge boson W_R, which mixes with the original SM W boson W_L. The weak eigenstates can be expressed in the mass eigenstates W_1 and W_2 as

$$W_L = W_1 \cos\xi + W_2 \sin\xi \ , \tag{2.13a}$$
$$W_R = e^{i\omega}(-W_1 \sin\xi + W_2 \cos\xi) \ , \tag{2.13b}$$

where ξ is the mixing angle and ω is a CP-violating phase. The coupling of W_R to quarks and leptons introduces the right-handed coupling g_R and the right-handed CKM element V_{ud}^R, the equivalents of the SM parameters. The expressions for a_{LR}, a_{RL}, and a_{RR} in terms of these parameters are given in Ref. [24]. A specific class of LR models are the symmetric LR models, in which P or C symmetry of the Lagrangian is imposed, which implies $g_L = g_R$ at the LR symmetric scale. We focus on bounds for such models in Sec. 2.4.2.

2.2.2 Lorentz violation

The study of Lorentz violation is motivated by the possibility of spontaneous breaking of Lorentz invariance predicted by theories of quantum gravity [25, 26, 27]. The natural energy scale for these theories of quantum gravity is the Planck scale, which lies 17 orders of magnitude higher than the electroweak scale. This precludes the direct detection of Planck-scale physics, but the effects of Lorentz violation at the Planck scale can become manifest at much lower energies, providing a "window on quantum gravity." At low energy, Lorentz violation can be systematically described by the Standard Model Extension (SME) [16], by using an EFT approach. The SME contains all possible Lorentz-violating terms that obey the SM gauge symmetries, which include CPT-violating terms, since Lorentz violation allows for the breaking of CPT invariance. In fact, CPT violation can occur only if Lorentz symmetry is also broken [1].

Spontaneous Lorentz violation arises as Lorentz-tensor fields acquire a vacuum-expectation value (VEV), resulting in Lorentz-violating tensor coefficients in the SME Lagrangian. These coefficients can be understood as constant background tensor fields. Because of to these tensor fields, the Lagrangian is no longer invariant under particle or active Lorentz transformations, i.e. boosts or rotations of the particles, because the background fields do not transform under the Lorentz group [16]. However, the low-energy theory remains invariant under observer Lorentz transformations, i.e. boosts or rotations of the observer's inertial frame. Because Lorentz symmetry is spontaneously broken, the underlying fundamental theory at the Planck scale remains Lorentz invariant, implying that important features such as energy-momentum conservation and microcausality are still valid. A possible experimental signature of Lorentz violation is a sidereal variation of observables, which arise as the laboratory moves through the Lorentz-violating background field when Earth rotates [other examples are given in e.g., Ref. [28]].

Schematically, terms in $\mathcal{L}_{\text{BSM}}$ in Eq. (2.8) can be written as [29]

$$\mathcal{L}_{\text{NP}} = \lambda^{(3)} \langle T \rangle \cdot \bar{\psi} \Gamma \psi + \frac{\lambda^{(4)}}{\Lambda} \langle T \rangle \cdot \bar{\psi} \Gamma (i\partial) \psi + \frac{\lambda^{(4+k)}}{\Lambda^k} \langle T \rangle \cdot \mathcal{O}^{(4+k)} \ , \tag{2.14}$$

where we summed over repeated indices and where $\lambda^{(i)}$ are dimensionless constants, $\langle T \rangle$ is the expectation value of tensor T, $\Gamma = 1, \gamma_5, \gamma_\mu, \gamma_\mu\gamma_5, \sigma_{\mu\nu}$ represents the gamma-matrix structure, and $\mathcal{O}^{(4+k)}$ are higher-dimensional operators. Furthermore, Λ represent the scale of the fundamental theory, which is naturally the Planck scale. The higher-dimensional operators are suppressed by powers of this high scale. The first two terms in Eq. (2.14) have mass dimensions 3 and 4, respectively. These terms are described in the original SME papers [16] and are now referred to as the minimal Standard-Model Extension (mSME). For our present discussion we limit ourselves to the mSME, although higher-dimensional coefficients have also been described [30, 31, 32, 33].

From an EFT point of view, the introduced Lorentz-violating dimension-3 and dimension-4 operators are unnatural. Naively, one would expect the dimension-3 operators to scale linearly with the large scale Λ, while the coefficients of the dimension-4 operators should be of order unity. The experimental bounds on these dimension-3 and dimension-4 operators are much smaller, of course. This problem does not occur for higher-dimensional operators, which are naturally suppressed by the scale Λ. To evade

these naturalness problems, the current limits on dimension-3 and dimension-4 coefficients require either large fine-tuning, or a symmetry that forbids these coefficients. However, even if dimension-3 and dimension-4 operators are forbidden at tree level, they will be induced by quantum corrections generated by higher-dimensional nonrenormalizable operators. These corrections scale quadratically with the cutoff scale, which might be as large as Λ. This can be circumvented by introducing new physics between the weak scale and the Planck scale. In that case, radiative corrections scale with a significantly lower cutoff scale (see e.g., Ref. [34]). Such a scenario occurs in supersymmetry (SUSY) [35, 36]. SUSY restricts Lorentz-violating operators to dimension 5 and higher, and forbids those of dimensions 3 and 4. Dimension-3 and dimension-4 operators are generated by loop corrections if SUSY is broken. This would naturally lead to a suppression of m^2/Λ and m/Λ for dimension-3 and dimension-4 operators, respectively, where m is the SUSY-breaking scale [35, 36]. In the mSME, it is assumed that dimension-3 and dimension-4 operators are suppressed by some unspecified higher-scale mechanism, and the experimental constraints are studied without any assumptions on the nature of this suppression mechanism [16, 37].

The SME contains a large number of coefficients that parametrize possible Lorentz violation. We list the relevant coefficients for β decay, which are the lepton, Higgs, and gauge terms. The Lorentz-violating terms for leptons are[4] [16]

$$\begin{aligned}\mathcal{L}_{\text{lepton}} &= \bar{L}_A \left[i(c_L^{\text{LV}})_{\mu\nu AB}\gamma^\mu D^\nu - (a_L^{\text{LV}})_{\mu AB}\gamma^\mu \right] L_B \\ &\quad + \bar{R}_A \left[i(c_R^{\text{LV}})_{\mu\nu AB}\gamma^\mu D^\nu - (a_R^{\text{LV}})_{\mu AB}\gamma^\mu \right] R_B \ , \end{aligned} \tag{2.15}$$

where L denotes the $SU(2)_L$ doublet and R denotes the singlet, defined in Eq. (2.1). The subscripts A, B are flavor indices, and D_μ is the covariant derivative. This introduces the Lorentz-violating coefficients $a_{L,R}^{\text{LV}}$ and $c_{L,R}^{\text{LV}}$, which are CPT-odd and CPT-even, respectively. We introduced the superscript LV for these coefficients, in order not to confuse them with the coefficients in Eq. (2.11).

Before electroweak symmetry breaking, the Higgs and gauge sectors are described by [16]

$$\begin{aligned}\mathcal{L}_{\text{Higgs+gauge}} &= \left[\frac{1}{2} k_{\phi\phi}^{\mu\nu} (D_\mu \phi)^\dagger D_\nu \phi + \text{H.c.} \right] + \left[i\, k_\phi^\mu \phi^\dagger D_\mu \phi + \text{H.c.} \right] \\ &\quad - \frac{1}{2} k_{\phi B}^{\mu\nu} \phi^\dagger \phi B_{\mu\nu} - \frac{1}{2} k_{\phi W}^{\mu\nu} \phi^\dagger W_{\mu\nu} \phi - \frac{1}{2} (k_G)_{\kappa\lambda\mu\nu} \text{Tr}(G^{\kappa\lambda} G^{\mu\nu}) \\ &\quad - \frac{1}{2} (k_W)_{\kappa\lambda\mu\nu} \text{Tr}(W^{\kappa\lambda} W^{\mu\nu}) - \frac{1}{4} (k_B)_{\kappa\lambda\mu\nu} B^{\kappa\lambda} B^{\mu\nu} \ , \end{aligned} \tag{2.16}$$

where $G^{\mu\nu}, W^{\mu\nu}$, and $B^{\mu\nu}$ are the $SU(3)_c, SU(2)_L$, and $U(1)_Y$ field-strength tensors, respectively, and ϕ is the Higgs doublet. The coefficient k_ϕ is CPT-odd, and the only coefficient with dimension of mass. The other coefficients are CPT-even and dimensionless. The coefficient $k_{\phi\phi}$ has symmetric real and antisymmetric imaginary components.

[4] The quark parameters c and d are defined equivalently by replacing the lepton doublet by the quark doublet and the lepton singlet by the quark singlet. Lorentz-violating quark parameters are discussed in Sec. 5.2.

The $k_{\phi W}$ and $k_{\phi B}$ coefficients are real and antisymmetric. The gauge couplings k_G, k_W, and k_B are real and have the symmetry properties of the Riemann tensor [16].

The SME parameters have been studied in a wide range of experiments [37]. The electromagnetic and gravity sector have been studied extensively, whereas the number of searches in the weak interaction is rather low. This changed recently [17, 38, 21], and the search for Lorentz violation has been extended to weak decays, in particular, β decay. β decay places strong constraints on Lorentz-violating coefficients in the Higgs and gauge sector. In addition, β decay has a unique sensitivity to some coefficients in the neutrino sector [39]. We discuss these constraints in Sec. 2.6.

2.3 Observables in β decay

2.3.1 Correlation coefficients in β decay

In β decay, the correlations between different observables, such as the β momentum and the nuclear spin, can be measured. The amount of correlation is expressed in terms of correlation coefficients. These correlation coefficients depend on SM couplings and possible new V, A, S, P, and T interactions. Using the general effective Lagrangian in Eq. (2.11), we can write the decay-rate distribution for polarized nuclei as [40]

$$\begin{aligned}
&\omega(\langle\vec{J}\rangle|E_e,\Omega_e,\Omega_\nu)dE_e d\Omega_e d\Omega_\nu \\
&= \frac{F(\pm Z,E_e)}{(2\pi)^5} p_e E_e (E_0-E_e)^2 dE_e d\Omega_e d\Omega_\nu \\
&\quad\times\bar{\xi}\left\{1 + a\frac{\vec{p}_e\cdot\vec{p}_\nu}{E_e E_\nu} + b\frac{m_e}{E_e} + c\left[\frac{1}{3}\frac{\vec{p}_e\cdot\vec{p}_\nu}{E_e E_\nu} - \frac{(\vec{p}_e\cdot\vec{j})(\vec{p}_\nu\cdot\vec{j})}{E_e E_\nu}\right]\left[\frac{J(J+1)-3\langle(\vec{J}\cdot\vec{j})^2\rangle}{J(2J-1)}\right]\right. \\
&\quad\left.+\frac{\langle\vec{J}\rangle}{J}\cdot\left[A\frac{\vec{p}_e}{E_e} + B\frac{\vec{p}_\nu}{E_\nu} + D\frac{\vec{p}_e\times\vec{p}_\nu}{E_e E_\nu}\right]\right\}\,,
\end{aligned} \tag{2.17}$$

where $E_{e(\nu)}$, $\Omega_{e(\nu)}$, and $p_{e(\nu)}$ denote the total $\beta(\nu)$ energy, direction, and momentum, respectively, E_0 is the energy available to the electron and the neutrino, $\langle\vec{J}\rangle$ is the expectation value of the spin of the initial nuclear state, and $\vec{j}$ is the unit vector in this direction; $F(\pm Z, E_e)$ is the Fermi function which modifies the phase space of the electron due to the Coulomb field of the nucleus. Also affecting the phase space is the Fierz-interference term, factorized with the coefficient b. This term is zero in the SM. We defined $\bar{\xi} \equiv G_F^2 V_{ud}^2/2\xi$, where ξ gives the strength of the interaction. The remaining terms describe the β-correlation coefficients: the β-neutrino asymmetry a, the P-odd "Wu parameter," the β asymmetry A, the neutrino asymmetry B, and the triple-correlation coefficient D. The c coefficient vanishes for nonoriented nuclei and for nuclei with $J = 1/2$, such as the neutron. The c coefficient has not been taken into account in any experiment to date. However, in future experiments, which use laser beams to trap and cool samples, the expectation value $\langle(\vec{J}\cdot\vec{j})^2\rangle$ may be affected, such that the c coefficient can play a role.

The decay rate integrated over the neutrino direction, but taking into account electron

Coefficient	Correlation	P	T
a ($\beta\nu$ angular correlation)	$\vec{p}_e \cdot \vec{p}_\nu / E_e E_\nu$	Even	Even
b (Fierz-interference term)	m_e/E_e	Even	Even
A (β asymmetry)	$\vec{J} \cdot \vec{p}_e / E_e$	Odd	Even
B (ν asymmetry)	$\vec{J} \cdot \vec{p}_\nu / E_\nu$	Odd	Even
G (longitudinal polarization)	$\vec{\sigma}_e \cdot \vec{p}_e / E_e$	Odd	Even
N	$\vec{J} \cdot \vec{\sigma}_e$	Even	Even
Q	$\vec{\sigma}_e \cdot \vec{p}_e \vec{J} \cdot \vec{p}_e / E_e$	Even	Even
D (triple correlation)	$\vec{J} \cdot (\vec{p}_e \times \vec{p}_\nu) / E_e E_\nu$	Even	Odd
R (triple correlation)	$\vec{\sigma}_e \cdot (\vec{J} \times \vec{p}_e) / E_e$	Odd	Odd

Table 2.2: Overview of symmetry properties under parity (P) transformations and time reversal (T) of the most relevant correlations in allowed β decay.

polarization, is [40]

$$\begin{aligned}\omega(\langle\vec{J}\rangle, \vec{\sigma}_e | E_e, \Omega_e) dE_e d\Omega_e = & \frac{F(\pm Z, E_e)}{(2\pi)^4} p_e E_e (E_0 - E_e)^2 dE_e d\Omega_e \\ & \times \bar{\xi} \left\{ 1 + b\frac{m_e}{E_e} + \frac{\vec{p}_e}{E_e} \cdot \left(A\frac{\langle\vec{J}\rangle}{J} + G\vec{\sigma}_e \right) \right. \\ & \left. + \vec{\sigma}_e \cdot \left[N\frac{\langle\vec{J}\rangle}{J} + Q\frac{\vec{p}_e}{E_e + m} \left(\frac{\langle\vec{J}\rangle}{J} \cdot \frac{\vec{p}_e}{E_e} \right) + R\frac{\langle\vec{J}\rangle}{J} \times \frac{\vec{p}_e}{E_e} \right] \right\} ,\end{aligned} \tag{2.18}$$

where $\vec{\sigma}_e$ is the spin vector of the β particle. This introduces the longitudinal β polarization G, the spin-correlation coefficients N and Q, and the triple-correlation coefficient R. The symmetry properties of the correlation coefficients are listed in Table 2.2. The A, B, and G coefficients are associated with parity violation. Depending on the type of transition they can have SM values close to ± 1, which is characteristic for maximal parity violation. The triple-correlation coefficients D and R are T-odd and unmeasurably small in the SM [41].

Integrating the decay rate over all kinematical variables gives the inverse lifetime,

$$\frac{1}{\tau} = \frac{m_e^5}{2\pi^3} f \bar{\xi} \left(1 + b \left\langle \frac{m_e}{E_e} \right\rangle \right) , \tag{2.19}$$

where f contains the integration over the modified phase space and $\langle m_e/E_e \rangle$ is the average inverse energy in units of the electron mass.

In Appendix 2.A we list the relevant correlation coefficients in terms of the couplings defined in Eq. (2.11) and the Fermi-Gamow-Teller matrix elements. The different correlation coefficients contain combinations of the complex V, A, S, P, and T couplings. Given the current experimental precision, we have neglected Coulomb corrections. These

corrections mainly introduce additional imaginary couplings (except for the D and R coefficients) [40].

We proceed by discussing how β-decay correlation experiments, combined with lifetime measurements, are used to obtain precise values for the SM V and A coupling strengths. In Sec. 2.4 we discuss constraints on exotic couplings.

2.3.2 Standard Model parameters in β decay

The correlation coefficients in Appendix 2.A reduce to the SM expressions when putting the scalar and tensor couplings to zero, $A_{LL,LR,RR,RL} = 0$ and $\alpha_{L(R)} = 0$, and by using only $V-A$ couplings, $a_{LR,RR,RL} = 0$. The Fierz-interference coefficient b is zero in the SM. The lifetime in Eq. (2.19) can be derived from the ft value, using the measured half-life t instead of τ. In the SM,

$$\frac{1}{ft} = \frac{m_e^5}{2\pi^3 \ln(2)} G_F^2 \, V_{ud}^2 \, g_V^2 |M_F|^2 (1 + |\rho|^2) \; . \tag{2.20}$$

The SM value for G_F is obtained from muon decay [42]. It is important to note that if one considers non-SM contributions these may influence muon decay as well. In principle, g_A is calculable using lattice QCD, but as mentioned before, current lattice calculations are not as accurate as values derived from experiments and henceforth $\lambda = |g_A|/g_V$ is considered a free parameter. In general, M_F and M_{GT} need to be derived from nuclear model calculations. For superallowed Fermi transitions $\rho = 0$ and $M_F = \sqrt{2}$, in the isospin limit. Hardy and Towner analyzed all available superallowed Fermi transitions, and derived a value for the ud CKM matrix element [43]. Since the ft values of superallowed transitions should be equal, a large number of measurements could be combined, leading to the most precise value of $V_{ud} = 0.97425(22)$ [43]. In the analysis, details of the isotope-dependent nuclear-structure corrections on the matrix element M_F (e.g., isospin breaking) and the phase-space modifications are also considered. The superallowed transitions also give the best bound on the Fierz coefficient b in Eq. (2.19) by considering the energy dependence of the lifetime (Sec. 2.4.1).

The parameters λ and V_{ud} can also be determined from β-decay correlations in neutron decay and from the neutron lifetime [11, 12, 13, 44]. The best current values are $\lambda = 1.2723(23)$ [19] and $V_{ud} = 0.9742(12)$ [13]. The latter is more than a5 times less precise; see also Fig. 22 in Ref. [13]. The strong Gamow-Teller dependence of neutron decay and the precision of the neutron-decay parameters is such that neutron decay also plays an important role in searches for tensor currents, as is discussed in Sec. 2.4.1.

Another class of nuclei for which the nuclear structure is relatively well known are the mirror nuclei [45]. Like neutron decay, mirror decays are mixed Fermi-Gamow-Teller transitions. Extraction of V_{ud} from lifetime measurements requires knowledge of the mixing parameter ρ, such that an additional measurement of at least one of the correlation coefficients is necessary. Naviliat-Cuncic and Severijns found $V_{ud} = 0.9719(17)$ [46], using five available transitions. The important structure corrections to Eq. (2.20) for mirror nuclei have been evaluated [45], in analogy to the work of Hardy and Towner [43] for superallowed Fermi decays. This new class of nuclei will broaden the spectrum of data and remove any possible bias in selecting only superallowed Fermi transitions in the

determination of V_{ud}. Measurements with this motivation were undertaken. For example, the lifetime of two relevant mirror nuclei ^{19}Ne and ^{37}K have been measured [47, 48, 49]. We will not review the status of this field here, but comment on their relevance in limiting left-handed tensor couplings via the Fierz-interference term in the next section. It demonstrates that the contribution of nuclear physics to high-precision SM data goes hand in hand with the searches for new physics in β decay.

2.4 Constraints on exotic couplings

β decay played an important role in establishing the $V-A$ structure of the SM, initially eliminating to a large extent the possible contributions of scalar and tensor interactions. Modern searches in nuclear β decay consider again scalar and tensor currents as possible very small deviations from the SM due to new physics [14, 50].

The searches in β decay are part of a much wider search in subatomic physics for new physics. Comparison between different searches has become possible in an EFT framework by using the effective Lagrangian in Eq. (2.11). At the quark level the relations between different observables are clean, but at the nucleon level they involve the nuclear form factors g_A, g_S, g_P, and g_T. Accurate values for these parameters are necessary in order to compare different limits. Recently, significant progress on the accuracy of both g_S and g_T has been reported. First results for g_P are also available. The most precise value for g_T is calculated with lattice QCD. Two recent results are $g_T = 1.038(16)$ [51], and $g_T = 1.047(61)$ [52].

The calculation method used in these works gives a much larger uncertainty for g_S. Estimates range from $g_S = 0.72(32)$ [52] to $g_S = 1.08(32)$ [51]. A value for g_S can also be derived using the CVC relation and lattice calculations [53],

$$g_S(0) = \frac{\delta M^{\rm QCD}}{\delta m_q} = 1.02(11) \ , \tag{2.21}$$

where both $\delta M^{\rm QCD} = (M_n - M_p)^{\rm QCD}$ [53] and $\delta m_q = m_d - m_u$ [54] are obtained separately from lattice calculations. However, the determination of g_S with Eq. (2.21) might underestimate the error, because correlations between the numerator and denominator are neglected. Such errors could be avoided by calculating the ratio in Eq. (2.21) directly on the lattice. Further efforts to reduce the error for g_S directly on the lattice are being pursued [52, 55].

The pseudoscalar constant g_P can be calculated by using the PCAC relation. Combined with lattice QCD results [53] one finds

$$g_P(0) = \frac{\bar{M}_N}{\bar{m}_q} g_A = 349(9) \ , \tag{2.22}$$

where $\bar{M} = (M_p + M_n)/2$ is the average nucleon mass and $\bar{m}_q = (m_u + m_d)/2 = 3.42(9)$ MeV is the average light-quark mass determined on the lattice [54]. According to Ref. [56], $\bar{m}_q = 3.5^{+0.7}_{-0.2}$ MeV at the renormalization scale $\mu = 2$ GeV, which gives a much larger error $g_P = 340^{+68}_{-19}$. Nevertheless, this shows that the pseudoscalar form factor is of the

order of $\mathcal{O}(10^2)$. In β decay, pseudoscalar terms are generally neglected, because they occur only as higher-order recoil corrections. This suppresses pseudoscalar interactions compared to scalar and tensor interactions. The large value of g_P cancels this suppression to a large extent, and β-decay experiments may be sensitive to pseudoscalar couplings after all. There are, however, already strong constraints on pseudoscalar couplings from pion decay, as discussed in Sec. 2.4.1.

In the remainder of this section we comment on searches for exotic couplings in β decay (Sec. 2.4.1), but consider only real couplings. We compare these results with constraints from the LHC experiments (Sec. 2.4.2) and due to the nonzero mass of the neutrino (Sec. 2.4.3). Bounds on imaginary couplings are discussed separately in Sec. 2.5.

2.4.1 Constraints from β decay

In nuclear β decays, exotic couplings are mainly searched for in either pure Fermi or pure Gamow-Teller decays. Pure Fermi transitions depend on vector and possibly scalar couplings, while pure Gamow-Teller transitions depend on axial-vector and possibly tensor couplings. The use of mixed transitions is necessary when searching for interference terms. Preferred are isotopes with a relatively simple nuclear structure, e.g., mirror nuclei, or the neutron. We discuss the constraints from Fermi, Gamow-Teller, and mixed decays separately, focusing on the best current experimental data. We discuss the constraints on scalar and tensor couplings, while assuming no additional vector or axial-vector interactions. For a fit of the data including these interactions we refer to Ref. [14], where also a review of the experimental techniques is given. We discuss $V + A$ couplings in Sec. 2.4.2.

Most β-correlation coefficients are measured by constructing asymmetry ratios. For example, the β asymmetry is measured from the quantity

$$A_{\text{measured}} = \frac{N(\uparrow) - N(\downarrow)}{N(\uparrow) + N(\downarrow)} \ , \tag{2.23}$$

where $N(\uparrow)$ and $N(\downarrow)$ are the decay rates derived from measuring β particles in a particular detector while the polarization P of the nucleus changes sign. The arrows indicate the direction of polarization. The rates $N(\uparrow), N(\downarrow)$ correspond to the integration of Eq. (2.17) over all unobserved degrees of freedom, which removes the dependence on the neutrino direction. In the numerator only the P-odd term remains, while in the denominator the odd term drops out. However, the Fierz-interference term remains in the sum $N(\uparrow) + N(\downarrow)$, so that

$$\begin{aligned} A_{\text{measured}} &= \frac{\int_{\Delta\Omega} \int_{E_{\min}}^{E_0} F(\pm Z, E_e) p_e (E_0 - E_e)^2 A |P| (p_e/E_e) \cos\theta_e dE_e d\Omega_e}{\int_{\Delta\Omega} \int_{E_{\min}}^{E_0} F(\pm Z, E_e) p_e (E_0 - E_e)^2 (1 + b/E_e) dE_e d\Omega_e} \\ &= \frac{A|P| \langle \beta_e \cos\theta_e \rangle}{1 + b \langle m_e/E_e \rangle} \ . \end{aligned} \tag{2.24}$$

This implies that actually not the coefficient A is measured, but

$$\tilde{A} = \frac{A}{1 + b \left\langle \frac{m_e}{E_e} \right\rangle} \ . \tag{2.25}$$

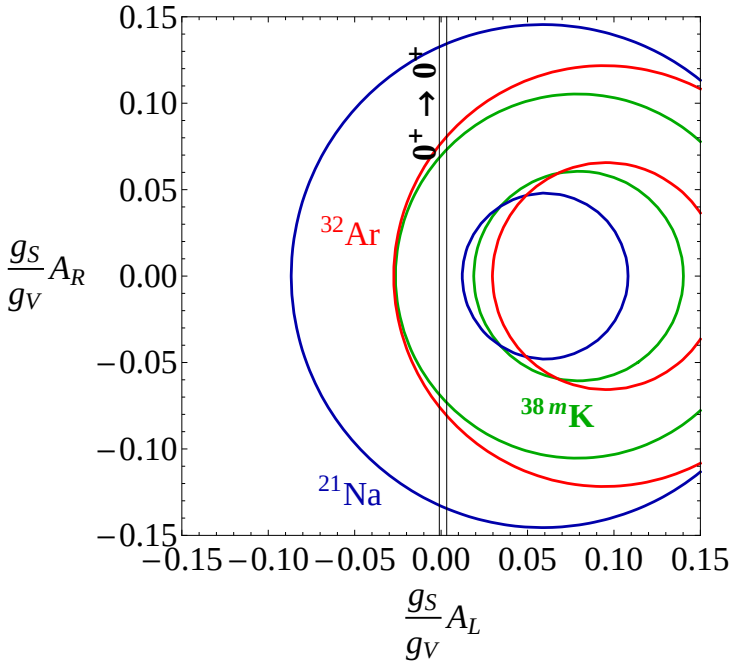

Figure 2.1: Bounds on scalar couplings with a left- and right-handed neutrino(90% C.L.). The narrow $0^+ \to 0^+$ band is from superallowed Fermi transitions Eq. (2.30) [43]. The ring-shaped boundaries are derived from β-ν correlation measurements in ^{38m}K [59] and ^{32}Ar [60], cf. Eq. (2.33). Also the bound from the mirror nucleus ^{21}Na [61] is given, neglecting tensor contributions.

The inverse average energy is approximated by

$$\left\langle \frac{m_e}{E_e} \right\rangle = \frac{\int_{E_{\min}}^{E_0} F(\pm Z, E_e) p_e (E_0 - E_e)^2 dE_e}{\int_{E_{\min}}^{E_0} F(\pm Z, E_e) p_e (E_0 - E_e)^2 E_e dE_e} \,, \tag{2.26}$$

which depends on the specific isotope and the experimental setup. In principle, the average energy could also depend on the angular distribution (θ_e). This makes it preferable that the analysis of $\langle m_e/E_e \rangle$ is done and published together with the observed correlation coefficients. At present, many of the values for $\langle m_e/E_e \rangle$ are derived by using the β-energy threshold E_{min} [14, 57, 58].

For the measured quantity $\tilde{X}$, $X = a, A, B, G$, etc., Eq. (2.25) applies. Except for B and N, the numerator of Eq. (2.25) depends only on the square of the coupling constants, while b has a linear dependence on left-handed couplings. In such cases one is most sensitive to b, and the measurement of $\tilde{X}$ provides in the first place a measurement of the Fierz coefficient b. Therefore, the exact value of the $\langle m_e/E_e \rangle$ will become increasingly important with increasing experimental precision.

Nuclear scalar searches

Throughout the discussion of limits on scalar and tensor couplings, we assume conventional left-handed vector couplings for the V-A part, such that $a_{LL} = 1$, and $a_{LR,RL,RR} =$

0. These and the other couplings are defined in Eq. (2.11). The notation is chosen such that the difference between the left-handed and right-handed coupling of the neutrino is emphasized, i.e., for the scalar couplings $A_L = A_{LL} + A_{LR}$ (left-handed neutrino coupling) and $A_R = A_{RR} + A_{RL}$ (right-handed neutrino coupling). Further details on the notation and some relevant expressions can be found in Appendix 2.A.

For pure Fermi transitions

$$\xi = 2|M_F|^2 g_V^2 \left\{ 1 + \left(\frac{g_S}{g_V} \right)^2 \left[A_L^2 + A_R^2 \right] \right\} , \tag{2.27}$$

$$\xi b_F = \pm 4\gamma |M_F|^2 g_V g_S A_L , \tag{2.28}$$

from Eq. (2.116) and (2.118), where b_F is the Fermi part of the Fierz coefficient b, the upper (lower) sign is for $\beta^-(\beta^+)$ decays and $\gamma = \sqrt{1 - Z^2\alpha^2}$, with Z the atomic number of the daughter nucleus and α the fine-structure constant. For the positron-emitting superallowed $0^+ \to 0^+$ Fermi decays

$$\frac{1}{ft_F} = \frac{m_e^5}{2\pi^3 \ln(2)} G_F^2 \, V_{ud}^2 \, g_V^2 \, |M_F|^2 \left\{ 1 + \left(\frac{g_S}{g_V} \right)^2 \left[A_L^2 + A_R^2 \right] - 2\gamma \left\langle \frac{m_e}{E_e} \right\rangle \frac{g_S}{g_V} A_L \right\} . \tag{2.29}$$

Hardy and Towner [43] obtained an average of all ft values, $\overline{\mathcal{F}t}$, after the appropriate corrections for radiative and nuclear-structure effects. The current best value of V_{ud} is derived from $\overline{\mathcal{F}t}$, assuming no exotic couplings. Allowing for scalar terms one can exploit [62] the different values of $\langle m_e/E_e \rangle$ to put a stringent limit on the Fermi Fierz-interference coefficient [43],

$$b_F = -0.0022(26) = -2 \frac{\frac{g_s}{g_V} A_L}{1 + \frac{g_S^2}{g_V^2}(A_L^2 + A_R^2)} \simeq -2 \frac{g_S}{g_V} A_L . \tag{2.30}$$

Although b_F is not sensitive to scalar currents with right-handed neutrinos (A_R), the value of $\overline{\mathcal{F}t}$ is sensitive to these. In fact, the bound on right-handed couplings, i.e. interactions involving a right-handed neutrino, is more than an order of magnitude larger than that of left-handed couplings, such that both contributions to the $\overline{\mathcal{F}t}$ values are of the same order, as can be seen in Eq. (2.29). Therefore, in searches for BSM physics one may not assume V_{ud} as given by the Particle Data Group (PDG) when such a search concerns also right-handed scalar terms. In the correlation coefficients, the value of V_{ud} mostly drops out, but in limits derived from measured lifetimes the actual value of V_{ud} is required.

Constraints on right-handed[5] scalar couplings can be extracted from the β-ν-correlation coefficient a defined in Eq. (2.117). We define $\delta_- = |a_{SM} - a_{exp}^-|$ as the lower bound and $\delta_+ = |a_{exp}^+ - a_{SM}|$ as the upper bound, where the experimental value, at 90% confidence level (C.L.), lies between a_{exp}^- and a_{exp}^+. Limits from a then give

$$2 \left(\frac{g_S}{g_V} \right)^2 [A_L^2 + A_R^2] < \delta_- , \tag{2.31}$$

[5]For simplicity we will refer to interactions with a right-handed neutrino as right-handed and with a left-handed neutrino as left-handed.

which gives a circular bound in the A_L, A_R plane. Thus, the bound on A_L and A_R would be the same,

$$\left|\frac{g_S}{g_V}A_{L(R)}\right| < \sqrt{\frac{\delta_-}{2}} \ . \tag{2.32}$$

In practice experiments normalize the correlation to the total number of counts, and the absolute normalization is not measured. This means that in fact $\tilde{a}$ is measured, as discussed below Eq. (2.23). In this way the Fierz-interference term b enters. The bounds remain circular, but the bound on A_L changes to

$$\frac{-\delta_-}{2\gamma\langle m_e/E_e\rangle} < \frac{g_S}{g_V}A_L < \frac{\delta_+}{2\gamma\langle m_e/E_e\rangle} \tag{2.33}$$

for β^+ and with opposite signs for β^-.

Figure 2.1 shows the bounds from the best current experiments. The superallowed Fermi decays constrain only left-handed couplings and give a narrow vertical band [43]. The right-handed coupling A_R is constrained only by the β-ν correlations, and depends on the square root of the experimental error δ_-. The most sensitive β-ν correlation measurements are from metastable ^{38m}K [59] and ^{32}Ar [60]. We also include the recent measurement of the mirror nucleus ^{21}Na [61], a mixed transition, where we have put tensor contributions to zero. In an earlier review this was erroneously shown with a bound as in Eq. (2.32) [50]. We show it because it is the first mixed transition available with such competitive precision.

The best current bounds on real scalar couplings from pure Fermi decays are found by minimizing the χ^2 of the b_F from Eq. (2.30) and the measurements of the β-ν correlation in ^{38m}K [59] and ^{32}Ar [60] (Table 2.3). At 90% C.L.,

$$-0.1\times10^{-2} < \frac{g_S}{g_V}A_L < 0.3\times10^{-2} \ , \tag{2.34a}$$

$$-6\times10^{-2} < \frac{g_S}{g_V}A_R < 6\times10^{-2} \ . \tag{2.34b}$$

For A_L the bound comes from the strong limit on the Fierz-interference term. The limit on A_R is less strong. Improving the bound on right-handed scalar couplings substantially is a daunting task: exploiting the forward-backward symmetry in the β-ν correlation would require collecting 10^{14} events to reach a bound $< 10^{-3}$ on $g_S A_R$.

Nuclear tensor searches

The nuclear Gamow-Teller matrix element M_{GT} can be evaluated only in the context of a nuclear model, because the spin of a nucleus is an observable, but the orbital angular momentum of a valence nucleon is not. For this reason M_{GT} cannot be evaluated sufficiently robustly to put a bound on the left-handed tensor couplings from ft values, as was done for the scalar coupling by using the superallowed Fermi decays. However, the Fierz-interference term will enter most observables via the normalization requirement discussed previously; cf. Eq. (2.25). The β-asymmetry coefficient A in Gamow-Teller

decays is a good example of this, where

$$\tilde{A} = \frac{A_{GT}}{1 + b_{GT}\left\langle \frac{m_e}{E_e} \right\rangle} \simeq \pm\lambda_{J'J}\left[-1 + 8\frac{g_T^2}{g_A^2}\alpha_L^2 - 4\frac{g_T}{|g_A|}\alpha_L\gamma\left\langle \frac{m_e}{E_e} \right\rangle\right] , \tag{2.35}$$

from Eq. (2.120). Thus in the absence of Coulomb corrections one finds that $\tilde{A}$ becomes independent of α_R and therefore only limits on α_L can be obtained from $\tilde{A}$. Defining now $\delta_- = |A_{SM} - A^-_{exp}|$ as the lower bound and $\delta_+ = |A^+_{exp} - A_{SM}|$ as the upper bound, where the experimental value, at 90% confidence level (C.L.), lies between A^-_{exp} and A^+_{exp}, gives

$$\frac{-\delta_-}{4\gamma\langle m_e/E_e\rangle} < \frac{g_T}{|g_A|}\alpha_L < \frac{\delta_+}{4\gamma\langle m_e/E_e\rangle} . \tag{2.36}$$

To obtain a bound on α_R one can exploit the β-ν correlation a. The result is similar to the result for a in Fermi decay. For β^- Gamow-Teller decay $a_{\rm SM} = -1/3$ and the bounds are

$$\begin{aligned} |\frac{g_T}{g_A}\alpha_R| &< \sqrt{\frac{3\delta_-}{8}} , \\ -\frac{3\delta_-}{4\gamma\langle m_e/E_e\rangle} &< \frac{g_T}{|g_A|}\alpha_L < \frac{3\delta_+}{4\gamma\langle m_e/E_e\rangle} . \end{aligned} \tag{2.37}$$

The limits on tensor interactions can be improved by combining scalar and tensor searches. In particular, the left-handed tensor couplings can be further constrained by using the measurements of the Fermi and Gamow-Teller-transition ratio of the longitudinal β polarization. These measurements were performed in the first place to study the manifest left-right symmetric model [63, 64]; see also Sec. 2.4.2. The ratio of longitudinal polarizations (P, see Appendix 2.A) of the emitted positrons was measured in the systems ^{26m}Al/^{30}P [63] and ^{14}O/^{10}C [64], where the first nucleus decays via a Fermi and the second a Gamow-Teller transition. The two transitions have nearly identical end-point energies, which eliminates systematic errors. The measured ratio is

$$\frac{P_F}{P_{GT}} \simeq \frac{\tilde{G}_F}{\tilde{G}_{GT}} \simeq 1 - 2\left\langle \frac{m_e}{E_e} \right\rangle \left(\frac{g_S}{g_V} A_L + 2\frac{g_T}{|g_A|}\alpha_L \right) . \tag{2.38}$$

Combining these measurements with the bounds on b_F in Eq. (2.30) gives a more precise left-handed tensor bound, but it does not constrain right-handed couplings.

Figure 2.2 shows the best constraints on tensor couplings. We use the P_F/P_{GT} values [63, 64], the β-ν correlation in ^{6}He [65, 66], and the β asymmetry in ^{60}Co [67] (see Table 2.3) to find the best bounds for nuclear searches, using χ^2 minimalization. For the P_F/P_{GT} values we have included the limits on scalar couplings in Eq. (2.34). The combined fit for real tensor couplings gives, at 90% C.L.,

$$-0.3 \times 10^{-2} < \frac{g_T}{|g_A|}\alpha_L < 0.6 \times 10^{-2} , \tag{2.39a}$$

$$-6 \times 10^{-2} < \frac{g_T}{|g_A|}\alpha_R < 6 \times 10^{-2} . \tag{2.39b}$$

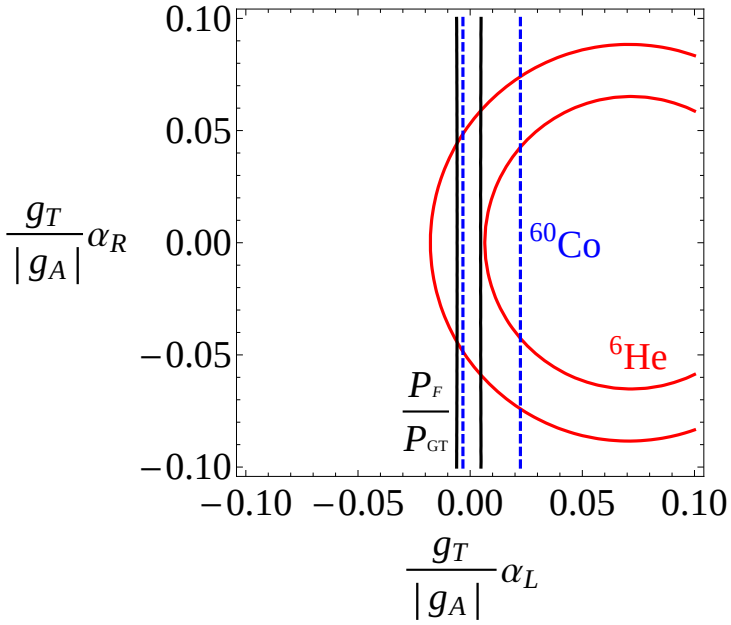

Figure 2.2: Bounds on left- and right-handed tensor couplings (90% C.L.). The measurement of the β-ν correlation in ^{6}He [65, 66] gives a ring-shaped boundary. The boundary of measurements of the β-asymmetry in the pure Gamow-Teller-decay of ^{60}Co [67] is given by dashed lines, the measurement only constrains left-handed couplings [Eq. (2.35)]. The strongest bounds on left-handed couplings are from measurements of the β-longitudinal polarization P_F/P_{GT} in Eq. (2.38) [63, 64], combined with the constraint on b_F.

Reducing the limits will require increased statistics and experimental improvements. Further constraints from β decay come from mixed decays which we discuss next.

Tensor constraints from neutron and mirror nuclei

Mirror transitions are mixed transitions and therefore sensitive to both scalar and tensor interactions. Mirror decays might be used to improve the bounds of pure Fermi and Gamow-Teller transitions discussed previously. At this point only the neutron can be considered. The prospects of using mirror nuclei are discussed at the end of this section. The neutron can serve as a laboratory for studying a range of fundamental interactions [11, 13, 12]). In neutron β decay, the main focus lies on determining the SM parameters V_{ud} and $\lambda = g_A/g_V$. Non-SM values are included by allowing λ to be complex and/or by allowing for scalar (A_L, A_R) and/or tensor (α_L, α_R) interactions. We still consider only real couplings and defer to Sec. 2.5.1 for complex λ and scalar and tensor couplings. To clarify the role of possible left- and right-handed scalar and tensor contributions, we keep the simplifying assumptions that the V and A couplings are those of the SM. For neutron

decay, with $M_{GT} = \sqrt{3}$ and $M_F = 1$, the ft value is given by

$$1/ft_n = \frac{m_e^5}{2\pi^3 \ln(2)} G_F^2 V_{ud}^2 g_V^2 \left\{ 1 + \left[\frac{g_S}{g_V}\right]^2 \left[A_L^2 + A_R^2\right] + 2\gamma \left\langle \frac{m_e}{E_e} \right\rangle \frac{g_S}{g_V} A_L + 3\lambda^2 \left(1 + \left[\frac{g_T}{g_A}\right]^2 \left[\alpha_L^2 + \alpha_R^2\right] - 4\gamma \left\langle \frac{m_e}{E_e} \right\rangle \frac{g_T}{|g_A|} \alpha_L \right) \right\} . \quad (2.40)$$

The current value recommended for the lifetime is $\tau_n = 880.3(1.1)$ s [19], which is nearly 6 s lower, but with the same error, as the recommended value of 2008. Of course, this affects the SM values for V_{ud} and λ, but cross-checks with other correlation coefficients are possible, allowing for consistency of the SM parameters [44]. Including scalar and tensor contributions increases the number of degrees of freedom and such cross-checks are no longer possible. The observable ft_n is most sensitive to α_L, because of the partial Gamow-Teller nature of neutron decay. One can combine various correlation coefficients from neutron decay to extract λ, while allowing for non-SM contributions. In combination with the experimental results from the superallowed Fermi transitions (b_F and $\overline{\mathcal{F}t}$), improved bounds on tensor contributions can be obtained. For example, with the recent limits on A from UCNA and PERKEOII Collaborations [68, 69] and neglecting right-handed neutrinos ($A_R = 0,\ \alpha_R = 0$), it is possible to obtain an analytical bound on α_L [57]. Allowing for right-handed neutrinos requires a fitting procedure.

A complete set of neutron correlation data has been compiled [13]. More recent results are obtained with the PERKEOII setup [68] and from the UCNA Collaboration [69]. Combined with the bounds from pure Fermi and Gamow-Teller transitions a fit can be made to obtain all relevant parameters ($\lambda, A_L, A_R, \alpha_L,$ and α_R) in a consistent way. This was recently done [58], to extract both left-handed and right-handed tensor-coupling limits. Their fitting method entails a grid search. For all α_L and α_R values, a value of χ^2 was obtained by minimizing χ^2 for the other three parameters. With this 2D χ^2 surface a contour plot can be made, by plotting the equal $\Delta\chi^2 \equiv \chi^2 - \chi_0^2$ lines, where χ_0^2 is the minimal χ^2.

Figure 2.3 shows the contour plot for the 1, 2, and 3 σ ($\Delta\chi^2 = 1, 4,$ and 9) bounds obtained with this method and by using the most relevant experiments listed in Table 2.3. It is important to note that the neutron lifetime requires the value of V_{ud}. The most precise value for V_{ud} is obtained from the $\mathcal{F}t$ of superallowed decays [70], under the assumption of no scalar interactions. We have corrected for this by using Eq. (2.127) for the neutron lifetime. For the neutron lifetime we use the average value of the PDG [56]. For the correlation coefficients the averages of the PDG cannot be used, because these are obtained by assuming only SM interaction. The possible different dependence on the Fierz-interference term is therefore not included. We consider the different values of A separately, for which we have calculated the energy dependence with Eq. (2.26). We have included the measurement of B, although for neutron decay this coefficient actually has a reduced sensitivity to the Fierz term b and to λ; see Eq. (2.133).

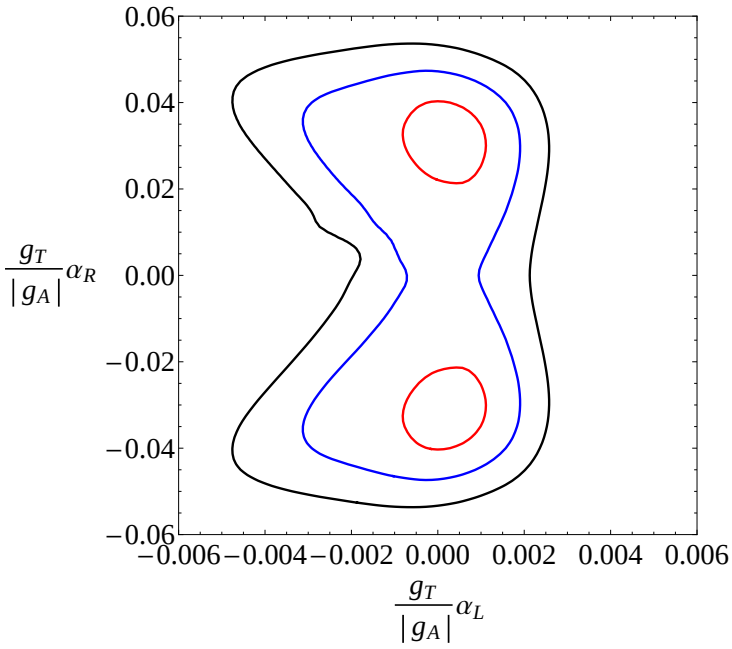

Figure 2.3: Contour plot of the 1, 2, and 3 σ contours, derived from the selection of available data listed in Table 2.3. In the fitting procedure we minimized A_L, A_R, and λ. Notice the scale difference of the two axes.

We find at 90% C.L[6]

$$-0.3 \times 10^{-2} < \frac{g_T}{|g_A|}\alpha_L < 0.06 \times 10^{-2} \quad , \tag{2.41a}$$

$$-4.6 \times 10^{-2} < \frac{g_T}{|g_A|}\alpha_R < 4.6 \times 10^{-2} \quad , \tag{2.41b}$$

$$-0.1 \times 10^{-2} < \frac{g_S}{g_V}A_L < 0.3 \times 10^{-2} \quad , \tag{2.41c}$$

$$-5 \times 10^{-2} < \frac{g_S}{g_V}A_R < 6 \times 10^{-2} \quad , \tag{2.41d}$$

$$1.2659 < \lambda < 1.2746 \quad . \tag{2.41e}$$

The scalar bounds are the same as the bounds in Eq. (2.34), but the tensor bounds are improved because of the inclusion of the neutron data. Especially the positive bound for α_R is reduced as compared to Eq. (2.39). This is caused by the large spread in experimental values for A. Using only the two most recent values of the PERKEOII setup [68] and from the UCNA Collaboration [69] gives $-0.3 \times 10^{-2} < g_T\alpha_L/|g_A| < 0.2 \times 10^{-2}$. For the tensor bounds, the neutron lifetime has a large influence [58]. We therefore anticipate that the error in the neutron lifetime and the spread in A will soon give the dominant error on the limit on tensor couplings.

Recently, also mirror decays have been used to constrain tensor couplings. The strong constraint on b_F from superallowed Fermi decays can be combined with measurements

[6]Bounds are extracted by scanning the 2D $\chi^2 + 1.64^2$ surface for scalar ($A_{L,R}$) and tensor ($\alpha_{L,R}$), while for λ we used the 1D probability density.

Isotope	Parameter	Decay	$\langle m_e/E_e \rangle$	Value	Error	Reference
^{6}He	$\tilde{a}_{GT}$	β^-, GT	0.286	-0.3308	0.003	[71]
						[65]
^{14}O/^{10}C	P_F/P_{GT} (Eq. (2.38))	β^+	0.292	0.9996	0.0037	[64]
^{26m}Al/^{30}P	P_F/P_{GT} (Eq. (2.38))	β^+	0.216	1.003	0.004	[63]
^{32}Ar	$\tilde{a}_F$	β^+, F	0.191	0.9989	0.0065	[60]
^{38m}K	$\tilde{a}_F$	β^+, F	0.133	0.9981	0.0045	[59]
^{60}Co	$\tilde{A}_{GT}$	β^-, GT	0.704	-1.027	0.022	[67]
$0^+ \to 0^+$	b_F	β^+, F	0.2560	-0.0022	0.0026	[43]
n	τ (Eq. (2.127))	β^-, F/GT	0.655	880 s.	0.9 s.	[56]
n	$\tilde{A}_n$	β^-, F/GT	0.56	-0.11952	0.00110	[69]
n	$\tilde{A}_n$	β^-, F/GT	0.534	-0.11926	0.00050	[68]
n	$\tilde{A}_n$	β^-, F/GT	0.582	-0.1160	0.0015	[72]
n	$\tilde{A}_n$	β^-, F/GT	0.558	-0.1135	0.0014	[73]
						[74]
n	$\tilde{A}_n$	β^-, F/GT	0.551	-0.1146	0.0019	[75]
n	$\tilde{B}_n$	β^-, F/GT	0.594	0.9801	0.0046	[76]
n	$\tilde{B}_n$	β^-, F/GT	0.63	0.9802	0.0050	[77]
n	$\tilde{a}_n$	β^-, F/GT	0.655	-0.1054	0.0055	[78]

Table 2.3: Experimental values used to construct Fig. 2.3. The values for $\langle m_e/E_e \rangle$ are mostly not calculated by the experimental groups and are derived with Eq. (2.26), except for the $0^+ \to 0^+$ decays, for which we use the value derived in Ref. [57]. Averages from the PDG are used only for the τ [56], since different measurements of $\tilde{A}$ and $\tilde{B}$ might also have a different energy dependence, which is not taken into account in the PDG averages. We have taken all experimental values for $\tilde{A}$ used by the PDG.

on mirror nuclei, to derive a value for b_{GT}. In Ref. [45] a complete survey of $\mathcal{F}t$ values of the available mirror transitions is given. The relation between the $\mathcal{F}t$ values of mirror transitions between $T = 1/2$ isospin doublets and the superallowed $0^+ \to 0^+$ is given by [45]

$$\mathcal{F}t^{\text{mirror}} \equiv \frac{2\mathcal{F}t^{0^+\to 0^+}\left\langle 1 + \frac{g_S^2}{g_V^2}\left[A_L^2 + A_R^2\right] - 2\gamma\left\langle \frac{m_e}{E_e}\right\rangle^{0^+\to 0^+}\frac{g_S}{g_V}A_L\right\rangle}{1 + \frac{g_S^2}{g_V^2}\left[A_L^2 + A_R^2\right] + \frac{f_A}{f_V}\rho^2\left[1 + 4\alpha_L^2 + 4\alpha_R^2\right] \pm 2\gamma\left\langle \frac{m_e}{E_e}\right\rangle\left(\frac{g_S}{g_V}A_L - 2\frac{g_T}{|g_A|}\alpha_L\rho^2\right)}\,, \tag{2.42}$$

where $f_A/f_V = 1.0143(29)$ is the ratio of the axial-vector and vector statistical rate functions [45]. The inverse energy dependence of the superallowed Fermi decays is denoted by $\langle m_e/E_e\rangle^{0^+\to 0^+}$ and calculated in Ref. [57]. If ρ is known, a value for α_L can be extracted from $\mathcal{F}t^{\text{mirror}}$.

The mirror β^+ decay of ^{19}Ne to ^{19}F was recently studied to determine the lifetime of ^{19}Ne [48]. In this work, the effectiveness of the method described above is shown. For mixed decays an independent measurement of ρ is necessary. For ^{19}Ne, $\rho = 1.5995(45)$ [79], was derived from the measurement of the β asymmetry A. Neglecting quadratic couplings in Eq. (2.42) and using the extracted value $\mathcal{F}t = 1719.8(13)$ s with $\langle m_e/E_e\rangle = 0.387022(18)$ [48] a limit on b_{GT} is derived. For left-handed tensor couplings this gives at 90% C.L. [48]

$$-1.5 \times 10^{-2} < \frac{g_T}{|g_A|}\alpha_L < 0.12 \times 10^{-2}\,. \tag{2.43}$$

The bounds are only an order of magnitude less precise than the combined limits in Eq. (2.41), and show the potential for this kind of measurements for improving the existing bounds.

Tensor constraints from radiative pion β decay

Reference [80] derived limits on tensor couplings from radiative pion decay $\pi^+ \to e^+ + \nu_e + \gamma$. These bounds can be translated into bounds on α_L [55] by using estimates for the pion form factor [81]. Assuming no right-handed couplings and using $g_T = 1.047(61)$, a limit at 90% C.L. is found,

$$-1.9 \times 10^{-3} < \frac{g_T}{|g_A|}\alpha_L < 2.3 \times 10^{-3}\,. \tag{2.44}$$

These bounds are the strongest bounds on tensor couplings from a single decay experiment and show that future β-decay experiments should probe $\alpha_L < 10^{-3}$ and beyond, in order to improve these existing limits.

Pseudoscalar constraints

Pseudoscalar interactions have so far been neglected in β-decay searches, since they are strongly suppressed because the nuclei are nonrelativistic. The suppression of these terms is $\mathcal{O}(1/M)$, where M is the nucleon mass. However, in β decay, the pseudoscalar interactions are always multiplied by g_P, the pseudoscalar form factor discussed in Eq. (2.22).

The large value $g_P = 349(9)$ [53] largely cancels this suppression, and β-decay experiments might be used to probe these interactions. There are, however, already strong constraints on pseudoscalar couplings from pion decay [24, 82, 55].

The ratio $R_\pi = \Gamma(\pi \to e\nu)/\Gamma(\pi \to \mu\nu)$ is sensitive to pseudoscalar couplings defined by

$$\mathcal{L} = \frac{G_F V_{ud}}{\sqrt{2}} \left[A_L^P\, \bar{e}(1-\gamma_5)\nu_e + A_R^P\, \bar{e}(1+\gamma_5)\nu_e\right]\, \bar{u}\gamma_5 d\ , \tag{2.45}$$

where we have neglected flavor-changing couplings, which can be found in Ref. [55]. The ratio R_π/R_π^{SM}, where R_π is the measured value, is sensitive to electron and muon pseudoscalar couplings $A^{P(e)}$ and $A^{P(\mu)}$, respectively. If these couplings are such that $A^{P(e)}/m_e = A^{P(\mu)}/m_\mu$, their contributions to the ratio cancel and no bounds on pseudoscalar interactions can be obtained. Since there is no reason to assume such a cancellation, we can place bounds on pseudoscalar interactions, because these would show up as $R_\pi/R_\pi^{\rm SM} \neq 1$. The current best value for this ratio is $R_\pi/R_\pi^{\rm SM} = 0.996(3)$ [83, 56], which leads to (90% C.L.) [55, 22]

$$-1.4 \times 10^{-7} < A_L^P < 5.5 \times 10^{-4}\ , \tag{2.46a}$$

$$-2.8 \times 10^{-4} < A_R^P < 2.8 \times 10^{-4}\ . \tag{2.46b}$$

In β decay the pseudoscalar term shows up in Gamow-Teller and mixed decays. The most relevant to experiments are its contributions to the Fierz-interference term,

$$b_{GT} = \mp 4\gamma \frac{g_T}{|g_A|}\alpha_L \mp \frac{1}{3}\gamma \frac{g_P}{|g_A|} A_L^P \frac{E_0 - E_e}{M}\ , \tag{2.47}$$

which enters with the usual $\langle m_e/E_e\rangle$ suppression. The $(E_0 - E_e)/M$ term is responsible for the suppression of pseudoscalar contributions, however, because $g_P(E_0 - E_e)/M \simeq 0.4$ pseudoscalar interactions are still suppressed compared to tensor interactions. Given the current limit on α_L, improving the bounds in Eq. (2.46a) seems unlikely in the near future.

The pseudoscalar couplings in Eq. (2.46) can also be translated into bounds on scalar and tensor couplings. If scalar and tensor interactions are present at the new-physics scale Λ, they will mix via radiative loop corrections, and pseudoscalar couplings will radiatively be generated [84, 82]. Current limits are at the level of [55, 22, 85]

$$|A_L| \lesssim 8 \times 10^{-2} \quad \text{and} \quad |A_R| \lesssim 5 \times 10^{-2}\ , \tag{2.48a}$$

$$|\alpha_L| \lesssim 2 \times 10^{-3} \quad \text{and} \quad |\alpha_R| \lesssim 1.2 \times 10^{-3}\ , \tag{2.48b}$$

and depend logarithmically on the scale of new physics Λ, for which $\Lambda = 10$ TeV is used. These bounds are of the same order of magnitude as global-fit limits from β decay in Eq. (2.41), except for the bound on α_R, which is an order of magnitude better. However, because the constraints for right-handed currents rely on the flavor structure of new physics [22], we do not further consider these bounds.

Left-handed scalar versus tensor

In Sec. 2.4.3 we discuss exotic couplings involving right-handed neutrinos. If right-handed neutrinos are absent, or too heavy to be energetically allowed in β decay, right-handed

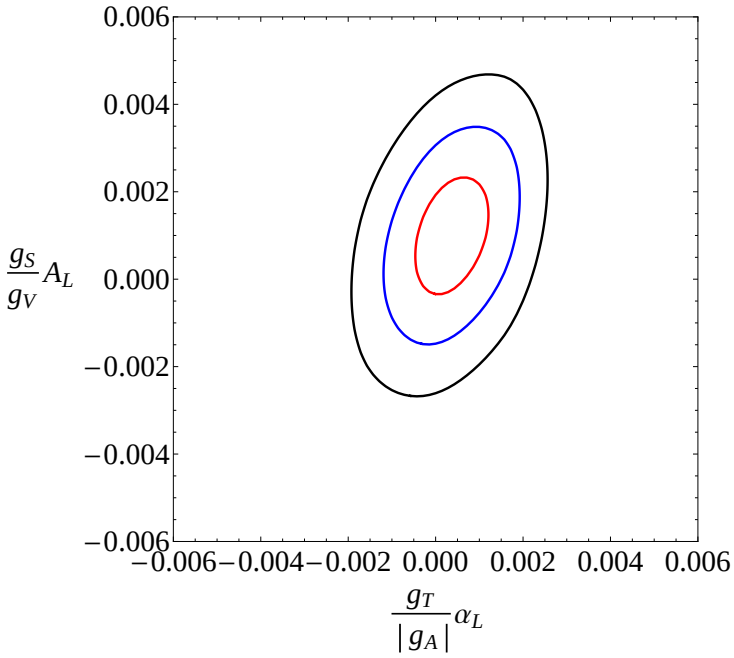

Figure 2.4: Contour plot of the 1, 2, and 3 σ contours, derived from the selection of available data listed in Table 2.3 without right-handed couplings, i.e. $A_R = \alpha_R = 0$.

neutrino couplings, i.e. A_R and α_R, can be neglected. The resulting reduction of parameter space allows us to use mixed decays to fit the correlations between left-handed tensor and scalar couplings. Figure 2.4 shows these correlations. For the complete set of data listed in Table 2.3 we find at 90% C.L.

$$-0.1 \times 10^{-2} < \frac{g_S}{g_V} A_L < 0.3 \times 10^{-2} \ , \tag{2.49a}$$

$$-0.2 \times 10^{-2} < \frac{g_T}{|g_A|} \alpha_L < 0.06 \times 10^{-2} \ , \tag{2.49b}$$

$$1.2715 < |\lambda| < 1.2744 \ . \tag{2.49c}$$

These bounds are not significantly different from the bounds from the complete fit in Eq. (2.41). For comparison: limits on right-handed couplings from neutron decay alone are given in Refs. [86, 13].

2.4.2 Constraints from the LHC experiments

Low-energy experiments are mostly viewed as complementary to high-energy collider searches for BSM physics. Experiments at the LHC can place bounds on new physics by looking for the on-shell production of new particles, as done in searches for a W_R boson [Eq. (2.13)] or supersymmetric particles. We focus here on the effect of a W_R boson, because this has been studied complementary by precision decay experiments and by the LHC, e.g., Ref. [87]. At the LHC, W_R is searched for by considering its possible decay channels. In the $W_R \to t\bar{b}$ channel, such direct searches at the CMS experiment constrain $M_R > 2$ TeV [88]. Constraints from the $W_R \to e\nu$ channel are similar, but depend on

assumptions for the right-handed neutrino. Constraints from neutral-kaon mixing give $M_R > 3$ TeV [89].

In β decay, strong limits come from CKM unitarity tests, for which the best bound is [70]

$$|V_{ud}|^2 + |V_{us}|^2 + |V_{ub}|^2 = 1.000\,08(56)\ , \tag{2.50}$$

which uses the value of V_{us} from Ref. [90]. The error has equal contributions from V_{ud} and V_{us}. This leads to a constraint on a_{LR}, i.e., left-handed lepton couplings and right-handed quark couplings, of [43]

$$-4 \times 10^{-3} < a_{LR} < 5 \times 10^{-3}\ , \tag{2.51}$$

at 90% C.L. The precision of both V_{ud} and V_{us} should improve simultaneously for such a test to remain significant.

In β decay, some correlation coefficients are sensitive to a_{LR}, a_{RL}, and a_{RR}, where the latter two are present only if light right-handed neutrinos are assumed. For example, the measurements of P_F/P_{GT} [63, 64] and A_{GT} in ^{60}Co [67], are used to constrain parameters of manifest LR-symmetric models[7]. Such models have a P symmetry, such that for the CKM matrices $V_{ud}^L = \pm V_{ud}^R$. There is no additional spontaneous CP violation, so $\omega = 0$. In this simplified model, $a_{RL} = \pm a_{LR} \sim -\xi$ and $a_{RR} = \delta = (M_1/M_2)^2$. Measurements of P_F/P_{GT} limit the combination $\delta \cdot \xi$ and do not give additional bounds, because of the strong bound on ξ from unitarity tests given in Eq. (2.51). Because ξ is strongly constrained, β-decay experiments can constrain only a_{RR} and thus the mass of the W_R. Derived limits are of the order of 200 GeV [67, 59], an order of magnitude below the bound from the LHC experiments presented above. In fact, when assuming manifest LR symmetry, the strongest bound on W_R comes from the K_L-K_S mass difference, from which $W_R > 20$ TeV was derived [92].

Besides constraining new physics by searching for direct on shell production, it is also possible for colliders to constrain exotic couplings. When the mass of the non-SM particle exceeds the energy accessible at the LHC, the new particles cannot be produced on-shell, but their effects can still be found in deviations from the SM predictions. In that way, the exotic interactions in Eq. (2.11) will also manifest themselves in proton-proton collisions. This makes it possible for LHC data to constrain the same tensor and scalar couplings relevant in β decay [55, 22].

In particular, the $pp \to e + \text{MET} + X$ channel is considered, where MET signifies missing transverse energy. This channel is closely related to β decay, since it involves the $\bar{u}d \to e\bar{\nu}$ process at quark level. At the LHC, both the ATLAS and CMS detectors are used to search for new physics in this channel [93, 94], by searching for an excess of events predicted at a large lepton transverse mass cut $\bar{m}_T$. At large $\bar{m}_T$, the SM cross section approaches zero more rapidly than the cross sections for new physics, making the sensitivity to non-SM physics larger at high momenta. The total cross section is

$$\begin{aligned} \sigma(m_T > \bar{m}_T) &= \sigma_{\text{SM}}(1 + |a_{LR}|^2 + |a_{RL}|^2) + \sigma_R |a_{RR}|^2 \\ &\quad + \sigma_S(|A_L|^2 + |A_R|^2) + \tfrac{1}{4}\sigma_T(|\alpha_L|^2 + |\alpha_R|^2)\ , \end{aligned} \tag{2.52}$$

[7]Here we comment only on manifest LR-symmetric models. The complementarity of β-decay experiments and other searches in generalized LR models is discussed in e.g., Ref. [91].

	$\lvert A_L\rvert$	$\lvert A_R\rvert$	$\lvert\alpha_L\rvert$	$\lvert\alpha_R\rvert$
β decay	2.5×10^{-3}	6×10^{-2}	3×10^{-3}	4.6×10^{-2}
LHC	6×10^{-3}	6×10^{-3}	2×10^{-3}	2×10^{-3}
Neutrino	-	1×10^{-3}	-	1×10^{-3}

Table 2.4: Comparison between β-decay limits on left- and right-handed scalar A_L and A_R and tensor couplings α_L and α_R, constraints from the LHC data [95], and from the neutrino mass [97]. Constraints are at 90% C.L., and all couplings are assumed to be real.

where $\sigma_{\rm SM}$ is the SM cross section and $\sigma_{R,S,T}$ are the cross sections for new physics. The explicit form of $\sigma_{\rm SM}$ and $\sigma_{R,S,T}$ is given, to lowest order in QCD corrections, in Ref. [22]. The coefficients a_{LR} and a_{RL} cannot be constrained, because their contribution is proportional to $\sigma_{\rm SM}$, and therefore small at large $\bar{m}_T$.

With the expected number of background events and the number of actual observed events, one can place an upper limit on the number of new-physics events, n_s^{up} [55]. This translates into an upper limit for σ, and finally into bounds on exotic couplings. First bounds were derived by Ref. [55], updated bounds are given in Ref. [95].

The bounds are derived by using the experimental data of CMS [96] at an integrated luminosity of 20 fb^{-1} and at a center-of-mass energy of $\sqrt{s} = 8$ TeV. Reference [95] also gave the combined limits for scalar and tensor couplings, assuming only left-handed couplings. In Table 2.4 we give the 90% C.L. bounds, obtained by allowing one exotic interaction and putting all other couplings to zero. To compare these results with β-decay constraints, we use the values from the global fit in Eq. (2.41) and the form factors $g_S = 1.02(11)$ [53] and $g_T = 1.047(61)$ [52]. Because the errors on the form factors are not Gaussian, we use the R-fit method [55], which treats all the values in a 1 σ interval with equal probability. Therefore, only the lower bounds are important. We stress again that the reduction of the error in g_S and g_T is important to make meaningful comparisons between the different experiments.

Table 2.4 shows that the LHC constraints on left-handed couplings are comparable to β-decay constraints, while for right-handed couplings the LHC constraints are an order of magnitude better than the β-decay limits. The current status is discussed in Sec. 2.4.4. Reference [95] also made a projection for the 14 TeV run at 50 fb^{-1}, and find that the expected bounds are a factor of 3 better.

2.4.3 Neutrino-mass implications

Besides strong bounds from the LHC experiments on right-handed interactions, there are also bounds from the neutrino mass. In the SM, neutrinos are assumed to be massless, but neutrino oscillations indicate the existence of at least two massive neutrinos. A direct upper limit on the neutrino mass comes from the shift of the end-point of the β spectrum. Recent measurements of the β spectrum of ^{3}H give $m_\nu < 2$ eV (95% C.L.) [98, 99]. The experiment of the KATRIN Collaboration aims to improve these limits by an order

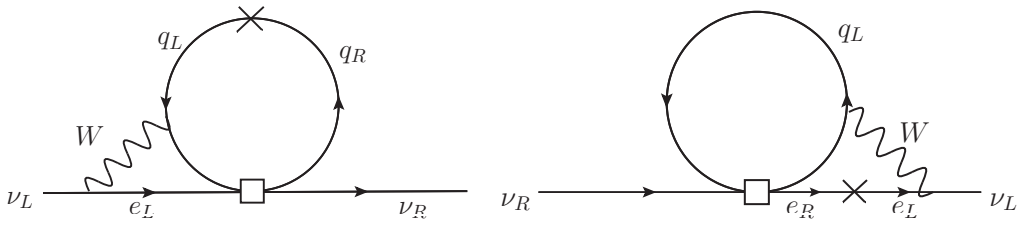

(a) Constrains A_{RR}, A_{RL}, and α_R (b) Constrains a_{RL}

Figure 2.5: The two-loop contribution to the neutrino mass, where the boxes indicate the exotic couplings. The crosses indicate mass insertions, with (a) $m_q = 4$ MeV and (b) $m_e = 0.511$ MeV [97]. For Majorana neutrinos one can substitute $\nu_R \to \nu_L^c$.

of magnitude [100]. Other bounds on the neutrino mass are derived from cosmological observations; WMAP Collaboration [101] limits $\sum m_\nu < 0.44$ eV and a recent study of Planck Collaboration [102], in which Planck data are combined with neutrino oscillation data, gives a similar limit $m_\nu < 0.15$ eV, for three degenerate neutrinos.

In Eq. (2.11), the couplings a_{RR}, a_{RL}, A_R, and α_R involve right-handed neutrinos. These couplings can be generated only if the decay to right-handed neutrinos is kinematically allowed, i.e., if right-handed neutrinos are light enough to be created in the decay. The possibility of these light right-handed neutrinos has been considered in various new-physics scenarios as a possible dark-matter candidate. If right-handed neutrinos are very heavy, as suggested in many see-saw mechanisms, we can omit all exotic couplings with first index R.

Prezeau and Ito showed that the small neutrino mass also limits the presence of exotic couplings in low-energy experiments that involve a (light) right-handed neutrino [103]. For β decay this strongly constrains the couplings A_R, α_R, and a_{RL} [97]. Neutrino masses can be either Dirac ($\bar{\nu}_L m_D \nu_R$) or Majorana ($\frac{1}{2}\bar{\nu}_L m_\nu \nu_L^c$), where $\nu_L^c = i\gamma_2\gamma_0\bar{\nu}_L^T$, or a combination of the two. However, the following results are general and apply to both types. Couplings to right-handed neutrinos contribute to the neutrino mass via loop interactions. Figure 2.5 shows the leading two-loop contribution to the neutrino mass, where the boxes indicate the non-SM couplings to right-handed particles. The crosses indicate the mass insertions needed to couple two fermions with different chiralities. Here the chirality-changing interactions are either proportional to (a) the quark or (b) the electron mass. In a power-counting scheme, one-loop contributions are in general less suppressed than two-loop contributions. However, the two-loop diagrams in Fig. 2.5 are enhanced by the W-boson mass, while the one-loop diagrams are suppressed only by the light-fermion mass. This makes the two-loop contribution dominant, as the additional loop suppression of $1/(4\pi)^2$ is diminished by the heavy W-boson mass.

One can estimate the two-loop contribution to the neutrino mass by considering only the logarithmic part of Fig. 2.5. The analytic parts are renormalization-scheme dependent and are therefore neglected [103]. By using dimensional regularization the contribution to δm_ν is estimated as [97]

$$\delta m_\nu \simeq 3g^2 G_F \bar{a} \frac{m_f M_W^2}{(4\pi)^4} \left(\ln \frac{\mu^2}{M_W^2}\right)^2 , \tag{2.53}$$

where $\bar{a} = \{A_{RL}, A_{RR}, \alpha_R, a_{RL}\}$ are the exotic couplings from Eq. (2.11), $g = 0.64$ is the gauge coupling, m_f is the inserted fermion mass, and μ is the renormalization scale, which should exceed the heaviest mass in the interaction $\mu > m_t$, where m_t is the top-quark mass. Assuming that the loop corrections do not exceed the mass of the neutrino[8], i.e. $\delta m_\nu < m_\nu$, setting $m_q = 4$ MeV, $\mu = 1$ TeV, and $m_\nu < 0.15$ eV in Eq. (2.53) gives

$$|a_{RL}| \lesssim 10^{-2} \,, \tag{2.54a}$$

$$|A_{RR}|\,, |A_{RL}|\,, |\alpha_R| \lesssim 10^{-3} \,. \tag{2.54b}$$

In Table 2.4 we compare these limits with current right-handed β-decay bounds and bounds from the LHC. The estimates from the neutrino mass are currently the strongest bounds on right-handed currents. They are more than an order of magnitude stronger than the β-decay bounds and comparable to the LHC bounds. For the bounds in Eq. (2.54) we have used the updated neutrino mass from the Planck space observatory, which might further improve in the future. The given bounds are conservative estimates, but nevertheless they show the large impact of the neutrino mass on β-decay measurements. Even stronger constraints of $\mathcal{O}(10^{-5})$ from the neutrino mass have been derived in Ref. [104].

2.4.4 Conclusions and outlook

We summarized the current status of the bounds on real scalar, pseudoscalar, and tensor interactions in β decay. We compared these bounds with those obtained from proton-proton collisions at the LHC experiments and the upper limit on the neutrino mass, mainly focusing on scalar and tensor interaction. The best current bounds are given in Table 2.4. We distinguished between bounds on left- and right-handed scalar and tensor interactions, where left or right denotes the chirality of the neutrino. The constraints on left-handed interactions are equally constrained by the LHC and β-decay experiments. On the other hand, β-decay experiments measuring right-handed interactions would have to improve orders of magnitude to compete with the bounds from the LHC experiments and the neutrino mass. This is illustrated in Fig. 2.6 for scalar interactions and in Fig. 2.7 for tensor interactions. Table 2.5 projects the competitive accuracies required for different β-decay parameters. For left-handed currents we give the necessary precision to compete with projected future LHC bounds [95]. For right-handed bounds, we give two accuracies. The first corresponds to the required sensitivity to compete with current LHC bounds; the number in brackets corresponds to the required precision to compete with the bounds from the neutrino mass (see Table 2.4).

The bounds on left-handed couplings are best pursued via measurements of the Fierz-interference coefficient b. For left-handed scalar couplings A_L the bound is most stringent because of the vast effort in the study of superallowed Fermi transitions. These studies also provide the best current value for V_{ud}. The left-handed tensor coupling α_L requires a larger effort, for which several measurements need to be combined. The best current bounds are from the global fit in which neutron and nuclear data are combined. In this fit, especially the uncertainties in the neutron lifetime and the A coefficient of the neutron have a significant impact. We pointed out that the large spread in the available

[8]There might be scenarios in which this is not obeyed, but these scenarios would have to be fine-tuned.

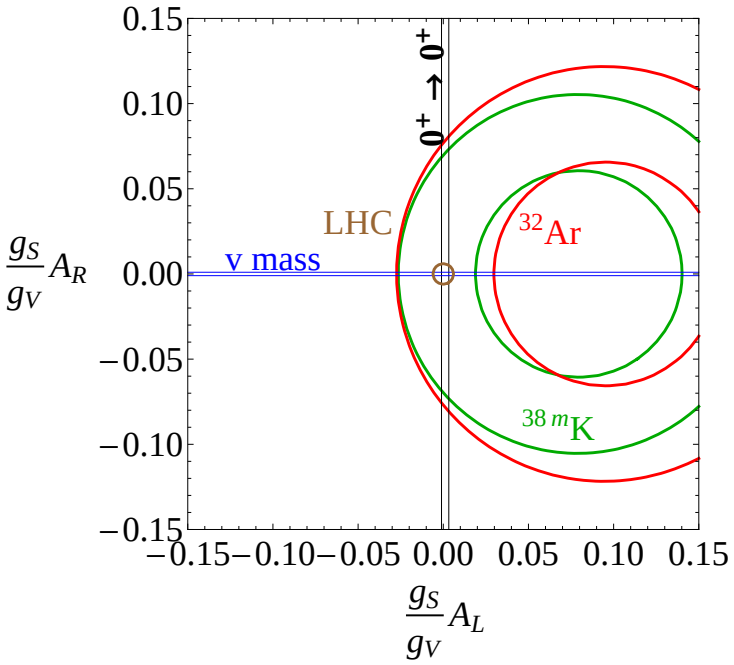

Figure 2.6: Scalar bounds from nuclear β decay as in Fig. 2.1 combined with limits derived from the neutrino mass (horizontal lines) and constraints from the LHC experiments (circular bounds).

A measurements influences the obtained bound significantly. The Gamow-Teller part b_{GT} of the Fierz-interference term and V_{ud} can also be constrained in mirror nuclei, in analogy to the superallowed Fermi transitions. However, this also requires the measurement of at least one correlation coefficient. Measurements with this aim are undertaken [105].

In Gamow-Teller transitions, measurements of the Fierz-interference term b_{GT} allow for bounds on the left-handed tensor terms. In Seattle, a ^{6}He factory has been set up to study this term. The lifetime of ^{6}He was already measured with high precision [106], but the shell-model calculations are not sufficiently accurate as yet to search for tensor interactions. One straightforward, but not so simple, approach is to measure the decay spectrum precisely. This would give access to b_{GT}. These measurements would also have to consider contributions from the SM weak-magnetism [cf. Eq. (2.4)]. Measurements of b_{GT} from electron-antineutrino correlation $\tilde{a}_{\beta\nu}$ and the spectrum are both ongoing and being set up [107, 108, 109, 110, 111, 112]. If these measurements reach $b < 10^{-3}$, they would allow for a strong limit on α_L. Such a precision is necessary to compete with the projected bounds from the 14 TeV run of the LHC. In neutron decay, many efforts are undertaken to improve the measurements of $a_{\beta\nu}$ and A [113, 114, 115, 116, 117, 118]. For comparison, limits on the Fierz terms from neutron decay alone are found in Refs. [13, 86], including limits derived from the electron energy dependence of the β-asymmetry $A_{\text{exp}}(E)$ alone.

Right-handed interactions, which imply the existence of a light right-handed neutrino, do not interfere with the SM interactions and can therefore only be measured directly, i.e. via quadratic terms. This makes it difficult to reach the sensitivity obtained for left-

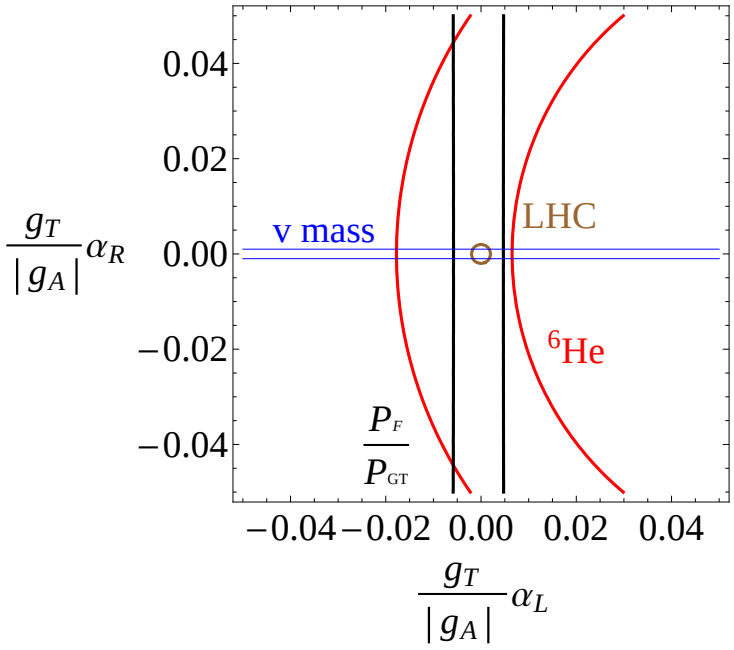

Figure 2.7: Tensor bounds from nuclear β decay as in Fig. 2.2 combined with limits derived from the neutrino mass (horizontal lines) and constraints from the LHC experiments (circular bounds).

handed couplings. In β decay, the right-handed tensor coupling α_R can be constrained by measuring the β-ν correlation, $\tilde{a}_{\beta\nu}$. The best measurement in pure Gamow-Teller decays of $a_{\beta\nu}$ stems from the measurement in ^{6}He [66]. Many efforts are undertaken to improve this limit in ^{6}He [109, 112, 119]. A dedicated effort to limit right-handed tensor couplings is ongoing in ^{8}Li, for which the daughter nucleus ^{8}Be breaks up into two α particles, $^8\mathrm{Li} \to e^- + \bar{\nu} + 2\alpha$. The a_{GT} coefficient can be measured by measuring the β-α correlation, and by taking advantage of the increased sensitivity due to the population of a 2^+ state in ^{8}Be. After putting the Fierz term $b = 0$, such that only right-handed interactions are constrained [120], one finds

$$\frac{g_T}{|g_A|}|\alpha_R| < 8 \times 10^{-2} \ . \tag{2.55}$$

The bound reaches the precision of the combined fits, but when considering the LHC or neutrino bounds the experiment would have to improve by more than 3 orders of magnitude to compete (see Table 2.5).

When comparing tensor and scalar bounds from different fields, the form factors g_S and g_T are important. Lattice QCD calculations have made great progress and will continue to do so in the next period. The lattice prediction of g_A will hopefully reach the experimental precision soon, which would allow for a cross-check between the experimental value and the theoretical lattice value.

Besides scalar and tensor searches, we also discussed searches for $V + A$ and pseudoscalar interactions. Pseudoscalar interactions are less suppressed than previously thought, due to the large value of g_P. However, strong bounds exist from radiative pion decay,

Parameter	Bound	Constraint at 90% C.L.
b_{GT}	10^{-3}	$\alpha_L < 3 \times 10^{-4}$
b_F	10^{-3}	$A_L < 5 \times 10^{-4}$
a_{GT}	10^{-4} (5×10^{-6})	$\alpha_R < 6 \times 10^{-3}$ $(\alpha_R < 10^{-3})$
a_F	8×10^{-6} (2×10^{-6})	$A_R < 2 \times 10^{-3}$ $(A_R < 10^{-3})$

Table 2.5: Required experimental precision on β-decay parameters to remain competitive with the LHC bounds; cf. Ref. [95]. Only the Fermi (F) and Gamow-Teller (GT) parts of the Fierz-interference term b and the β-ν correlation a are listed. The third column gives the corresponding limit on scalar couplings A_L and A_R and tensor couplings α_L and α_R. The Fierz term is the leading term in most β-correlation experiments (Sec. 2.4.1). The indicated bounds for b assumes that future LHC data lead to bounds indicated in the last column. The a parameter is the most direct way to obtain a bound on right-handed couplings, which should be the motivation to measure a. Here the current bounds of the LHC are assumed, while the values in parentheses are the required accuracies when the bounds derived from the limit of the neutrino mass are considered (Table 2.4).

and pseudoscalar interactions can still be neglected in the upcoming β-decay experiments. Strong constraints on $V + A$ currents are extracted from CKM unitarity tests, to which β-decay experiments contribute by providing the most accurate value of V_{ud}. Besides this, measurements of correlation coefficients can be used to constrain parameters of (manifest) left-right symmetric models. For these specific models, strong limits from the LHC experiments and the neutral-kaon mass difference exist.

2.5 Limits on time-reversal violation

So far we have considered only the real parts of the exotic couplings. In this section we focus on their imaginary parts. A nonzero measurement of an imaginary coupling would imply that time-reversal (T) symmetry and, by the CPT-theorem, CP symmetry is violated[9]. Because of the matter-antimatter asymmetry of the universe, new sources of CP violation are expected [121]. Many models of BSM physics predict such additional sources of CP violation; see, e.g., Refs. [122, 123, 124]. This makes T or CP violation one of the main portals to search for new physics. These searches range from experiments at the LHC to atomic-physics experiments. As such the observables can be quite diverse. With advances in theory, in particular via EFT methods, relations between the different observables have become more clear (cf. Sec. 2.4.2 and 2.4.3).

In this section we focus on the connection between T-violating observables in β decay and the bounds on EDMs. The P- and T-odd EDM measurements are a powerful probe

[9]In any Lorentz-symmetric local field theory, CP violation is equivalent to T violation, according to the CPT theorem. For CPT-violation; see Sec. 2.6.

of CP violation beyond the SM [125]. High-precision EDM searches have been made for the neutron, paramagnetic and diamagnetic atoms, and molecules. The EDM is a static observable, and, therefore, allows for very precise atomic-physics experiments. It is also a background-free observable, because the electroweak SM contributions to the EDM are strongly suppressed. Therefore, EDM experiments give strong limits on new T-violating physics. BSM physics contributions to the EDM can be parametrized by dimension-6 operators [126, 127, 128, 129, 130]. At low energy this leads to a relation between the T-violating correlations in β decay and EDMs.

Many correlation coefficients in β decay depend on the square of the underlying coupling constants. As such they depend only on the imaginary couplings squared, which are therefore difficult to access. A more direct way to probe imaginary couplings is to consider the T-odd triple correlations $\vec{J}\cdot(\vec{p}_e\times\vec{p}_\nu)$ and $\vec{\sigma}_e\cdot(\vec{J}\times\vec{p}_e)$ multiplied by the D [Eq. (2.17)] and R [Eq. (2.18)] coefficients, respectively. The first is P even and T odd, while the latter is P and T odd. They probe left-handed imaginary couplings, which are absent in the SM.

Since the interactions contributing to D, R, and EDMs are generated by the same operators, a limit on the EDM also limits the D and R coefficients. We consider these relations and discuss the relative precision of the two types of experiments.

2.5.1 Limits on triple-correlation coefficients in β decay

A finite D coefficient arises from the interference between the imaginary parts of the left-handed vector couplings and is proportional to Im a_{LR}. The R coefficient arises from the interference between the imaginary parts of scalar or tensor couplings and SM couplings, making this coefficient sensitive to both Im A_L and Im α_{LL}.

The SM contributes to both the R and D coefficients through electromagnetic final-state interactions (FSI) and through SM CP violation. The FSI are only motion-reversal odd, i.e., the initial and final state are no longer interchangeable, due to radiative corrections. In this way, FSI mimic time-reversal violation, but in fact are T even. We denote their contributions by R_f and D_f, and write $D = D_t + D_f$ and $R = R_t + R_f$ [131], where D_t and R_t are the true T-violating contributions. The contributions from FSI are comparable to the current experimental precision and depend on the momentum of the β particle. We will discuss their values for specific isotopes later. True T violation in the SM arises from the CP-violating phase of the CKM matrix and the QCD θ term. These sources contribute only at the level of $\mathcal{O}(10^{-12})$ [41], much below the current experimental precision.

D coefficient

To first order in exotic couplings, the D_t coefficient can be expressed as [132]

$$D_t = a_D \text{Im } a_{LR} \ , \tag{2.56}$$

from Eq. (2.122), with

$$a_D = \frac{4\delta_{J'J}\sqrt{\frac{J}{J+1}}\rho}{1+\rho^2} \ . \tag{2.57}$$

The D coefficient can be accessed only in mixed transitions and has been measured in both neutron and ^{19}Ne decay, which have $a_D = 0.87$ and $a_D = -1.03$, respectively. For ^{19}Ne the best measurement is $D = 1(6) \times 10^{-4}$ [133], and from neutron decay $D = -0.94(2.10) \times 10^{-4}$ [134, 135].

The value of the FSI depends on the kinematics of the experiment. For ^{19}Ne the FSI have been derived as $D_f = 2.6 \times 10^{-4} p_e/p_e^{\max}$[136], which is of the same order as the experimental precision. For neutron decay the FSI are also calculated in chiral perturbation theory [137]. This derivation reproduces the original result of Ref. [136]. However, Ref. [137] includes higher-order corrections, which are of the order of $\mathcal{O}(10^{-7})$, allowing for an accurate expression for the FSI,

$$D_f = (0.228\frac{p_e^{\max}}{p_e} + 1.083\frac{p_e}{p_e^{\max}}) \times 10^{-5} - 5.88\frac{p_e^{\max}}{p_e} \times 10^{-8} \ , \tag{2.58}$$

where the first two terms are the original terms [136], and the last term represents the higher-order corrections. Equation (2.58) is accurate to better than 1%. For the current best neutron experiment the FSI are estimated at $D_f \simeq 1.2 \times 10^{-5}$ [134]. The uncertainty in D_f stems from the uncertainty of the β momentum in the experiment. The T-violating part of the neutron D measurement gives at 90% C.L.

$$|D_t| < 4 \times 10^{-4} \ , \tag{2.59}$$

and with $a_D = 0.87$,

$$|\text{Im } a_{LR}| < 4 \times 10^{-4} \ . \tag{2.60}$$

Given the current experimental precision, it is clear that the FSI become increasingly more important. In this respect, neutron experiments are favored over nuclei, because the FSI can be calculated with a higher precision. Eventually the accuracy to which the FSI are known will limit measurements of true T violation.

R coefficient

Neglecting quadratic non-SM couplings, the R_t coefficient is given by [132]

$$R_t = \frac{(a_D \mp b_D)}{|g_A|} g_T \text{Im } \alpha_L - \frac{a_D}{2g_V} g_S \text{Im } A_L \ , \tag{2.61}$$

from Eq. (2.123), where the upper (lower) sign is for $\beta^-(\beta^+)$ decay, a_D is given in Eq. (2.57), and

$$b_D = \frac{4\lambda_{J'J}\rho^2}{1+\rho^2} \ , \tag{2.62}$$

with $\lambda_{J'J}$ as given in Appendix 2.A. The R coefficient can be measured in both mixed or pure Gamow-Teller transitions, where the latter limits Im α_L. The leading contributions to the FSI are given by the Coulomb corrections [40],

$$R_f = \frac{Z\alpha m_e}{2p_e}(\mp a_D + b_D) \ . \tag{2.63}$$

The R coefficient has been measured in the pure Gamow-Teller decay of ^{8}Li, where $a_D = 0$ and $b_D = 4/3$. The FSI give $R_f \simeq 7 \times 10^{-4}$, leading to $R_t = (0.9 \pm 2.2) \times 10^{-3}$ [138]. This constrains at 90% C.L.

$$g_T|\text{Im } \alpha_L| < 3 \times 10^{-3} \ . \tag{2.64}$$

The best measurement of R in a mixed decay has been obtained for neutron decay, for which $a_D = 0.87$ and $b_D = 2.2$. Ref. [139] found $R = (4 \pm 12 \pm 5) \times 10^{-3}$. The FSI are calculated with Eq. (2.63). By using the energy distribution seen by the experimental setup one obtains $R_f \simeq 6 \times 10^{-4}$ [139]. The error in R_f is less than 10%. R_f can be neglected given the current experimental precision. At 90% C.L.

$$-1.1 g_T \text{Im } \alpha_L - 0.44 g_S \text{Im } A_L < 2.4 \times 10^{-2} \ . \tag{2.65}$$

With the constraint given in Eq. (2.64) one finds at 90% C.L.

$$g_S|\text{Im } A_L| < 6 \times 10^{-2} \ \ . \tag{2.66}$$

Alternative correlations

The measurement of the D coefficient requires the detection of the recoiling nucleus instead of detecting the neutrino. This imposes strong experimental constraints on any measurement scheme. Current schemes consider atomic trapping in a magneto-optical trap, which has led to the best value for the β-ν correlation a. Measuring D requires a modification of this trap technique, to allow for a polarized sample. It will be extremely challenging to achieve high statistical precision and systematical accuracy with this technique. An alternative lies in the β-γ correlations of polarized nuclei [140, 141], where the photon with momentum $\vec{k}$ is emitted from the state populated by the β decay. In this way one measures the correlation proportional to

$$E\vec{J} \cdot (\vec{p}_e \times \vec{k})(\vec{J} \cdot \vec{k}) \ , \tag{2.67}$$

when the emission is due to an $E1$ transition. The correlation coefficient $E \propto \text{Im } a_{LR}$ is nonzero only for mixed decays. ^{36}K has been identified as a promising candidate for such a measurement [142], since this isotope allows for the comparison between a mixed and a Gamow-Teller transition. The latter is insensitive to T violation and can be used to test the experimental setup and reduce systematic errors. Secondary beams of high intensity can be produced, stopped, and polarized in a buffer gas allowing one to measure β-γ correlations [38] with high precision. Correlations alternative to measuring R are also possible [the L and M coefficients [132, 143]] but, similar to R, will always require one to measure the polarization of the β particle, which is an inefficient process.

In radiative β decay, it is possible to have triple-correlation coefficients without nuclear or electron spin [144, 145, 146], such as

$$K\vec{k} \cdot (\vec{p}_\nu \times \vec{p}_e) \ . \tag{2.68}$$

This coefficient has not been measured, but Ref. [147] shows that EDMs provide extremely strong constraints on the coefficient K.

EDM	e cm (90% C.L.)	Reference	Connection to β decay
n	2.9×10^{-26}	[150]	D
^{199}Hg	2.6×10^{-29}	[151]	D, R
^{205}Tl	0.9×10^{-24}	[152]	R
YbF	$\lvert d_e \rvert < 10.5 \times 10^{-28}$	[153]	R
ThO	$\lvert d_e \rvert < 8.7 \times 10^{-29}$	[154]	R

Table 2.6: The current best EDM limits of the neutron, diamagnetic Hg, paramagnetic Tl, and molecular YbF and ThO. The neutron EDM and Hg can be connected to the D coefficient (and E coefficient). Other EDM measurements, except the neutron, can be connected to the R coefficient. The limit from molecular YbF and ThO are expressed as a constraint on the electron EDM d_e.

2.5.2 EDM limits

Limits exist for the neutron EDM, the electron EDM, and several atomic EDMs. The best current bounds are listed in Table 2.6, where the limits from molecular YbF and ThO are expressed as a limit on the electron EDM d_e. The last column of Table 2.6 indicates if a connection to the triple-correlation coefficients D and R exists [148, 149].

Limits on D from EDM limits

Any new vector interaction that contributes to Im a_{LR} (and thus to D_t) also contributes to nuclear EDMs [148, 131]. This makes it possible to translate bounds on the EDMs of the neutron and diamagnetic atoms into bounds on Im a_{LR}. The D coefficient is P even and T odd, while the EDM is both P and T odd. Nevertheless, loop corrections, containing the W boson, allow for a relation between these observables.

The relevant CP-odd dimension-6 operator is [148]

$$\mathcal{L}^{(\text{eff})} = \frac{c}{\Lambda^2} \bar{u}_R \gamma^\mu d_R \, \tilde{\varphi}^\dagger i D_\mu \varphi + \text{h.c.} \tag{2.69}$$

where c is a complex coefficient, Λ is the scale of new physics, D_μ is the covariant derivative, and φ is the Higgs doublet with $\tilde{\varphi}^I = \epsilon^{IJ} \varphi^{J*}$, where ϵ^{IJ} is the antisymmetric tensor. Figure 2.8 shows the energy evolution of this operator. First, electroweak symmetry breaking generates the coupling of the W boson to right-handed quarks,

$$\mathcal{L}^{(\text{eff})} = \frac{g v^2}{2\sqrt{2}\Lambda^2} (c \, \bar{u}_R \gamma^\mu d_R W_\mu^+ + c^* \bar{d}_R \gamma^\mu u_R W_\mu^-) \, , \tag{2.70}$$

where φ acquired its vacuum-expectation value $v/\sqrt{2}$ and g is the $SU(2)_L$ coupling constant. The W boson can couple to a lepton current or a quark current. At lower energy,

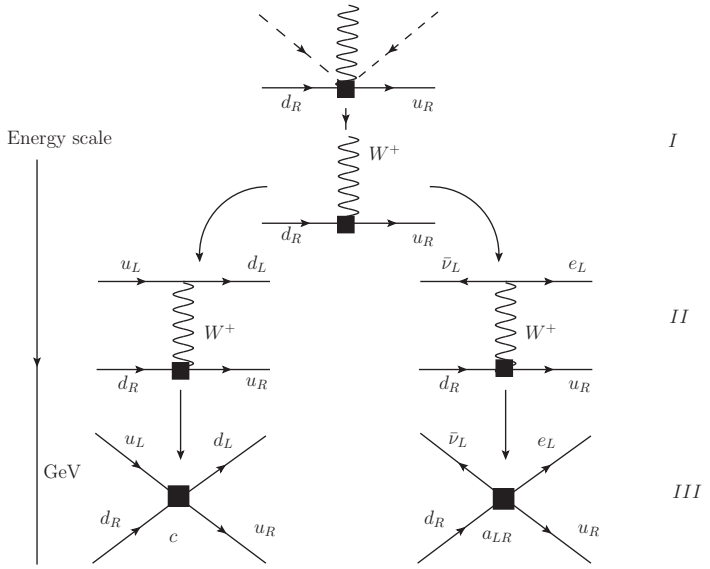

Figure 2.8: Generation of the four-fermion operators that contribute to the EDM (left) and β decay (right). The boxes denote the four-fermion couplings c and a_{LR}, respectively. The coupling of the W boson to the right-handed quarks is generated by the dimension-6 operator in Eq. (2.69).

the W boson is integrated out. This generates a P- and T-odd four-quark coupling and the lepton-quark coupling a_{LR} in β decay. The effective Lagrangian is

$$\mathcal{L}^{(\text{eff})} = -\frac{c}{\Lambda^2}\left(\bar{u}_R\gamma^\mu d_R \bar{e}_L\gamma_\mu \nu_{eL} + V_{ud}\bar{u}_R\gamma^\mu d_R \bar{d}_L\gamma_\mu u_L\right) + \text{h.c.}\ , \tag{2.71}$$

which shows that the two couplings c and a_{LR} have a common origin. They are related by

$$\text{Im}\ a_{LR} = \frac{\text{Im}\ c}{2\sqrt{2}G_F\Lambda^2}\ . \tag{2.72}$$

When evolving to the QCD scale, the second term in Eq. (2.71) is affected by QCD renormalization. However, this has only a small numerical effect [155], which can be neglected given the uncertainties coming from the calculation of the neutron EDM.

Bounds on Im c thus lead to an upper limit on Im a_{LR}. The dependence of the EDM on Im c involves theoretical calculations at different energy scales. Especially for diamagnetic atoms such as ^{199}Hg, differences in nuclear calculations lead to a large uncertainty in the interpretation of the bounds on atomic EDMs. Therefore, we do not consider bounds from ^{199}Hg. No such problem occurs for the neutron, and the link between the neutron EDM and Im c is [129, 156]

$$d_n = -1\times 10^{-20}\frac{\text{Im}\ c}{2\sqrt{2}G_F\Lambda^2} e\ \text{cm}\ . \tag{2.73}$$

This result differs by an order of magnitude from the result used by Ref. [148], which was obtained using Refs. [157, 71]. In Refs. [129, 156] it was pointed out that, due to the

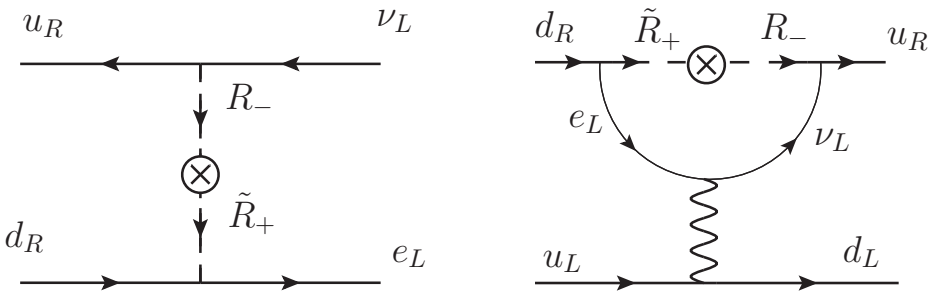

(a) Tree-level contribution to β decay (b) Loop contribution to the neutron EDM

Figure 2.9: Example of scalar LQ exchange that contributes to (a) β decay at tree level, and to (b) the neutron EDM via an electroweak loop. The scalar LQ are denoted by R_- and $\tilde{R}_+$, where $\pm$ refers to the weak isospin component. After Ref. [148].

use of a relativistic meson-nucleon field theory, Refs. [157, 71] overestimated the neutron EDM by an order of magnitude.

The current bound on the neutron EDM $|d_n| < 2.9 \times 10^{-26}\ e$ cm [150] and Eq. (2.73) gives at 90% C.L.

$$|\text{Im } a_{LR}| < 3 \times 10^{-6} \ . \tag{2.74}$$

This bound is at least 2 orders of magnitude below the bound obtained from β decay. Improving this bound in β decay requires a measurement of $D_t < 10^{-6}$, which is an order of magnitude below the contribution of the FSI.

The result above is obtained in a model-independent EFT approach, by introducing dimension-6 operators. The constraints apply to left-right symmetric models, exotic fermion models, and the R-parity violating minimal supersymmetric Standard Model (MSSM) [148]. Evasion of the bounds in Eq. (2.74) is possible only in either a strongly fine-tuned model or in a model in which the dimension-6 operators do not exist or do not contribute to either EDMs or β decay. An example of the latter is leptoquarks (LQs). LQs are particles with both baryon and lepton numbers, which can be either vector or scalar particles depending on their spin. These were previously considered "EDM safe," but in fact they are not [148]. LQs can contribute to β decay at tree level, for example, via the exchange of scalar LQs as depicted in Fig. 2.9a. Leptoquarks also contribute to EDMs, but only via W exchange [Fig. 2.9b]. These loop contributions are not suppressed by the light-quark masses $m_{u,d}^2$ [148], as was previously argued [24]. Therefore, the constraints from EDMs in the LQ scenario are much more stringent than previously thought.

Estimates of the limit on D_t in this scenario depend on the LQ mass and on whether light right-handed neutrinos exist. Assuming the existence of light right-handed neutrino [148],

$$\text{Im } a_{LR} = D_t/a_D < 3 \times 10^{-4} \left(\frac{300 \text{ GeV}}{m_{LQ}} \right)^2 \ , \tag{2.75}$$

while without them

$$\text{Im } a_{LR} = D_t/a_D < 7 \times 10^{-5} \left(\frac{300 \text{ GeV}}{m_{LQ}} \right)^2 \ . \tag{2.76}$$

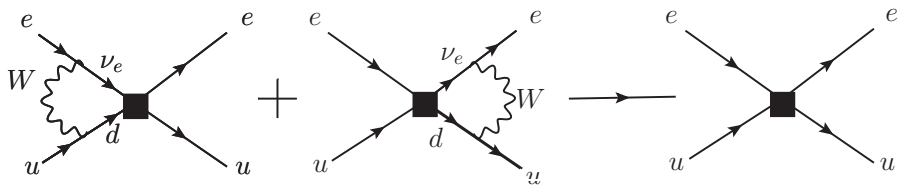

Figure 2.10: Contribution of β-decay coupling to the effective P- and T-odd electron-quark coupling through the exchange of the W boson.

Taking conservatively $m_{LQ} = 300$ GeV (as in Ref. [148]), gives, assuming the existence of light right-handed neutrinos, $D_t < 3 \times 10^{-4}$. This limit is of the same order as the current β-decay bounds. Nevertheless, improving the current β decay limit seems a difficult task, since there are many experiments ongoing or planned that aim to improve the bounds on the neutron EDM [158, 159, 160, 161, 162, 163]. In addition, strong bounds on the scalar LQ mass exist from the ATLAS and CMS experiments at the LHC. The bounds on their masses range from 607 to 830 GeV, depending on the assumed LQ branching ratio [19], which suggests much stronger bounds on D_t.

Limits on R from EDM limits

The R coefficient and the EDM are both P and T odd. EDM measurements in atoms and molecules limit both the electron EDM and BSM scalar and tensor electron-nucleon interactions. Reference [149] showed the relation between these electron-nucleon interactions and the electron-quark interaction of β decay. The scalar and tensor electron-nucleon interactions are defined by

$$\mathcal{L} = \sum_N \frac{G_f}{\sqrt{2}} \left[C_S \bar{N} N \bar{e} i\gamma_5 e + C_T \bar{N} \sigma_{\mu\nu} N \bar{e} i\gamma_5 \sigma^{\mu\nu} e \right] \ , \tag{2.77}$$

where C_S (C_T) is the scalar (tensor) coupling and we have neglected pseudoscalar couplings. The limits on C_S and C_T can be related to both Im A_L and Im α_{LL}, the couplings contributing to the R coefficient [149, 164]

The best current limit on nucleon scalar couplings is due to the EDM limit on molecular ThO, $|C_S| < 5.9 \times 10^{-9}$ (90% C.L.) [154]. The best bound on the nucleon tensor coupling $|C_T| < 1.3 \times 10^{-9}$ (90% C.L.) is derived from the EDM limit on atomic Hg [151, 165]. These couplings must be translated to quark couplings in order to compare them to the β-decay couplings in Eq. (2.11). At the quark level, scalar and tensor couplings in the electron-quark (e-q) interaction are described by [166]

$$\mathcal{L} = \sum_{q=u,d} \frac{G_F}{\sqrt{2}} \left[k_{Sq} (\bar{e} i\gamma_5 e \bar{q} q) + k_{Tq} (\bar{e} i\gamma_5 \sigma_{\mu\nu} e \bar{q} \sigma^{\mu\nu} q) \right] \ , \tag{2.78}$$

where $k_{Sq}(k_{Tq})$ is the scalar (tensor) coupling in the e-q interaction. The nucleon couplings can be translated into quark couplings [166, 131], which are of the same order of magnitude. Conservatively, we find that the k_{Sq} and k_{Tq} couplings are $< 10^{-8}$ (90% C.L.)

	Im a_{LR}	Im A_L	Im α_L
β decay	4×10^{-4}	6×10^{-2}	3×10^{-3}
EDM	3×10^{-6} (3×10^{-4})	10^{-5}	10^{-6}

Table 2.7: Comparison between β-decay limits on imaginary couplings and constraints from EDMs. The bound in parentheses is derived in a model with leptoquarks and right-handed neutrinos. For the β-decay coefficients we use $g_S = 1.02(11)$ [53] and $g_T = 1.047(61)$ [52] and the R-fit mentioned in Sec. 2.4.2. Constraints are at 90% C.L.

Figure 2.10 shows that the electroweak corrections to the exotic β-decay couplings contribute to the EDM e-u couplings, k_{Su} and k_{Sd}. The effective P- and T-odd e-u interactions in Fig. 2.10 are estimated as [149]

$$\frac{-G_F}{\sqrt{2}}\frac{\alpha}{4\pi}\ln\left(\frac{\mu^2}{M_W^2}\right) V_{ud}\,\mathrm{Im}\,(2A_L + 24\alpha_L)\left[\bar{e}i\gamma_5 e\bar{u}u + \tfrac{1}{2}\bar{e}i\gamma_5\sigma_{\mu\nu}e\bar{u}\sigma^{\mu\nu}u\right] , \tag{2.79}$$

where μ is the renormalization scale. Limits on the scalar electron-nucleon interaction C_S thus limit both A_L and α_L. The effective e-d interaction contains only A_L and gives similar constraints.

Comparing Eq. (2.78) and (2.79) we arrive at an expression for k_{Su} and k_{Tu}. By using $k_{Su} < 10^{-8}$ (90% C.L.) and the conservative assumption that $\ln(\mu^2/m_W^2) = 1$ [149], we estimate that at 90 % C.L.

$$|\mathrm{Im}\ A_L| < 10^{-5} , \tag{2.80a}$$
$$|\mathrm{Im}\ \alpha_L| < 10^{-6} . \tag{2.80b}$$

Both bounds are at least 2 orders of magnitude better than those obtained from the R coefficient in β decay.

2.5.3 Conclusion

Table 2.7 summarizes the limits on imaginary couplings. Bounds obtained from EDMs are several orders of magnitude better than current bounds from T-violating β-decay coefficients. The many ongoing efforts in the EDM field will strengthen the EDM bounds even further.

The D coefficient should be measured with a precision of 10^{-6} to improve the current EDM limits. Such a measurement is below the FSI interactions, and would require precise knowledge of the FSI for the used isotope. Measurements of the D coefficient are considered as part of a larger effort to measure 11 coefficients (R) in neutron decay [167]. Measurements of D are also considered in nuclear decays [168, 169]. The E coefficient in Eq. (2.67) depends on the same BSM coupling as the D coefficient and is thus subject to the same EDM constraints.

It might be possible that the connection between EDMs and β decay is diminished in a specific new-physics model, when such a model is strongly fine-tuned. For the D

coefficient examples are leptoquark models. Conservatively, this model relaxes the EDM constraint by maximally 2 orders of magnitude to $|D_t| < 3 \times 10^{-4}$ [148]. This is of the same order as current β-decay limits. Direct bounds on leptoquarks from the LHC experiments already suggest a stronger bound. Besides that, new bounds on the neutron EDM are also expected before any new D measurement could realistically be done. This would further improve the bounds in Table 2.7.

Improving the current bounds on Im α_L requires a measurement of $R_t < 10^{-6}$, which is an improvement of the current result by more than 3 orders of magnitude. An R measurement in ^{8}Li is ongoing at the Mott polarimeter for T-violation (MTV) [170]. Specific models may again weaken the connection between β decay and EDMs. Such models would have to be strongly fine-tuned. For example, in R-parity violating SUSY [131] such a cancellation would have to occur over 3 orders of magnitude. Such a severe cancellation is highly unnatural. Besides EDM limits there are also strong limits from the ratio $R_\pi = \Gamma(\pi \to e\nu)/\Gamma(\pi \to \mu\nu)$, which give Im $A_L < 4 \times 10^{-4}$ [171, 131].

Our EFT approach applies only when new physics can be parametrized by the heavy scale of new physics. If new particles are very light, the EFT approach does not apply anymore. However, the absence of experimental evidence for such light degrees of freedom supports the validity of the EFT approach. We therefore conclude that new measurements of the D and R coefficients should take the EDM bounds into account and stress that the bounds can be evaded only in specific and strongly fine-tuned models.

2.6 Lorentz violation

We now review the new field of searches for the violation of Lorentz symmetry in the weak interaction. Recently, it was found that β decay offers unique possibilities to test Lorentz and/or CPT-invariance in the weak interaction, in both the gauge and neutrino sectors. We discuss these two sectors separately.

2.6.1 Gauge sector

In the gauge sector, Lorentz violation can be studied in a general theoretical framework, developed to study allowed and forbidden β decay and orbital electron capture [17, 21, 172]. This framework considers a broad class of Lorentz-violating effects on the W boson, by adding a general tensor $\chi^{\mu\nu}$ to the Minkowski metric. At low energies, this modifies the W-boson propagator to

$$\langle W^{\mu+} W^{\nu-} \rangle = \frac{-i(g^{\mu\nu} + \chi^{\mu\nu})}{M_W^2} \ , \tag{2.81}$$

where $g^{\mu\nu}$ is the Minkowski metric and M_W is the W-boson mass. Vertex corrections are described by

$$-i\Gamma = -ig(g^{\mu\nu} + \chi^{\mu\nu}) \ . \tag{2.82}$$

However, such vertex modifications also require the modification of the electron and neutrino spinors [17]. We restrict ourselves to propagator corrections, for which Hermiticity

of the Lagrangian implies that $\chi^*_{\mu\nu}(p) = \chi_{\nu\mu}(-p)$. In terms of the SME discussed in Sec. 2.2.2, one finds, at lowest order,

$$\chi^{\mu\nu} = -k^{\mu\nu}_{\phi\phi} - \tfrac{i}{2g}k^{\mu\nu}_{\phi W} + 2k^{\rho\mu\sigma\nu}_W \frac{q_\rho q_\sigma}{M_W^2} \ , \tag{2.83}$$

where q is the momentum of the W boson and g is the $SU(2)$ coupling constant.

Bounds on χ have been derived from allowed [173, 38, 174] and forbidden β decay [21], pion decay [175, 176], muon decay [177], and nonleptonic kaon decay [178]. Here we discuss allowed and forbidden β decay.

Allowed β decay

For allowed β decay, Ref. [17] derived the Lorentz-violating differential decay rate using the modified W-boson propagator in Eq. (2.81). The complete expression is given in Eq. (2.136). Lorentz violation gives many additional correlations, since the observables (momentum and spin) can now also couple to the tensor χ. In β decay, a variety of correlations can be used to access different (combinations of) χ components. The necessary expressions can be derived by integrating over one or more kinematic variables. Momentum-dependent terms are always suppressed by some power of a heavy mass (M_W in the least-suppressed case), and can therefore be neglected given the current experimental precision. Neglecting momentum-dependent contributions to the propagator, the relation $\chi^*_{\mu\nu}(p) = \chi_{\nu\mu}(-p)$ implies that χ can only be real and symmetric or imaginary and antisymmetric, i.e. $\chi^{0l}_r = \chi^{l0}_r$, $\chi^{0l}_i = -\chi^{l0}_i$, $\chi^{\mu\mu}_i = 0$, $\chi^{lk}_r = \chi^{kl}_r$ and $\chi^{lk}_i = -\chi^{kl}_i$. The subscripts r and i denote the real and imaginary parts of χ, respectively. This leaves 15 independent CPT-even components of $\chi^{\mu\nu}$ that need to be measured.

With this simplification and in the absence of tensor polarizations, the decay rate is [17, 179]

$$\begin{aligned}
dW \ = \ & \frac{F(\pm Z, E_e)}{(2\pi)^5}|\vec{p}_e|E_e(E_e - E_0)^2 dE_e d\Omega_e d\Omega_\nu \bar{\xi} \\
& \times \Bigg\{ 1 + (2a - c')\chi^{00}_r + \left(-(2a - c')\chi^{0l}_r + 2\breve{g}\tilde{\chi}^l_i\right)\frac{p^l_e}{E_e} \\
& + \frac{p^j_\nu p^l_e}{E_e E_\nu}\left[(a + c' + 2\breve{a}\chi^{00}_r)\delta_{jl} - 4\breve{g}\chi^{jl}_r\right] - (2a - c')\chi^{0s}_i \frac{(\vec{p}_\nu \times \vec{p}_e)^s}{E_e E_\nu} \\
& + \frac{\langle J^k\rangle}{J}\left(-2\breve{L}\tilde{\chi}^k_i + \frac{p^l_e}{E_e}\left[(A + B\chi^{00}_r)\delta_{kl} - B\chi^{kl}_r\right]\right) + A\chi^{0s}_i \frac{(\vec{p}_e \times \langle\vec{J}\rangle)^s}{JE_e} \\
& + \frac{p^j_\nu}{E_\nu}\left((-2a + c')\chi^{0j}_r - 2\breve{g}\tilde{\chi}^j_i\right) + \frac{\langle J^k\rangle p^j_\nu}{JE_\nu}\left[(B + A\chi^{00}_r)\delta_{kj} - A\chi^{kj}_r\right] \\
& - B\chi^{0s}_i \frac{(\vec{p}_\nu \times \langle\vec{J}\rangle)^s}{JE_\nu} \Bigg\} \ ,
\end{aligned} \tag{2.84}$$

where $\langle\vec{J}\rangle$ is the expectation value of the spin of the parent nucleus, $\tilde{\chi}^l = \epsilon^{lmk}\chi^{mk}$, and Latin indices run over spatial directions. The last line of Eq. (2.84) contains only the

neutrino momentum or the neutrino momentum and the nuclear polarization, and can therefore mostly be ignored. In fact, the neutrino correlations give access to a similar combination of χ components as the electron correlations. The latter are considerably easier to obtain, and we further consider only the electron correlations[10]. The coefficients $\bar{\xi}, a, A$, and B are the standard β-decay coefficients listed in Appendix 2.A and the coefficient c' is a modified c coefficient. The coefficients with a breve ($\breve{}$) multiply Lorentz-violating coefficients. They are given by

$$\begin{aligned} c' &= \frac{\rho^2}{1+\rho^2}\bar{\Lambda}_{J'J} \ , \\ \breve{g} &= \frac{\frac{1}{3}\rho^2}{1+\rho^2} + \tfrac{1}{2}c' \ , \\ \breve{L} &= \pm\frac{\frac{1}{2}\lambda_{J'J}\rho^2}{1+\rho^2} \ , \\ \breve{a} &= \frac{1+\frac{1}{3}\rho^2}{1+\rho^2} + \tfrac{1}{2}c' \ , \end{aligned} \tag{2.85}$$

where the upper(lower) sign refers to $\beta^{\mp}$ decay, and $\lambda_{J'J}$ and $\bar{\Lambda}_{J'J} = \Lambda_{J'J}\frac{\langle(\vec{J}\cdot\vec{j})^2\rangle - \frac{1}{3}J(J+1)}{J(2J-1)}$ are the standard β-decay coefficients given in Eqs. (2.113) and (2.114), respectively. The coefficient c' vanishes for nonoriented nuclei and for nuclei with $J' = J = 1/2$.

The effect of Lorentz violation in β decay can already be studied by measuring the dependence of the decay rate as a function of the direction of the emitted β particles. The modified Fermi decay rate integrated over neutrino energy and direction and summed over electron spin is

$$dW_F = dW^0\left(1 + 2\chi_r^{00} - 2\chi_r^{0l}\frac{p_e^l}{E_e}\right) \ , \tag{2.86}$$

while for Gamow-Teller transitions of randomly oriented nuclei

$$dW_{GT} = dW^0\left(1 - \frac{2}{3}\chi_r^{00} + \frac{2}{3}(\chi_r^{l0} + \tilde{\chi}_i^l)\frac{p_e^l}{E_e}\right) \ , \tag{2.87}$$

where

$$dW^0 = \frac{1}{8\pi^4}p_e E_e (E_0 - E_e)^2 F(\pm Z, E_e) dE_e \, d\Omega_e \bar{\xi} \ . \tag{2.88}$$

The component $\tilde{\chi}_i$ can also be accessed by measuring the Gamow-Teller decays of polarized nuclei as a function of the spin direction,

$$dW_{GT} = dW^0\left(1 - \frac{2}{3}\chi_r^{00} \mp \lambda_{J'J}\tilde{\chi}^l\frac{\langle J^l\rangle}{J}\right) \ . \tag{2.89}$$

As an example of a mixed decay, one has for the neutron $a = -0.11, A = -0.12, B = 0.98$,

[10] In electron capture, the neutrino correlations play an important role [172] (Sec. 4.2).

and $\breve{g} = \breve{L} = \lambda^2/(1+3\lambda^2) = 0.27$. Integrated over the neutrino direction[11]

$$\begin{aligned} dW &= dW^0 \Bigg\{ 1 - 0.21\chi_r^{00} + (0.21\chi_r^{0l} + 0.55\tilde{\chi}_i^l)\frac{p_e^l}{E_e} \\ &\quad + \frac{\langle J^k \rangle}{J}\left[-0.55\tilde{\chi}_i^k + (-0.12 + 0.98\chi_r^{00})\frac{p_e^k}{E_e} - 0.98\chi_r^{lk}\frac{p_e^l}{E_e} \right] \\ &\quad -0.12\chi_i^{0s}\frac{(\vec{p_e} \times \langle \vec{J} \rangle)^s}{JE_e} \Bigg\} \ . \end{aligned} \tag{2.90}$$

Equation (2.84) depends on SM parameters, which are often not known better than at the 1%-0.1% level. This dependence on SM coefficients can be avoided by measuring asymmetries that do not depend on the accuracy of the SM coefficients. The Lorentz-violating part of Eq. (2.86) can, for example, be accessed by measuring the decay asymmetry of a Fermi transition with the β particles measured in opposite directions,

$$A_F = \frac{W_F^+ - W_F^-}{W_F^+ + W_F^-} = -2\beta\chi_r^{0l}\ \hat{p}_e^l \ , \tag{2.91}$$

where $\beta = |\vec{p}_e|/E_e$ and $W_F^\pm$ is the rate of β particles measured in the $\pm\ \hat{p}_e$-direction. Similarly, the decay asymmetry in Gamow-Teller decays is

$$A_{GT} = \frac{W_{GT}^+ - W_{GT}^-}{W_{GT}^+ + W_{GT}^-} = \tfrac{2}{3}\beta(\chi_r^{0l} + \tilde{\chi}_i^l)\hat{p}_e^l \ . \tag{2.92}$$

The coefficient $\tilde{\chi}$ can also be obtained by measuring the spin asymmetry in a pure Gamow-Teller transition

$$A_J = \frac{W_{GT}^\uparrow - W_{GT}^\downarrow}{W_{GT}^\uparrow + W_{GT}^\downarrow} = PA\tilde{\chi}_i^k\ j^k \ , \tag{2.93}$$

where $W_{GT}^{\uparrow(\downarrow)}$ are the integrated decay rates independent of the β direction, but in the inverted polarization direction $\vec{j}$, and P is the degree of nuclear polarization. A is the β asymmetry coefficient (for Gamow-Teller decays $A = \mp\lambda_{J'J}$). The remaining components of χ require more complicated measurements that involve at least two observables. The decay asymmetry between the spin and the β particles can, for example, be measured from

$$A_{J\beta} = \frac{W_L^\uparrow W_R^\downarrow - W_R^\uparrow W_L^\downarrow}{W_L^\uparrow W_R^\downarrow + W_R^\uparrow W_L^\downarrow} = -2P\beta(A\chi_i^{0s}\epsilon^{slk} + B\chi_r^{lk})j^l\hat{p}_e^k \ , \tag{2.94}$$

where $W_{L,R}$ is obtained by measuring the β particles in the opposite $\hat{p}_e$ direction, while the nuclei are polarized in the $\uparrow$ ($\downarrow$) opposite $\vec{j}$ direction. Similarly, χ_i^{0s} can also be obtained by measuring the decay asymmetry between the neutrino and electron in perpendicular directions.

The spatial directions of χ are defined in the laboratory frame and their absolute orientation depends on the orientation of Earth. It is therefore necessary to choose a standard absolute reference frame, for which the Sun-centered inertial reference frame is

[11] This formula corrects Eq. (38) in Ref. [17] (see also Appendix 2.B).

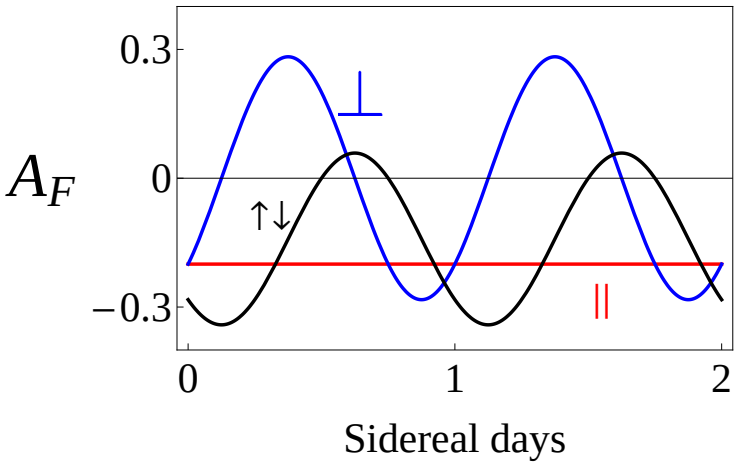

Figure 2.11: Illustration of the oscillation of the asymmetry A_F in Eq. (2.91), for $X_r^{0l} = 0.1$ and $\zeta = 45°$. Three different detection directions of the β particles are depicted. When β particles are detected parallel ($\|$) to the Earth's rotation axis there is no sidereal variation (red line). The top curve (blue line) shows the asymmetry when the β particles are detected in the east-west direction ($\perp$) and the black line shows when they are detected perpendicular to the Earth's surface ($\uparrow\downarrow$). Both show a sidereal variation, the latter with a constant offset.

commonly chosen [37]. The movement of this reference frame can safely be ignored. The transformation of $\chi^{\mu\nu}$ in the laboratory frame to the Sun-centered frame, in which we denote $\chi^{\mu\nu}$ by $X^{\mu\nu}$, is [17]

$$\chi^{\mu\nu} = R^{\mu}{}_{\rho} R^{\nu}{}_{\sigma} X^{\rho\sigma} \ . \tag{2.95}$$

The transformation matrix is

$$R(\zeta, t) = \begin{pmatrix} 1 & 0 & 0 & 0 \\ 0 & \cos\zeta\cos\Omega t & \cos\zeta\sin\Omega t & -\sin\zeta \\ 0 & -\sin\Omega t & \cos\Omega t & 0 \\ 0 & \sin\zeta\cos\Omega t & \sin\zeta\sin\Omega t & \cos\zeta \end{pmatrix} , \tag{2.96}$$

where ζ is the colatitude of the experiment and Ω is Earth's sidereal rotation frequency. In the laboratory frame, $\hat{x}$ points in the north to south direction, $\hat{y}$ points west to east, and $\hat{z}$ is perpendicular to the Earth's surface. The coefficients χ_r^{0l} and $\tilde{\chi}_i^l$ can be transformed to X_r^{0l} and $\tilde{X}_i^l$, respectively. This transformation shows that the asymmetries A_F, A_{GT}, and A_J can oscillate with the rotational frequency of Earth. These sidereal variations of the signal are a unique signature of Lorentz violation and can therefore be separated from other limits on BSM physics. A generic example of how sidereal oscillations can be observed is shown in Fig. 2.11, for $X_r^{0l} = 0.1$. This example also shows that if the β particles are detected parallel ($\|$) to the Earth's rotation axis, the asymmetry will have no sidereal dependence (red curve). The top curve (blue curve) shows the case where the β particles are detected in the east-west ($\perp$)direction. It has no offset because it is measured perpendicular to the Earth's rotation axis. The black line gives the asymmetry

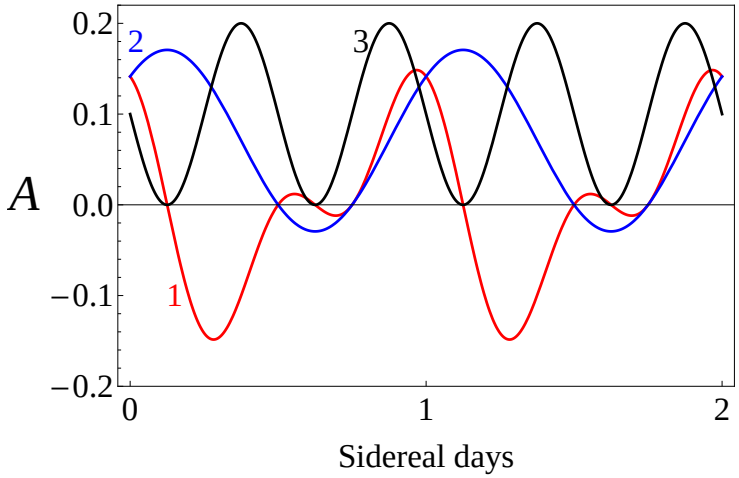

Figure 2.12: Illustration of the possible sidereal variations of tensor Lorentz violation parametrized as $\chi_r^{lk} j^l \hat{p}_e^k$, with $X_r^{\mu\nu} = 0.1$. Line (1) shows the modulations when $\vec{j}$ is in the $\hat{z}$ (up-down) direction and $\hat{p}_e$ in the $\hat{y}$ (east-west) direction. Line (2) is for $\vec{j}$ in the $\hat{z}$ direction and the β particles detected parallel to the Earth's rotation axis. Line (3) shows the modulations when both $\vec{j}$ and $\hat{p}_e$ are in the east-west direction.

for β particles detected in the up-down ($\uparrow\downarrow$) direction perpendicular to the Earth's surface ($\hat{z}$ direction in the labframe). It shows a sidereal oscillation on a constant offset. Detection of the β particles perpendicular to the rotation axis is preferred, since an offset could be the result of systematic errors in the measurement.

Tensor contributions involving χ^{jk} lead to terms that may oscillate with twice the Earth's rotational frequency. Figure 2.12 illustrates three possible scenarios for an asymmetry that depends on $\chi^{lk} j^l \hat{p}_e^k$. Line (1) shows the modulations when the polarization is in the up-down direction, while the β particles are detected in the east-west direction. Line (2) shows the modulations in the same polarization direction, but when the β particles are detected parallel to the Earth's rotation axis. It shows an oscillation with the period of the sidereal rotational frequency on top of a constant offset. Line (3) shows an oscillation with twice the period of the sidereal frequency. It arises when both the polarization and the β particles are detected in the east-west direction.

In allowed β decay, Lorentz violation was for the first time tested in polarized ^{20}Na [38], by measuring the spin asymmetry A_J (Eq. (2.93)). ^{20}Na first decays with a β^+ $2^+ \to 2^+$ Gamow-Teller transition, followed by a γ decay of the daughter nucleus. The parity-odd β decay was used to determine the polarization P by measuring the β asymmetry [38]. The parity-even γ decay was used to measure the lifetime $\tau^{\uparrow(\downarrow)}$ and to determine the γ asymmetry

$$A_\gamma = \frac{\tau^\downarrow - \tau^\uparrow}{\tau^\uparrow + \tau^\downarrow} = P A \vec{\tilde{\chi}}_i \cdot \vec{j} \,, \tag{2.97}$$

where the polarization direction is in the $\vec{j}$ direction. To reduce systematic errors, the polarization direction is preferably in the $\hat{y}$ (east-west) direction. The analysis of the setup in this direction places bounds of the order of $\mathcal{O}(10^{-3})$ [180].

Lorentz violation has also been searched for in polarized neutron decay [174]. Two

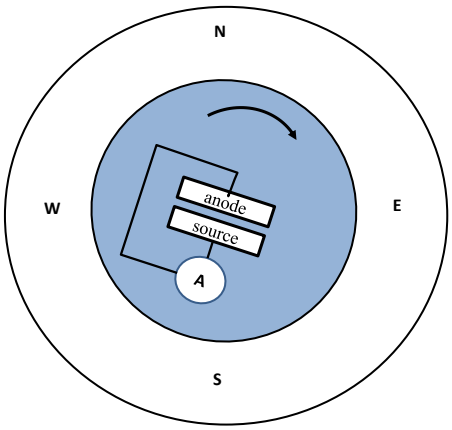

Figure 2.13: Schematic setup of the rotating ^{90}Y experiment [181].

different asymmetries, that depend on the nuclear polarization and the β direction, were measured and are currently being analyzed. The asymmetries depend on combinations of $\vec{\tilde{\chi}}_i$ and $\vec{\chi}_r$ and preliminary bounds are $\mathcal{O}(10^{-2})$ [174]. This setup probably also allows for a measurement of $A_{J\beta}$ defined in Eq. (2.94). Such a measurement would measure the so-far unconstrained coefficients χ_i^{0l}.

Forbidden β decay

"Forbidden" (slow) transitions are suppressed with respect to allowed transitions, because the lepton pair carries away angular momentum. Theoretically, the simplest of these transitions are the unique first-forbidden transitions ($\Delta J = 2$), since they depend on only one nuclear matrix element. Because Lorentz violation includes rotational violation, it also implies the violation of angular-momentum conservation. Forbidden β decays are then more sensitive to rotational invariance violation in the weak interaction. In the 1970s, two experiments were performed with this motivation. Newman and Wiesner searched for anisotropies in the angular distribution of β particles in first-forbidden ^{90}Y decay [181]. Ullman searched for sidereal modulations of the count rates for first-forbidden ^{137}Cs β decay and second-forbidden ^{99}Tc β decay [182]. The strongest bounds were found in the experiment by Newman and Wiesner [181]. In this experiment the β-decay distribution of ^{90}Y from a high-intensity source was measured in a rotating setup. Schematically, the setup is depicted in Fig. 2.13. The rotation of the setup allowed for the determination of three decay asymmetries

$$\delta_{NS} = 2\frac{W_N - W_S}{W_N + W_S} \ , \quad \delta_{EW} = 2\frac{W_E - W_W}{W_E + W_W} \ , \tag{2.98}$$

and

$$\delta_{2\nu} = 2\frac{W_N + W_S - W_E - W_W}{W_N + W_S + W_E + W_W} \ , \tag{2.99}$$

where N, S, E, W are north, south, east, and west and W is the decay rate measured by the β particles in that direction. These asymmetries were fitted with

$$\delta = a_0 + a_1 \sin(\Omega t + \phi_1) + a_2 \sin(2\Omega t + \phi_2) \ , \tag{2.100}$$

to search for a sidereal time dependence and to reduce systematic errors. The extracted bounds on a_0, a_1, and a_2 are $\mathcal{O}(10^{-8})$ [181]. In Ref. [21] this data was reinterpreted, after extending the allowed β-decay framework to include higher-order terms in the multipole expansion, i.e., all possible forbidden decays. The modified W-boson propagator gives an unconventional contraction of the nucleon and lepton currents, such that angular momentum is no longer conserved. In the Lorentz-symmetric case, rotational invariance implies that $\Delta J \leq J_{\text{lep}}$, where ΔJ is the spin change of the nucleus and J_{lep} is the total angular momentum of the leptons. In contrast, when contracting with χ^{0l}, transitions with $\Delta J = J_{\text{lep}} + 1$ are possible, and when contracting with χ^{lk} also $\Delta J = J_{\text{lep}} + 2$ transitions are allowed. It is thus possible to have transitions in which the leptons carry away less angular momentum than in the Lorentz-symmetric case. Because the suppression of the forbidden decays is proportional to the angular momentum of the leptons, the Lorentz-violating terms are enhanced compared to the Lorentz-symmetric case.

For unique first-forbidden transitions [21]

$$\frac{dW}{d\Omega_e dE_e} \propto p_e^2 + p_\nu^2 + p_e^2 \frac{\alpha Z}{p_e R} \left[\tfrac{3}{10} \tfrac{p_e}{E_e} \left(\chi_r^{ij} \hat{p}^i \hat{p}^j - \tfrac{1}{3} \chi_r^{00} \right) - \tfrac{1}{2} \tilde{\chi}_i^l \hat{p}^l + \chi_r^{l0} \hat{p}^l \right] \ , \tag{2.101}$$

where $\alpha Z / p_e R \simeq \mathcal{O}(10^1)$. Equation (2.101) shows that the Lorentz-violating contributions are enhanced. Higher-order forbidden decays do not have additional enhancement compared to the simpler first-forbidden transitions. The bounds from Ref. [181] were translated using Eq. (2.101) [21]. This led to strong limits on several combinations of $X^{\mu\nu}$. Assuming no cancellations between coefficients, this results in the limits [21]

$$X_r^{\mu\nu} = \begin{bmatrix} 10^{-6} & 10^{-7} & 10^{-7} & 10^{-8} \\ 10^{-7} & 10^{-6} & 10^{-6} & 10^{-6} \\ 10^{-7} & 10^{-6} & 10^{-6} & 10^{-6} \\ 10^{-8} & 10^{-6} & 10^{-6} & 10^{-6} \end{bmatrix}, \quad \text{and} \quad X_i^{\mu\nu} = \begin{bmatrix} \times & - & - & - \\ - & \times & 10^{-8} & 10^{-7} \\ - & 10^{-8} & \times & 10^{-7} \\ - & 10^{-7} & 10^{-7} & \times \end{bmatrix} . \tag{2.102}$$

These are the strongest constraints on $\chi^{\mu\nu}$. The only coefficients not constrained by forbidden decays are χ_i^{0l}. These coefficients can be studied in allowed β decay by considering Eq. (2.94) or equivalent correlations. The bounds on χ were also translated into bounds on the SME parameters [21], providing strong direct bounds on the SME parameters $k_{\phi\phi}$ and $k_{\phi W}$ defined in Eq. (2.16).

Conclusion and outlook

We discussed the efforts to search for Lorentz violation in the weak interaction in forbidden and allowed β decays. The bounds from forbidden β decay are several orders of magnitude stronger than the current bounds in allowed β decay, due to the intense sources that

were used [181, 182]. In allowed β decay, Lorentz-violating effects are not enhanced and matching the statistical precision of forbidden β-decay experiments would require long-running experiments with high-intensity sources. An interesting alternative lies in orbital electron capture, where it is possible to use such high-intensity sources [172].

Allowed β decay offers various correlations in which Lorentz violation could be probed. Observables can be chosen such that they give direct constraints on χ compared to the combination of coefficients constrained by forbidden decays. Two relatively simple experiments that probe the β asymmetry in Fermi and Gamow-Teller decays, A_F and A_{GT}, respectively, give direct bounds on χ_r^{0l} and $\tilde{\chi}_i$. These asymmetries could be studied parallel to the efforts to measure the β-spectrum shape discussed in Sec. 2.4.4 [179]. Another interesting possibility is to exploit the γ_r^2 enhancement of decay asymmetries by considering fast-moving nuclei [179, 178, 175]. The total decay rate in the rest frame of the nucleus is proportional to χ_r^{00} [see Eqs. (2.86) and (2.87)]. For a fast-moving nucleus, the expression can be related to the Sun-centered frame with a boost. If the nucleus is moving ultrarelativistically in the $\hat{v}$ direction,

$$\chi_r^{00} = \gamma_r^2 \left(X_r^{TT} + 2X_r^{TL}\hat{v}^L + X_r^{LK}\hat{v}^L\hat{v}^K \right) , \tag{2.103}$$

where γ_r is the Lorentz-boost factor and T, L, and K are coordinates in the Sun-centered reference frame. This relation was, for example, used to extract bounds of $\mathcal{O}(10^{-4})$ from pion decay [175]. For allowed β decay, β-beam facilities, currently considered for producing neutrino beams [183], could be exploited. See also Sec. 4.1.

So far the coefficients χ_i^{0l} remain unconstrained. In Fermi decays, this coefficient could be measured by considering the correlation $\chi_i^{0l}(\vec{p}_e \times \vec{p}_\nu)^l$. The coefficients can also be constrained by measuring the polarized β asymmetry $A_{J\beta}$ in Eq. (2.94). Such an asymmetry could probably be explored in the neutron-decay measurement pursued in Ref. [174].

2.6.2 Neutrino sector

A different possibility to study Lorentz violation in β decay lies in the neutrino sector of the SME [31, 184]. Most interesting for β decay are the modified versions of a^{LV} and c^{LV} defined in Eq. (2.15).

Unlike the weak gauge sector, the neutrino sector has been studied extensively in several experiments. Strong bounds exist from neutrino oscillations and time-of-flight measurements [37]. However, there are four operators that do not show up in oscillations and have no effect on the neutrino group velocity. These operators are called "countershaded" [185]. Recently, it was shown that β decay has a unique sensitivity to these operators [39]. The four countershaded coefficients are denoted by $a_{\text{of}}^{(3)}$. The operators are dimension 3 and CPT odd. These coefficients modify the neutrino dispersion relation and the available phase space of the neutrino, which affects β decay in two ways, in the β end point and in the correlation coefficients.

End point in β decay

The β-spectrum end-point is very sensitive to the neutrino phase space and to the neutrino mass (see also Sec. 2.4.3). Independent of the neutrino mass, the countershaded neutrino

coefficients also shift the end-point, as can be seen from the modified decay rate [39, 186]

$$\frac{dW}{dT} \sim (\Delta T + \delta T_{\rm LV})^2 - \tfrac{1}{2} m_\nu^2 \ , \tag{2.104}$$

where $\Delta T = T_0 - T_e$, $T_e = E_e - m_e$ is the electron kinetic energy, and T_0 is the end-point energy for $m_\nu = 0$. $\delta T_{\rm LV}$ is the Lorentz-violating modification, which depends on sidereal time. Independent of the neutrino mass, a bound on the countershaded coefficients can be set by using the available data of the Troitsk [99] and Mainz [98] experiments; see Ref. [39]. Since these experiments collected data over a long period of time, all the oscillations average out and only the time-averaged Lorentz-violating coefficients can be constrained. Therefore, only two of the four countershaded coefficients could be bounded. Conservatively, this gives bounds of order $\mathcal{O}(10^{-8})$ GeV [39]. These limits improve and complement previous limits. A dedicated analysis of the data of the Troitsk, Mainz, or the expected KATRIN [100] experiments could improve these results. If the data analysis also takes into account the sidereal time, bounds on all the countershaded coefficients could be set.

Correlation coefficients

The Lorentz-violating neutrino coefficients of Eq. (2.15) also modify the neutrino spinor solutions. Near the end point, this modification can be neglected because the phase space dominates. However, the derivation of the complete modified decay rate requires both the modified spinors and the phase-space modification. The modified neutrino phase space is $d^3\vec{p}_\nu \simeq (E_\nu^2 - 2E_\nu a_{\rm of}^{(3)}) dE_\nu d\Omega_\nu$. The modification of the spinors requires the replacement of $\vec{p}_\nu$ by $\tilde{\vec{p}}_\nu = (\vec{p}_\nu + \vec{a}_{\rm of}^{(3)} - \dot{a}_{\rm of}^{(3)} \hat{p}_\nu)$, where $\dot{a}_{\rm of}^{(3)}$ is the isotropic component. The modified neutron-decay rate is

$$\begin{aligned} \frac{dW}{d\Omega_e\, d\Omega_\nu\, dT} \ &\simeq \ F(Z,E)|\vec{p}_e|E_e(E_\nu^2 + 2E_\nu \delta T_{\rm LV}) \\ &\quad \times \left(1 + a\vec{\beta}\cdot\tilde{p}_\nu + A\frac{\langle \vec{J}\rangle}{J}\cdot\frac{\vec{p}_e}{E_e} + B\frac{\langle \vec{J}\rangle}{J}\cdot\frac{\tilde{p}_\nu}{E_\nu})\right) \ . \end{aligned} \tag{2.105}$$

The neutrino coefficients modify the decay rate in a similar way as χ does, since there are now additional correlations between $\vec{J}$ and $\vec{p}_e$ and $a_{\rm of}^{(3)}$.

The countershaded coefficients could, for example, affect the β-ν correlation. The β-ν correlation can be measured as an asymmetry, defined by

$$\tilde{a} = \frac{N_+ - N_-}{N_+ + N_-} \ , \tag{2.106}$$

where $N_+(N_-)$ is the number of decays in which the neutrino and electron are emitted (anti)parallel. The Lorentz-violating neutrino coefficients modify this correlation coefficient to [186]

$$\tilde{a} = a|\vec{\beta}| + \sqrt{\frac{3}{\pi}}\frac{(a\beta^2 + a|\vec{\beta}|)}{E_\nu}(a_{\rm of}^{(3)})_{10}^{\rm lab} \ , \tag{2.107}$$

where the coefficients should be transformed to the Sun-centered frame and would depend on the sidereal frequency of the Earth.

No experiment has searched for these variations, but Ref. [39] estimates that a 0.1% measurement of a would limit the countershaded coefficients at the level of 10^{-8} GeV. Similar, for a 0.1% measurement of the correlation coefficient B, the limits are estimated at $\mathcal{O}(10^{-6})$ GeV. A dedicated experiment measuring either a or B would thus provide interesting new bounds on Lorentz-violating parameters in the neutrino sector. Note that χ and $a_{\rm of}^{(3)}$ have a similar influence on the decay rate. In a dedicated experiment both coefficients might influence the asymmetry. A measurement of Eq. (2.106) might also be sensitive to χ_r^{0l} and $\tilde{\chi}_i$, depending on the experimental setup.

2.6.3 Conclusion

To summarize, β decay offers a unique way to study Lorentz violation in both the gauge and neutrino sectors. The large variety of correlations allows for direct measurements of different components of χ, while in the neutrino sector β decay allows for the study of countershaded coefficients.

In the gauge sector, strong bounds on the order of 10^{-6} - 10^{-8} exist from forbidden β-decay experiments. Unconstrained are the coefficients χ_i^{0l}, which can be accessed in β decay by considering the interaction of χ with two observables [Eq. (2.94)]. Improving the existing bounds requires high statistics and precise knowledge of the systematic uncertainties. Beneficial for this would be to exploit the γ_r^2 enhancement of boosted β decay or to consider electron capture. The real and imaginary parts of χ can be constrained by measuring the asymmetries in Eqs. (2.91) and (2.92), respectively. Such an effort could be combined with measurements of the Fierz-interference term.

Further, we discussed the possibilities to improve constraints on Lorentz violation in the countershaded neutrino sector. In that sector no dedicated experiment has been preformed so far, but using available data from tritium gives bounds of the order of 10^{-8} GeV. The parameters not constrained so far could be bound in β-decay correlation experiments. Lorentz violation gives a unique signal compared to other BSM physics when searched for in a dedicated experiment. Estimates for 0.1% measurements of the coefficients a and B gives a constraint on Lorentz violation of 10^{-8} GeV, which shows the potential for these future experiments.

2.7 Summary and discussion

In this chapter we addressed the current status and role of nuclear and neutron β decay in the search for physics beyond the SM. In these searches, the statistical precision is becoming increasingly important. However, systematic errors, despite improved detection methods, and higher-order corrections such as FSI, still appear to be the main limits. In the meantime, thanks to the evolution of EFT methods, constraints obtained in other fields weigh in, establishing bounds on the scalar and tensor contributions. This is illustrated in Figs. 2.6 and 2.7, where measurements at the LHC (Sec. 2.4.2) and limits from the neutrino mass (Sec. 2.4.3) give constraints that outperformed the β-correlation

measurements in the right-handed sector. This is quantified in Table 2.4.

The study of fundamental aspects of β decay will be most fruitful in the study of left-handed scalar (Sec. 2.4.1) and tensor currents (Sec. 2.4.1), where the left denotes the helicity of the neutrino, as these appear linearly in most observables via the Fierz-interference term. Fortunately, these interactions can be studied in parallel to precision studies of SM parameters (Sec. 2.3.2). For example, extracting the CKM matrix element V_{ud} from superallowed Fermi transitions has, as a by-product, the most strict limit on left-handed scalar interactions. Lacking still is a similar effective measurement of tensor contributions. An interesting option to obtain such a bound could come from measuring the detailed shape of the β spectrum in Gamow-Teller transitions. Also the potential of mirror transitions, both for obtaining tensor limits and for obtaining a value for V_{ud} independent of the superallowed Fermi transitions, has been recognized. In Table 2.5 we indicate the precision required to impose new bounds on left- and right-handed scalar and tensor currents. Measuring the Fierz-interference term in β decay remains competitive in determining bounds on left-handed coupling constants. In contrast, Table V shows that, for right-handed couplings, the limits from the LHC and the limits derived from the neutrino mass are by far superior to the best bounds derived from the $\beta\nu$-correlation a, and future experiments in β decay are unlikely to reach this precision.

Concerning the most fundamental measurement of T-violation, we discussed in Sec. 2.5 the strong bounds on the triple-correlation coefficients D and R derived from the limits on permanent EDMs. These bounds are summarized in Table 2.7. Not only are the bounds from EDMs several orders of magnitude stronger than those of β decay, but the EDM limits also have a large potential to improve faster than those from β decay. One reason is that EDMs can be measured in stable or long-lived particles, but also because of the widely perceived urgency for improved limits in this sector.

A new twist to the discussion of symmetry violations in β decay has been added, since β decay also offers an interesting sensitivity to Lorentz violation in the weak interaction. In Sec. 2.6, we reviewed these limits for the first time. Because the discrete symmetries C, P, and T are each violated in the weak interaction, this interaction is a promising portal to search for new physics when considering CPT violation and thus Lorentz violation. The familiar β-decay correlations are now extended to include correlations between spin and momentum and a Lorentz-violating background tensor. Consequently, spin and momentum appear to have preferred directions in absolute space, resulting in unique signals that can be distinguished from other BSM searches.

In weak decays, Lorentz violation has been parametrized with the complex tensor χ. The bounds on most components of this tensor are of the order of 10^{-6} to 10^{-8} (Sec. 2.6.1). Fine-tuning between the tensor components allows one to weaken these bounds. Relatively simple new experiments can improve these bounds using very strong sources, also removing the possibility of fine-tuning. Obtaining sufficient high counting statistics is the main challenge. The searches for Lorentz violation can be expanded in a parallel effort with the more traditional searches. Alternatively, one can study β decay in flight, exploiting the γ_r^2 enhancement. In this respect there may be as yet unexplored possibilities related to semileptonic decays in high-energy physics. Because this field of research is relatively unexplored, both experimentally and theoretically, the best approach may still emerge.

Improvements in theory and experimental techniques, as well as new radioactive-beam facilities, provide new possibilities to study fundamental aspects of β decay, both in the search for exotic interactions and in the search for Lorentz violation. These studies should be done by considering also the other searches in high-energy physics and precision physics at low energies. Nuclear and neutron β decay will remain an important topic on the research agenda.

Appendix 2.A Decay coefficients

Our formalism can be linked to the original work of Refs. [23, 132], where[12]

$$\begin{aligned}\mathcal{L}_{\text{eff}} = &\bar{p}n\ \bar{e}(C_S - C'_S\gamma_5)\nu_e \\ &+ \bar{p}\gamma^\mu n\ \bar{e}\gamma_\mu(C_V - C'_V\gamma_5)\nu_e \\ &+ \bar{p}\gamma^\mu\gamma_5 n\ \bar{e}\gamma_\mu(C'_A - C_A\gamma_5)\nu_e \\ &+ \frac{1}{2}\bar{p}\sigma^{\mu\nu}n\ \bar{e}\sigma_{\mu\nu}(C_T - C'_T\gamma_5)\nu_e\ . \end{aligned} \tag{2.108}$$

This notation can be related to our couplings in Eq. (2.11) by using the normalized couplings

$$C_i = \frac{G_F}{\sqrt{2}}V_{ud}\,\bar{C}_i\ , \tag{2.109}$$

and

$$\begin{aligned}\bar{C}_V &= g_V(a_L + a_R)\ , \\ \bar{C}'_V &= g_V(a_L - a_R)\ , \\ \bar{C}_A &= -|g_A|(a'_L + a'_R)\ , \\ \bar{C}'_A &= -|g_A|(a'_L - a'_R)\ , \\ \bar{C}_S &= g_S(A_L + A_R)\ , \\ \bar{C}'_S &= g_S(A_L - A_R)\ , \\ \bar{C}_T &= 2g_T(\alpha_L + \alpha_R)\ , \\ \bar{C}'_T &= 2g_T(\alpha_L - \alpha_R)\ . \end{aligned} \tag{2.110}$$

For simplicity we have defined

$$\begin{aligned}a_L &\equiv a_{LL} + a_{LR}\ , \\ a_R &\equiv a_{RR} + a_{RL}\ , \\ a'_L &\equiv a_{LL} - a_{LR}\ , \\ a'_R &\equiv a_{RR} - a_{RL}\ , \\ A_L &\equiv A_{LR} + A_{LL}\ , \\ A_R &\equiv A_{RL} + A_{RR}\ . \end{aligned} \tag{2.111}$$

We write α_L and α_R as in Eq. (2.11), because $\sigma_{\mu\nu}\gamma_5 = i/2\epsilon_{\mu\nu\alpha\beta}\sigma^{\alpha\beta}$. The coefficients $a_{\epsilon\delta}, A_{\epsilon\delta}$, and α_ϵ are related to the ϵ coefficients in Refs. [22, 95] by using

$$\{a_{LL}, a_{LR}, a_{RL}, a_{RR}, A_{LL} + A_{LR}, A_{RR} + A_{RL}, \alpha_L, \alpha_R\} = \{1 + \epsilon_L, \epsilon_R, \tilde{\epsilon}_L, \tilde{\epsilon}_R, \epsilon_S, \tilde{\epsilon}_S, 2\epsilon_T, 2\tilde{\epsilon}_T\}\ . \tag{2.112}$$

A full list of correlation coefficients in allowed β decay including Coulomb corrections is given in Refs. [132, 40]. Here we give the most important decay coefficients in terms of couplings defined in Eq. (2.9). We emphasize that only b, B, and N depend linearly on

[12] Using our definition of γ_5 and neglecting pseudoscalar couplings.

scalar and tensor couplings. We define $\lambda = |g_A|/g_V > 0$ and neglect Coulomb interactions. The spin factors are

$$\lambda_{J'J} = \begin{cases} 1, & J \to J' = J-1 \\ \frac{1}{J+1}, & J \to J' = J \\ \frac{-J}{J+1}, & J \to J' = J+1 \end{cases} , \tag{2.113}$$

and

$$\Lambda_{J'J} = \begin{cases} 1, & J \to J' = J-1 \\ \frac{-(2J-1)}{J+1}, & J \to J' = J \\ \frac{J(2J-1)}{(J+1)(2J+3)}, & J \to J' = J+1 \end{cases} , \tag{2.114}$$

where J and J' are the spin of the initial and final nucleus, respectively. In the following equations, M_F and M_{GT} are the Fermi and Gamow-Teller matrix elements, the upper (lower) sign refers to β^- (β^+) decay, and $\gamma = \sqrt{1-\alpha^2 Z^2}$, with Z the atomic number of the daughter nucleus and α the fine-structure constant.

Because of our normalization of the couplings in Eq. (2.11) we define

$$\bar{\xi} \equiv \frac{G_F^2 V_{ud}^2}{2} \xi \ , \tag{2.115}$$

with

$$\begin{aligned} \xi = {} & 2g_V^2 |M_F|^2 \left\{ |a_L|^2 + |a_R|^2 + \frac{g_S^2}{g_V^2} \left(|A_L|^2 + |A_R|^2 \right) \right\} \\ & + 2g_V^2 \lambda^2 |M_{GT}|^2 \left\{ |a'_L|^2 + |a'_R|^2 + 4\frac{g_T^2}{g_A^2} \left(|\alpha_L|^2 + |\alpha_R|^2 \right) \right\} \ . \end{aligned} \tag{2.116}$$

Neglecting Coulomb interactions, the decay coefficients are [40, 132]

$$\begin{aligned} a\xi = {} & 2g_V^2 |M_F|^2 \left\{ |a_L|^2 + |a_R|^2 - \frac{g_S^2}{g_V^2} \left[|A_L|^2 + |A_R|^2 \right] \right\} \\ & + 2g_V^2 \lambda^2 \frac{|M_{GT}|^2}{3} \left\{ -|a'_L|^2 - |a'_R|^2 + 4\frac{g_T^2}{g_A^2} \left[|\alpha_L|^2 + |\alpha_R|^2 \right] \right\} \ , \end{aligned} \tag{2.117}$$

$$\begin{aligned} b\xi = {} & \pm 2g_V^2 \gamma \Big\{ 2|M_F|^2 \frac{g_S}{g_V} \Big[\mathrm{Re}(A_L a_L^*) + \mathrm{Re}(A_R a_R^*) \Big] \\ & - 4\frac{g_T}{|g_A|} \lambda^2 |M_{GT}|^2 \Big[\mathrm{Re}(\alpha_L a_L^*) + \mathrm{Re}(\alpha_R a_R^*) \Big] \Big\} \ , \end{aligned} \tag{2.118}$$

$$c\xi = 2g_V^2 \lambda^2 \Lambda_{J'J} |M_{GT}|^2 \left\{ -|a'_L|^2 - |a'_R|^2 + 4\frac{g_T^2}{g_A^2} \left[|\alpha_L|^2 + |\alpha_R|^2 \right] \right\} \ , \tag{2.119}$$

$$
\begin{aligned}
A\xi = \; & \pm 2g_V^2\lambda^2|M_{GT}|^2\lambda_{J'J}\left\{4\frac{g_T^2}{g_A^2}\left[|\alpha_L|^2-|\alpha_R|^2\right]-\left[|a'_L|^2-|a'_R|^2\right]\right\} \\
& + 2g_V^2\lambda\delta_{J'J}|M_F||M_{GT}|\sqrt{\frac{J}{J+1}}\left\{4\frac{g_Tg_S}{|g_A|g_V}\Big[\mathrm{Re}(A_L\alpha_L^*)-\mathrm{Re}(A_R\alpha_R^*)\Big]\right. \\
& \left. + 2\Big[|a_{LL}|^2-|a_{LR}|^2-|a_{RR}|^2+|a_{RL}|^2\Big]\right\}\,, \qquad (2.120)
\end{aligned}
$$

$$
\begin{aligned}
B\xi = \; & 2g_V^2\lambda^2|M_{GT}|^2\lambda_{J'J}\Big\{\frac{-4g_T}{|g_A|}\frac{m_e\gamma}{E_e}\Big[\mathrm{Re}(\alpha_La'^*_L)-\mathrm{Re}(\alpha_Ra'^*_R)\Big] \\
& \pm\frac{4g_T^2}{g_A^2}\left[|\alpha_L|^2-|\alpha_R|^2\right]\pm\left[|a'_L|^2-|a'_R|^2\right]\Big\} \\
& - 2g_V^2\lambda\delta_{J'J}|M_F||M_{GT}|\sqrt{\frac{J}{J+1}}\Big\{\frac{4g_Tg_S}{g_V|g_A|}\Big[\mathrm{Re}(A_L\alpha_L^*)-\mathrm{Re}(A_R\alpha_R^*)\Big] \\
& - 2\Big[|a_{LL}|^2-|a_{LR}|^2-|a_{RR}|^2+|a_{RL}|^2\Big] \\
& \pm\frac{m_e\gamma}{E_e}\Big(-\frac{2g_S}{g_V}\Big[\mathrm{Re}(A_La'^*_L)-\mathrm{Re}(A_Ra'^*_R)\Big]+\frac{4g_T}{|g_A|}\Big[\mathrm{Re}(a_L\alpha_L^*)-\mathrm{Re}(a_R\alpha_R^*)\Big]\Big)\Big\}\,, \qquad (2.121)
\end{aligned}
$$

$$
\begin{aligned}
D\xi = \; & 2g_V^2\lambda\delta_{J'J}|M_F||M_{GT}|\sqrt{\frac{J}{J+1}}\Big\{\frac{4g_Tg_S}{g_V|g_A|}\Big[\mathrm{Im}(A_L\alpha_L^*)+\mathrm{Im}(A_R\alpha_R^*)\Big] \\
& + 2\Big[\mathrm{Im}(a_La'^*_L)+\mathrm{Im}(a_Ra'^*_R)\Big]\Big\}\,, \qquad (2.122)
\end{aligned}
$$

$$
\begin{aligned}
R\xi = \; & \pm 2g_V^2\lambda^2|M_{GT}|^2\lambda_{J'J}\frac{-4g_T}{|g_A|}\Big[\mathrm{Im}(\alpha_La'^*_L)-\mathrm{Im}(\alpha_Ra'^*_R)\Big] \\
& + 2g_V^2\lambda\delta_{J'J}|M_F||M_{GT}|\sqrt{\frac{J}{J+1}}\Big\{-2\Big[\mathrm{Im}(A_La'^*_L)-\mathrm{Im}(A_Ra'^*_R)\Big] \\
& - \frac{4g_T}{|g_A|}\Big[\mathrm{Im}(a_L\alpha_L^*)-\mathrm{Im}(a_R\alpha_R^*)\Big]\Big\}\,, \qquad (2.123)
\end{aligned}
$$

and

$$
\begin{aligned}
N\xi = \; & 2g_V^2\lambda^2|M_{GT}|^2\lambda_{J'J}\Big\{\frac{m_e\gamma}{E_e}\Big[|a'_L|^2+|a'_R|^2+4\frac{g_T^2}{g_A^2}\left[|\alpha_L|^2+|\alpha_R|^2\right]\Big] \\
& \mp\frac{4g_T^2}{g_A^2}\Big[\mathrm{Re}(\alpha_La_L^*)+\mathrm{Re}(\alpha_Ra_R^*)\Big]\Big\} \\
& + 2g_V^2\lambda\delta_{J'J}|M_F||M_{GT}|\sqrt{\frac{J}{J+1}}\Big\{-\frac{2g_S}{g_V}\Big[\mathrm{Re}(A_La'^*_L)+\mathrm{Re}(A_Ra'^*_R)\Big] \\
& + \frac{4g_T}{|g_A|}\Big[\mathrm{Re}(a_L\alpha_L^*)+\mathrm{Re}(a_R\alpha_R^*)\Big]\pm\frac{\gamma m_e}{E_e}\Big(\frac{4g_Tg_S}{g_V|g_A|}\Big[\mathrm{Re}(A_L\alpha_L^*)+\mathrm{Re}(A_R\alpha_R^*)\Big] \\
& - 2\Big[|a_{LL}|^2-|a_{LR}|^2+|a_{RR}|^2-|a_{RL}|^2\Big]\Big)\Big\}\,. \qquad (2.124)
\end{aligned}
$$

The longitudinal electron polarization is [40, 132]

$$P = \frac{G\frac{v_e}{c}}{1 + b\left\langle \frac{m_e}{E_e} \right\rangle} \,, \tag{2.125}$$

with

$$\begin{aligned} G\xi = & \pm 2|M_F|^2 g_V^2 \left\{ \frac{g_S^2}{g_V^2} \left[|A_L|^2 - |A_R|^2 \right] - |a_L|^2 + |a_R|^2 \right\} \\ & \pm 2|M_{GT}|^2 g_V^2 \lambda^2 \left\{ \frac{4g_T^2}{g_A^2} \left[|\alpha_L|^2 - |\alpha_R|^2 \right] - \left[|a'_L|^2 - |a'_R|^2 \right] \right\}. \end{aligned} \tag{2.126}$$

The neutron lifetime [Eq. (2.40)] depends on V_{ud}, which is extracted from the $0^+ \to 0^+$ superallowed Fermi decays. However, the extracted value of V_{ud} might also depend on new physics. Taking into account this possibility,

$$\tau_n = K \frac{1 - 2\frac{g_S}{g_V} A_L \gamma \left\langle \frac{m_e}{E_e} \right\rangle^{0^+\to 0^+} + \frac{g_S^2}{g_V^2} A_L^2 + \frac{g_S^2}{g_V^2} A_R^2}{1 + \frac{g_S^2}{g_V^2} A_L^2 + \frac{g_S^2}{g_V^2} A_R^2 + 3\lambda^2 (1 + 4\frac{g_T^2}{g_A^2}\alpha_L^2 + 4\frac{g_T^2}{g_A^2}\alpha_R^2) + \gamma \left\langle \frac{m_e}{E_e} \right\rangle (2\frac{g_S}{g_V} A_L - 12\lambda^2 \frac{g_T}{|g_A|}\alpha_L)} \,, \tag{2.127}$$

where $\langle m_e/E_e \rangle^{0^+\to 0^+}$ is the inverse average energy of the superallowed decays [57]. The constant K is [57]

$$K \equiv \frac{2\pi^3}{m_e^5 f_n (1 + \Delta_{RC}) G_F^2 V_{ud}^2} = (1.9342 \pm 0.002) \cdot 10^{-4} \,, \tag{2.128}$$

where $f_n = 1.6887(2)$ is the statistical rate function [187] and Δ_{RC} are the SM electroweak corrections [188].

The SM expressions can be obtained by setting $a_{LL} = 1$ and neglecting all other couplings. Defining $\rho \equiv |g_A| M_{GT}/g_V M_F$, the remaining SM expressions are

$$a_{SM} = \frac{1 - \rho^2/3}{1 + \rho^2} \,, \tag{2.129a}$$

$$A_{SM} = \frac{\mp\lambda_{J'J}\rho^2 + 2\delta_{J'J}\sqrt{J/(J+1)}\rho}{1 + \rho^2} \,, \tag{2.129b}$$

$$B_{SM} = \frac{\pm\lambda_{J'J}\rho^2 + 2\delta_{J'J}\sqrt{J/(J+1)}\rho}{1 + \rho^2} \,, \tag{2.129c}$$

$$G_{SM} = \mp 1 \,, \tag{2.129d}$$

while all other coefficients vanish. For neutron decay, $\rho = \sqrt{3}|g_A|$ and $J = J' = 1/2$.

2.A.1 Linear terms in B

The B coefficients contains terms linear in exotic couplings. Neglecting quadratic couplings, we can write

$$B\xi = \pm\lambda_{J'J}\rho^2 + 2\rho\delta_{J'J}\sqrt{J/(J+1)} + \left\langle \frac{m_e\gamma}{E_e} \right\rangle b_B \xi \,, \tag{2.130}$$

where

$$b_B\xi = -\rho^2\lambda_{J'J}\frac{4g_T}{|g_A|}\text{Re }\alpha_L \\ \mp\delta_{J'J}\rho\sqrt{\frac{J}{J+1}}\Big[-\frac{2g_S}{g_V}\text{Re }A_L+\frac{4g_T}{|g_A|}\text{Re }\alpha_L\Big]\ . \tag{2.131}$$

Most B measurements measure

$$\tilde{B}=\frac{B_{SM}+b_B\gamma\left\langle\frac{m_e}{E_e}\right\rangle}{1+b\left\langle\frac{m_e}{E_e}\right\rangle}\ . \tag{2.132}$$

For pure Gamow-Teller transitions, with $\rho\to\infty$, $\tilde{B}_{GT}=\pm\lambda_{J'J}$ and the linear dependence cancels. For neutron decay and assuming real couplings, $B_{SM}\simeq 1$ and

$$\begin{aligned}\tilde{B}&\simeq B_{SM}+\left\langle\frac{m_e}{E_e}\right\rangle(\gamma b_B-bB_{SM})\\ &\simeq\frac{2(\lambda+\lambda^2)}{1+3\lambda^2}+\left\langle\frac{m_e\gamma}{E_e}\right\rangle\frac{-\lambda-2\lambda^2+3\lambda^3}{(1+3\lambda^2)^2}\left[2\frac{g_S}{g_V}A_L+4\frac{g_T}{|g_A|}\alpha_L\right]\\ &\simeq 1+\left[0.1\frac{g_S}{g_V}A_L+0.2\frac{g_T}{|g_A|}\alpha_L\right]\left\langle\frac{m_e\gamma}{E_e}\right\rangle\ .\end{aligned} \tag{2.133}$$

For comparison, for neutron decay, the Fierz-interference term is

$$\begin{aligned}b_{\text{neutron}}&=\frac{2\frac{g_S}{g_V}A_L-12\lambda^2\frac{g_T}{|g_A|}\alpha_L}{1+3\lambda^2}\\ &\simeq 0.35\frac{g_S}{g_V}A_L-3.3\frac{g_T}{|g_A|}\alpha_L\ .\end{aligned} \tag{2.134}$$

For the measured $\tilde{A}$ coefficient in neutron decay, with $A_{\text{SM}}\simeq -0.11$,

$$\tilde{A}_{\text{neutron}}=A_{\text{SM}}\mp A_{\text{SM}}\frac{m_e\gamma}{E_e}(0.35\frac{g_S}{g_V}A_L-3.3\frac{g_T}{|g_A|}\alpha_L)\ . \tag{2.135}$$

So for neutron decay, B actually has a reduced sensitivity to scalar and in particular tensor terms compared to for example A.

Appendix 2.B Lorentz violation

The Lorentz-violating β-decay rate including Coulomb corrections and electron spin, to first order in $\chi^{\mu\nu}$, is [17]

$$
\begin{aligned}
dW = {} & \frac{1}{(2\pi)^5} E_e p_e (E_0 - E_e)^2 F(\pm Z, E_e) \bar{\xi} dE_e d\Omega_e d\Omega_\nu \\
& \times \left\{ \left(1 \mp \frac{\vec{p}_e \cdot \hat{s}_e}{E_e} \right) \left[\tfrac{1}{2} \left(1 + B \frac{\vec{p}_\nu \cdot \langle \vec{J} \rangle}{J E_\nu} \right) + t + \frac{\vec{w}_1 \cdot \vec{p}_\nu}{E_\nu} + \vec{w}_2 \cdot \frac{\langle \vec{J} \rangle}{J} + T_1^{km} j^k j^m \right. \right. \\
& \left. + T_2^{kj} \frac{\langle J^k \rangle p_\nu^j}{J E_\nu} + \frac{S_1^{kmj} j^k j^m p_\nu^j}{E_\nu} \right] \\
& + \left(\left(1 \mp \frac{(E_e - \gamma m_e)(\vec{p}_e \cdot \vec{\sigma}_e)}{E_e^2 - m_e^2} \right) \frac{p_e^l}{E_e} \mp \frac{\gamma m_e}{E_e} \hat{\sigma}_e^l \mp \frac{m_e}{E_e} \sqrt{1 - \gamma^2} (\hat{p}_e \times \hat{\sigma}_e)^l \right) \\
& \times \left[\tfrac{1}{2} A \frac{\langle J^k \rangle}{J} - \tfrac{3}{2} c' \frac{\vec{p}_\nu \cdot j}{E_\nu} j^l + \tfrac{1}{2} (a + c') \frac{p_\nu^l}{E_\nu} + w_3^l + \frac{T_3^{lj} p_\nu^j}{E_\nu} + T_4^{lk} \frac{\langle J^k \rangle}{J} \right. \\
& \left. \left. + S_2^{lmk} j^m j^k + \frac{S_3^{lmj} \langle J^m \rangle p_\nu^j}{J E_\nu} + \frac{R^{lmkj} j^m j^k p_\nu^j}{E_\nu} \right] \right\} ,
\end{aligned}
\tag{2.136}
$$

where $\gamma = \sqrt{1 - \alpha^2 Z^2}$. The Lorentz-violating constants are[13]

$$
\begin{gathered}
t = (a - \tfrac{1}{2} c') \chi_r^{00} , \\
w_1^j = -x \chi_r^{0j} + \breve{g} (\chi_r^{j0} - \tilde{\chi}_i^j) , \qquad w_2^k = \breve{K} (\chi_r^{k0} - \chi_r^{0k}) - \breve{L} \tilde{\chi}_i^k , \qquad w_3^l = -x \chi_r^{0l} + \breve{g} (\chi_r^{l0} + \tilde{\chi}_i^l) , \\
T_1^{km} = \tfrac{3}{2} c' \chi_r^{km} , \qquad T_2^{kj} = \tfrac{1}{2} A \chi_r^{00} \delta^{jk} + \breve{L} (\chi_r^{jk} + \chi_i^{s0} \epsilon^{sjk}) - \breve{K} (\chi_r^{kj} + \chi_i^{0s} \epsilon^{sjk}) , \\
T_3^{lj} = (x + \breve{g}) \chi_r^{00} \delta^{lj} - (x \chi_i^{0s} + \breve{g} \chi_i^{s0}) \epsilon^{sjl} - \breve{g} (\chi_r^{jl} + \chi_r^{lj}) , \\
T_4^{lk} = \tfrac{1}{2} B \chi_r^{00} \delta^{lk} - \breve{L} (\chi_r^{lk} - \chi_i^{s0} \epsilon^{ksl}) - \breve{K} (\chi_r^{kl} - \chi_i^{0s} \epsilon^{ksl}) , \\
S_1^{kmj} = -\tfrac{3}{2} c' (\chi_r^{k0} \delta^{mj} - \chi_i^{ms} \epsilon^{sjk}) , \qquad S_2^{lmk} = -\tfrac{3}{2} c' (\chi_r^{m0} \delta^{kl} + \chi_i^{ms} \epsilon^{slk}) , \\
S_3^{lmj} = \breve{L} \left(\chi_r^{l0} \delta^{jm} - \chi_i^{sl} \epsilon^{sjm} - \chi_r^{j0} \delta^{ml} + \tilde{\chi}_i^m \delta^{jl} - \chi_i^{sj} \epsilon^{lms} \right) \\
+ \breve{K} \left(\chi_i^{00} \epsilon^{ljm} - \chi_r^{0l} \delta^{jm} - \chi_r^{0j} \delta^{ml} + (\chi_r^{0m} + \chi_r^{m0}) \delta^{jl} - \chi_i^{ms} \epsilon^{sjl} \right) , \\
R^{lmkj} = \tfrac{3}{2} c' \left(\chi_i^{m0} \epsilon^{lkj} - \chi_r^{mk} \delta^{lj} + \chi_r^{ml} \delta^{kj} + \chi_r^{mj} \delta^{kl} \right) ,
\end{gathered}
\tag{2.137}
$$

where r and i denote the real and imaginary parts of $\chi^{\mu\nu}$, respectively, $\tilde{\chi}^l = \epsilon^{lmk} \chi^{mk}$, and p^l denotes the electron momentum in the l direction. a, A, B, and $\bar{\xi}$ are the standard β-decay coefficients, given in Eq. (2.129);, the other coefficients are

$$
\begin{gathered}
x = \frac{1}{1 + \rho^2} , \qquad y = \frac{-\rho}{1 + \rho^2} , \\
c' = (1 - x) \bar{\Lambda}_{JJ'} , \\
\breve{g} = \tfrac{1}{3} (1 - x)(1 + \tfrac{3}{2} \bar{\Lambda}_{JJ'}) , \qquad \breve{K} = -y \sqrt{\frac{J}{J+1}} \delta_{JJ'} , \qquad \breve{L} = \pm \tfrac{1}{2} \frac{\rho^2}{1 + \rho^2} \lambda_{JJ'} ,
\end{gathered}
\tag{2.138}
$$

[13] Note the sign error in w_3^l in Ref. [17].

where upper(lower) signs refer to $\beta^-(\beta^+)$ decay. The coefficient $\lambda_{J'J}$ is given in Eq. (2.113) and

$$\bar{\Lambda}_{J'J} \equiv \Lambda_{J'J} \frac{\left\langle (\vec{J}\cdot\vec{j})^2 \right\rangle - \frac{1}{3}J(J+1)}{J(2J-1)} \ , \tag{2.139}$$

with $\Lambda_{J'J}$ given in Eq. (2.114).

Chapter 3

T violation in radiative β decay and electric dipole moments

In radiative β decay, T violation can be studied through a spin-independent T-odd correlation. We consider contributions to this correlation by beyond the standard model (BSM) sources of T-violation, arising above the electroweak scale. At the same time such sources, parametrized by dimension-6 operators, can induce electric dipole moments (EDMs). As a consequence, the manifestations of the T-odd BSM physics in radiative β decay and EDMs are not independent. Here we exploit this connection to show that current EDM bounds already strongly constrain the spin-independent T-odd correlation in radiative β decay.

3.1 Introduction

The Standard Model of particle physics (SM) cannot account for the baryon asymmetry of the universe [121, 189, 190, 191], and additional sources of CP violation might be expected to arise beyond the SM (BSM). Searches for additional time-reversal (T) violation, and equivalently CP violation, are, therefore, promising probes of BSM physics. Especially interesting are observables with a very low SM background, such as the electric dipole moments (EDMs) of hadrons, nuclei, atoms, and molecules.

In β decay, T violation is probed by the triple-correlation coefficients D and R [132]. However, these observables are not independent from EDM measurements [131, 148, 149, 192]. In fact, the stringent neutron EDM limit bounds D more than an order of magnitude better [148] than current β-decay experiments [134, 135]. Molecular and atomic EDMs constrain scalar and tensor electron-nucleon couplings [151, 153, 154, 165], which leads to strong constraints on the R coefficient [149, 192]. These constraints are several orders of magnitude better than the current best β-decay bounds [138, 193] (Sec. 2.5).

In radiative decays it is possible to study spin-independent T-odd triple-correlations [144, 145, 146], which are not present in β decay. In this chapter, we consider such a correlation in radiative β decay generated by high-energy BSM sources of CP violation.

Published: K. K. Vos and W. Dekens, Phys. Lett. B **751**, 500 (2015).

As in β decay, we find that this T-odd correlation and EDMs are connected, which allows EDM bounds to strongly constrain the spin-independent T-odd correlation.

We work in an effective field theory (EFT) framework in which dimension-6 operators parametrize the new sources of CP violation. We first discuss these operators. Then we consider their contributions to radiative β decay in section 3.3, while discussing the contribution of these operators to the EDM in section 3.4. Finally, we give the current EDM bounds on these operators while assuming only one coupling is nonzero at a time. We then briefly discuss the constraints that arise when turning on two couplings simultaneously and end with a brief discussion.

3.2 Formalism

We consider the effects of new T-violating physics on the correlation $K\vec{p}_\nu \cdot (\vec{p}_e \times \vec{k})$, where $\vec{k}$ is the photon momentum, and neglect the small T-violating SM contributions generated by the CP-odd phase of the CKM matrix and the QCD θ-term [41]. Besides these true SM T-odd sources, there are also electromagnetic final-state interactions (FSI) that mimic T-violation and that also contribute to the triple-correlation (similar FSI contribute to D and R). These FSI have been studied for the neutron, ^{19}Ne, and ^{35}Ar [145, 146, 194], and contribute to the T-odd asymmetry at $\mathcal{O}(10^{-3}) - \mathcal{O}(10^{-5})$, depending on the detectable photon energy and the used isotope.

The effects of new T-violating physics, arising at a high scale Λ, can be studied in an EFT framework. At low energies, the new physics is effectively described by higher-dimensional operators. We consider dimension-six operators, for which the complete set of gauge-invariant operators has been derived in Refs. [7, 195]. We divide the operators relevant for radiative β decay into two groups.

(i) The first group consists of four-fermion operators that also contribute to β decay [7, 8, 22]. The relevant part of the effective β-decay Lagrangian is [24]

$$\mathcal{L}^{(\text{eff})}_{S,P,T} = \frac{-4G_F}{\sqrt{2}} \sum_{\epsilon,\delta=L,R} \left\{ A_{\epsilon\delta}\, \bar{e}\nu^\epsilon_e \cdot \bar{u}d_\delta + \alpha_\epsilon\, \bar{e}\frac{\sigma^{\mu\nu}}{\sqrt{2}}\nu^\epsilon_e \cdot \bar{u}\frac{\sigma_{\mu\nu}}{\sqrt{2}}d_\epsilon \right\} + \text{h.c.}, \tag{3.1}$$

where we have set $V_{ud} = 1$ for convenience. G_F is the Fermi coupling constant and we sum over the chirality (L, R) of the final states. These four-fermion operators modify the $V-A$ coupling of the SM, by generating scalar/pseudoscalar (A) and tensor (α) couplings [23, 40]. Besides contributing to β decay, the operators in Eq. (3.1) also contribute to radiative β decay after being dressed with bremsstrahlung photons [144, 146].

(ii) The second group of T-violating operators is given in Table 3.1[1]. At the scale of new physics, Λ, the relevant terms for radiative β decay, are

$$\begin{aligned}\mathcal{L}_6 \;=\; & C_{\varphi\tilde{W}B}(\Lambda)\frac{gc_w v^2}{2} i\varepsilon^{\mu\nu\alpha\beta} W^+_\mu W^-_\nu F_{\alpha\beta} + C_{\varphi ud}(\Lambda)\frac{v^2 g}{2\sqrt{2}}\bar{u}_R\gamma^\mu d_R W^+_\mu \\ & + 2vC_{uW}(\Lambda)\,(\bar{d}_L\sigma^{\mu\nu}\overleftrightarrow{D}_\nu u_R)W^-_\mu + 2vC_{dW}(\Lambda)\,(\bar{u}_L\sigma^{\mu\nu}\overleftrightarrow{D}_\nu d_R)W^+_\mu \\ & + \text{h.c.} + \ldots, \end{aligned} \tag{3.2}$$

[1] In principle, the operator $Q_{eW} = (\bar{l}\sigma^{\mu\nu}e)\tau^I\varphi W^I_{\mu\nu}$ also contributes to radiative β decay, however, it does not contribute to K at leading recoil order.

$Q_{\varphi ud}$	$i(\tilde{\varphi}^\dagger D_\mu \varphi)(\bar{u}\gamma^\mu d)$
$Q_{\varphi \tilde{W} B}$	$\varphi^\dagger \tau^I \varphi \tilde{W}^I_{\mu\nu} B^{\mu\nu}$
Q_{uW}	$(\bar{q}\sigma^{\mu\nu}\tau^I \tilde{\varphi}\, u) W^I_{\mu\nu}$
Q_{dW}	$(\bar{q}\sigma^{\mu\nu}\tau^I \varphi\, d) W^I_{\mu\nu}$

Table 3.1: Dimension-six operators that contribute to T-violating radiative β decay. Here τ^I are the Pauli matrices, φ is the Higgs doublet and $\tilde{\varphi} = i\tau_2\varphi^*$. Furthermore, $D_\mu = \partial_\mu - i\frac{g}{2}\tau^I W^I_\mu - i\frac{g'}{2}B_\mu$ is the covariant derivative of the Higgs doublet, while $W^I_{\mu\nu} = \partial_\mu W^I_\nu - \partial_\nu W^I_\mu + g\varepsilon^{IJK} W^J_\mu W^K_\nu$ and $B_{\mu\nu} = \partial_\mu B_\nu - \partial_\nu B_\mu$ are the field strengths of the $SU(2)$ and $U(1)_Y$ gauge fields respectively. Finally, the duals of the field strengths are $\tilde{X}_{\mu\nu} = \varepsilon_{\mu\nu\alpha\beta}X^{\alpha\beta}$, where $\varepsilon^{0123} = +1$.

where $v \approx 246\,\text{GeV}$ is the vacuum expectation value of the Higgs field $\langle\varphi\rangle = \frac{1}{\sqrt{2}}v$, the photon field is denoted by A_μ and $s_w = \sin\theta_w$ is the sine of the Weinberg angle ($c_w = \cos\theta_w$). The covariant derivative $D_\mu = \partial_\mu - is_w g q_f A_\nu$, where q_f is the charge of the fermion. C_X is the coupling constant associated with the operator Q_X defined in Table 3.1.

Fig. 3.1 shows how these operators contribute to radiative β decay. At low energies, $\mu \approx 1\,\text{GeV}$, after integrating out the $W^\pm$ boson, we obtain

$$\begin{aligned}
\mathcal{L}_6^{\text{eff}} \;=\; & -\frac{8ic_w}{gv^2} V_{ud}\,\text{Re}\,C_{\varphi\tilde{W}B}(\Lambda)\,\varepsilon^{\mu\nu\alpha\beta}(\bar{u}_L\gamma_\mu d_L)(\bar{e}_L\gamma_\nu\nu_L)F_{\alpha\beta} \\
& + \frac{1}{M_W^2} C_{\varphi ud}(\Lambda)(\bar{u}_R\gamma_\mu d_R)\Gamma^{\mu\nu}(\bar{e}_L\gamma_\nu\nu_L) \\
& - \frac{8is_w}{\sqrt{2}v}\eta_{qW} C^*_{Wu}(\Lambda)\,(\bar{u}_R\sigma^{\mu\nu} d_L)(\bar{e}_L\gamma_\mu\nu_L)A_\nu \\
& - \frac{8is_w}{\sqrt{2}v}\eta_{qW} C_{Wd}(\Lambda)\,(\bar{u}_L\sigma^{\mu\nu} d_R)(\bar{e}_L\gamma_\mu\nu_L)A_\nu + \text{h.c.} + \ldots,
\end{aligned} \tag{3.3}$$

where $\Gamma^{\mu\nu} = g^{\mu\nu}D^2 - D^\nu D^\mu - igs_w F^{\mu\nu}$, whose leading contribution to K arises from Fig. 3.1a. Furthermore, $\eta_{qW} = \left(\frac{\alpha_s(\Lambda)}{\alpha_s(m_t)}\right)^{4/21}\left(\frac{\alpha_s(m_t)}{\alpha_s(m_b)}\right)^{4/23}\left(\frac{\alpha_s(m_b)}{\alpha_s(m_c)}\right)^{4/25}\left(\frac{\alpha_s(m_c)}{\alpha_s(\mu)}\right)^{4/27}$ is a running factor (numerically, $\eta_{qW} = 0.39\,(0.33)$ for $\Lambda = 1\,(10)\,\text{TeV}$), arising from the QCD renormalization of the Q_{qW} operators [196, 197]. The dots represent terms which are necessary to maintain gauge invariance, but that do not contribute to K at leading recoil order.

The first term in Eq. (3.3) is similar to the interaction studied in Eq. (2) of Ref. [146]. Although we find that such a term is not T-violating when it arises from a pseudo-Chern-Simons term (i.e. Eq. (1) in Ref. [146]), it is clear that it can be generated by BSM physics such as $Q_{\varphi\tilde{W}B}$.

3.3 T-violating radiative β decay

The new sources of T violation contribute to the radiative β decay rate

$$d\Gamma = 32e^2G_F^2 M_n M_p d\Gamma_0 \left[K\vec{p}_\nu\cdot(\vec{p}_e\times\vec{k}) + \cdots\right], \tag{3.4}$$

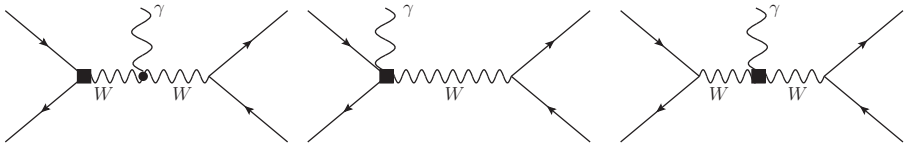

(a) $Q_{\varphi ud}$ (b) $Q_{uW,dW}$ (c) $Q_{\varphi\tilde{W}B}$

Figure 3.1: The relevant T-violating effective interactions for radiative β decay. The box indicates one of the BSM interactions of Table 3.1, the dot indicates the SM coupling of two W bosons and a photon.

where $M_{n,p}$ are the neutron and proton masses and $d\Gamma_0$ contains the integral over the phase space. The dots represent higher-order recoil terms as well as T-even terms that are present in the SM [198]. The K coefficient can be inferred from the asymmetry [145, 146]

$$\mathcal{A} = \frac{\Gamma^+ - \Gamma^-}{\Gamma^+ + \Gamma^-} \ , \tag{3.5}$$

where Γ^+ corresponds to the ϕ_ν range $[0, \pi]$ and Γ^- to the ϕ_ν range $[\pi, 2\pi]$ if $\vec{p}_e$ is in the $\hat{z}$ direction, such that $\vec{k}$ and $\vec{p}_e$ fix the $\hat{z} - \hat{x}$ plane [145, 146]. The asymmetry depends on the Q-value of the interaction and on the threshold energy of the photon detector $\omega_{\min}$, typically in the range of MeV. The asymmetry grows with increasing $\omega_{\min}$, following Ref. [146] we evaluate the integrals at $\omega_{\min} = 0.3$MeV. We discuss the form of K and the contribution to $\mathcal{A}$ for the two groups of operators.

(i) The first group contributes to radiative β decay after being dressed with bremsstrahlung photons [146]. For neutron decay,

$$K = 2\frac{1}{M_p}\frac{1}{k\cdot p_e}\text{Im}\left[g_T\alpha_L(g_S^* A_L^* + g_P^* A'^*_L) - g_T\alpha_R(g_S^* A_R^* + g_P^* A'^*_R)\right] \ , \tag{3.6}$$

where $A_L \equiv A_{LL} + A_{LR}$, $A_R \equiv A_{RR} + A_{RL}$, $A'_L \equiv A_{LL} - A_{LR}$ and $A'_R \equiv A_{RR} - A_{RL}$. The couplings g_Λ are defined by $\langle p|\bar{u}\Gamma d|n\rangle = g_\Gamma \bar{p}\Gamma n$, with $\Gamma = 1, \gamma_5, \gamma_\mu, \gamma_\mu\gamma_5, \sigma^{\mu\nu}$. For $\omega_{\min} = 0.3$ MeV, the asymmetry is

$$\mathcal{A} = 2.1\times 10^{-5}\text{Im}\left[g_T\alpha_L(g_S^* A_L^* + g_P^* A'^*_L) - g_T\alpha_R(g_S^* A_R^* + g_P^* A'^*_R)\right] \ , \tag{3.7}$$

which is in part small due to the nucleon mass suppression in Eq. (3.6). The asymmetry only contains quadratic couplings, which also appear in the R correlation [40]. The current best β decay bounds are Im $g_T\alpha_L < 3\times 10^{-3}$ (90% C. L.) from the pure Gamow-Teller decay of ^{8}Li [138]. Combining this constraint with the bound on R from neutron decay [193] gives Im $g_S A_L < 6\times 10^{-2}$ (90% C. L.). Given these experimental constraints, improving these bounds in radiative β decay would require a measurement of the asymmetry in Eq. (3.7) to better than 10^{-9}. Besides that, the EDM bound on molecular ThO [154] and the EDM bound on ^{199}Hg [151] also limit the R coefficient [149, 192] and thus the couplings in Eq. (3.7). Conservative bounds are Im $A_L < 10^{-5}$ and Im $\alpha_L < 10^{-6}$ (90% C. L.) [149, 192]. A similar conclusion was drawn in Ref. [146].

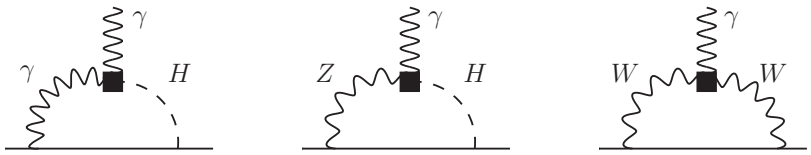

Figure 3.2: One-loop contributions of $Q_{\varphi\tilde{W}B}$ to the quark and electron EDMs.

(*ii*) At leading order, the interactions in Eq. (3.3) give

$$\begin{aligned} K &= -16\frac{c_w}{eg}\frac{E_e}{k\cdot p_e}(g_A^2+g_V^2)\mathrm{Re}\, C_{\varphi\tilde{W}B} - 8s_w\frac{1}{k\cdot p_e}\frac{\sqrt{2}M_W}{eg}g_A g_T \eta_{qW}\mathrm{Im}(C^*_{Wd}+C_{Wu}) \\ &\quad +\frac{s_w}{eg}\mathrm{Im}C_{\varphi ud}\left(8\frac{E_e}{k\cdot p_e}(g_A^2-g_V^2)+4\frac{1}{\omega}(g_A^2+g_V^2)\right) . \end{aligned} \tag{3.8}$$

For $\omega_{\rm min} = 0.3$ MeV, the asymmetry for neutron radiative β decay is

$$\begin{aligned} \mathcal{A} &= -2\times 10^{-11}\ \mathrm{Re}\, C'_{\varphi\tilde{W}B} + 2\times 10^{-7}\ \mathrm{Im}(C'^*_{Wd}+C'_{Wu}) \\ &\quad +4\times 10^{-12}\ \mathrm{Im}C'_{\varphi ud}\ , \end{aligned} \tag{3.9}$$

in terms of the couplings at $\Lambda = 1$ TeV. We used $g_A = 1.27$, $s_w^2 = 0.23$, $g = 0.64$, $g_T \sim 1$ and $M_W = 80.4$ GeV. For clarity we have redefined $C' \equiv v^2 C$, such that the couplings C' are dimensionless. Clearly, the contribution of these operators to the asymmetry is rather small. However, the sensitivity of the asymmetry to the T-odd BSM sources can be improved by choosing isotopes with larger Q-values. For ^{37}K [199], we find, for example, that it is 20 times more sensitive than neutron decay. In the next section we discuss the stringent limit from EDMs on these couplings.

3.4 Constraints from EDMs

The second class of operators also contribute to the neutron EDM (nEDM) and electron (eEDM). At the scale M_W, these operators induce

$$\begin{aligned} \mathcal{L}_{\rm EDM} &= -\frac{i}{2}\sum_{f=u,d,e} d_f e Q_f m_f\, \bar{\psi}_f \sigma^{\mu\nu}\gamma_5\psi_f F_{\mu\nu} - i\,\mathrm{Im}\,\Xi_1\Big[\bar{u}_R\gamma^\mu d_R\,\bar{d}_L\gamma_\mu u_L - \bar{d}_R\gamma^\mu u_R\,\bar{u}_L\gamma_\mu d_L\Big] \\ &\quad -i\,\mathrm{Im}\,\Xi_8\Big[\bar{u}_R\gamma^\mu t^a d_R\,\bar{d}_L\gamma_\mu t^a u_L - \bar{d}_R\gamma^\mu t^a u_R\,\bar{u}_L\gamma_\mu t^a d_L\Big], \end{aligned} \tag{3.10}$$

where $d_{u,d}$ represent the up- and down-quark EDM, d_e is the electron EDM ($d_e^{\rm exp} \equiv e m_e d_e$), and $\Xi_{1,8}$ are CP-odd four quark operators. The contributions from $C_{\varphi ud}$, $C_{\varphi\tilde{W}B}$, and C_{qW} to the couplings in Eq. (3.10) are listed in Table 3.2.

$Q_{\varphi ud}$

Table 3.2 shows that, at leading order $C_{\varphi ud}$, only contributes to Ξ_1. This interaction is generated after integrating out the $W^\pm$ boson through a tree-level diagram. The relevant interaction is similar to Fig. 3.1b without the photon, and where the $W^\pm$ should now

	$C_{\varphi ud}(\Lambda)$	$\frac{1}{gg'}\mathrm{Re}\, C_{\varphi\tilde{W}B}(\Lambda = 1\,(10)\,\mathrm{TeV})$	$\frac{\sqrt{2}vs_w}{em_qQ_q}\mathrm{Im}\, C_{qW}(\Lambda = 1\,(10)\,\mathrm{TeV})$
$d_u(M_W)$	–	$-6.2\,(-11)\times 10^{-2}$	$-0.80\,(-0.69)$
$d_d(M_W)$	–	$-11\,(-19)\times 10^{-2}$	$0.80\,(0.69)$
$d_e(M_W)$	–	$-5.3\,(-10)\times 10^{-2}$	–
$\Xi_1(M_W)$	1	–	–
$\Xi_8(M_W)$	–	–	–

Table 3.2: The couplings in Eq. (3.10) at the scale M_W in terms of the BSM couplings $C_{\varphi ud}$, $C_{\varphi\tilde{W}B}$, and C_{qW} at the scale $\Lambda = 1\,(10)$ TeV. The row headings are given by the column headings multiplied by the corresponding table entry, a dash indicates there is no contribution at leading order in perturbation theory. For more details, see Ref. [155].

be coupled to quarks instead of leptons [148]. As $Q_{\varphi ud}$ does not evolve under QCD renormalization, the relation in Table 3.2 is independent of Λ.

$Q_{\varphi\tilde{W}B}$

In contrast, $Q_{\varphi\tilde{W}B}$ does not contribute to the interactions in Eq. (3.10) at the tree-level, but it induces quark EDMs at the one-loop-level. This operator also contains Higgs$-\gamma\gamma$ and Higgs$-Z\gamma$ interactions. These interactions and the $WW\gamma$ interaction in Eq. (3.2) contribute to the quark EDMs through the diagrams in Fig. 3.2 [155, 200]. As a consequence, the operator $Q_{\varphi\tilde{W}B}$ mixes with the quark EDMs when it is evolved from the scale of new physics, Λ, down to M_W. The electron EDM (eEDM) is induced through the same mechanism. The results in Table 3.2 take into account both the mixing between $C_{\varphi\tilde{W}B}$ and d_q, and the running of d_q[2] [196, 197].

Q_{uW} and Q_{dW}

Finally, the Q_{qW} operators contribute to $d_{u,d}$ directly, and we have,

$$d_u(\Lambda) = -\frac{\sqrt{2}vs_w}{eQ_um_u}\mathrm{Im}\, C_{uW}(\Lambda), \qquad d_d(\Lambda) = \frac{\sqrt{2}vs_w}{eQ_dm_d}\mathrm{Im}\, C_{dW}(\Lambda). \tag{3.11}$$

After taking into account the running of the quark EDMs, we obtain the results in Table 3.2.

The induced interactions at the scale M_W have to be evolved to the low energies where EDM experiments take place. The renormalization group equations (RGEs) for the quark EDMs and the four-quark operators give [155, 157, 196, 197, 201]

$$\begin{gathered} d_q(M_{\mathrm{QCD}}) = 0.48\, d_q(M_W), \\ \mathrm{Im}\,\Xi_1(M_{\mathrm{QCD}}) = 1.1\,\Xi(M_W), \qquad \mathrm{Im}\,\Xi_8(M_{\mathrm{QCD}}) = 1.4\,\Xi(M_W), \end{gathered} \tag{3.12}$$

where $M_{\mathrm{QCD}} \approx 1\,\mathrm{GeV}$ is the QCD scale, while the eEDM does not evolve under one-loop QCD renormalization.

[2]Like $Q_{\varphi ud}$, the operator $Q_{\varphi\tilde{W}B}$ does not evolve under one-loop QCD renormalization.

nEDM	Im $C'_{\varphi ud}(\Lambda)$	Re $C'_{\varphi \tilde{W} B}(\Lambda)$	Im $C'_{dW}(\Lambda)$	Im $C'_{uW}(\Lambda)$
$\Lambda = 1\,\text{TeV}$	1.0×10^{-5}	1.8×10^{-4}	2.9×10^{-10}	9.7×10^{-10}
$\Lambda = 10\,\text{TeV}$	1.0×10^{-5}	1.0×10^{-4}	3.0×10^{-10}	1.0×10^{-9}

eEDM	Re $C'_{\varphi \tilde{W} B}(\Lambda)$
$\Lambda = 1$ TeV	2.3×10^{-6}
$\Lambda = 10\,\text{TeV}$	1.2×10^{-6}

Table 3.3: 90% C.L. bounds on the couplings of the dimension-six operators in Table 3.1 ($C'_i \equiv v^2 C_i$) due to the limits on the neutron and electron EDM. The constraints are shown for two values of the scale of new physics, $\Lambda = 1,\ 10\,\text{TeV}$. To obtain these results we employed the central values in Eq. (3.13), and assumed one coupling to be dominant at the scale of new physics. Only $Q_{\varphi \tilde{W} B}$ gives rise to a significant eEDM.

3.4.1 Constraints on single couplings

We first discuss the bounds on the couplings in Table 3.2, while assuming only one nonzero coupling at a time. To calculate the nEDM in terms of d_q and $\Xi_{1,8}$ we use the following lattice-QCD [202, 203] and naive dimensional analysis [204, 205] (NDA) results, respectively,

$$\begin{aligned} d_n^{d_q} &= -0.22(3) d_u(M_{\text{QCD}}) + 0.74(7) d_d(M_{\text{QCD}}) \ , \\ d_n^{\Xi} &= \mathcal{O}\left(\frac{e M_{\text{QCD}}}{(4\pi)^2}\right) \text{Im}\, \Xi_{1,8}(M_{\text{QCD}}). \end{aligned} \tag{3.13}$$

The results for $d_n^{d_q}$ is in agreement with QCD sum-rule results [206, 125], while the estimate of d_n^{Ξ} agrees with the results of Refs. [92, 129, 156]. Combining Table 3.2, Eq. (3.12), and the central values in Eq. (3.13) with the upper limit on the nEDM, $|d_n| \leq 2.9 \times 10^{-26} e\,\text{cm}$ [150], and the upper limit on eEDM from ThO, $|d_e^{\text{exp}}| \leq 8.7 \times 10^{-29} e\,\text{cm}$ [154], we finally obtain the bounds shown in Table 3.3.

3.4.2 Two-coupling analysis

In a specific BSM scenario one might expect several dimension-six operators to be generated at the same time. To investigate the possibility of cancellations between these couplings we perform a two-coupling analysis. Because the contributions to hadronic EDMs, especially of $\Xi_{1,8}$, have significant uncertainties, we use conservative values for the relevant matrix elements.

We first consider the interplay between C_{uW} and C_{dW}. To constrain these couplings simultaneously, both the bounds on the nEDM and on the Hg EDM are needed. The dominant contribution to EDM of diamagnetic atoms, such as ^{199}Hg, arises from the

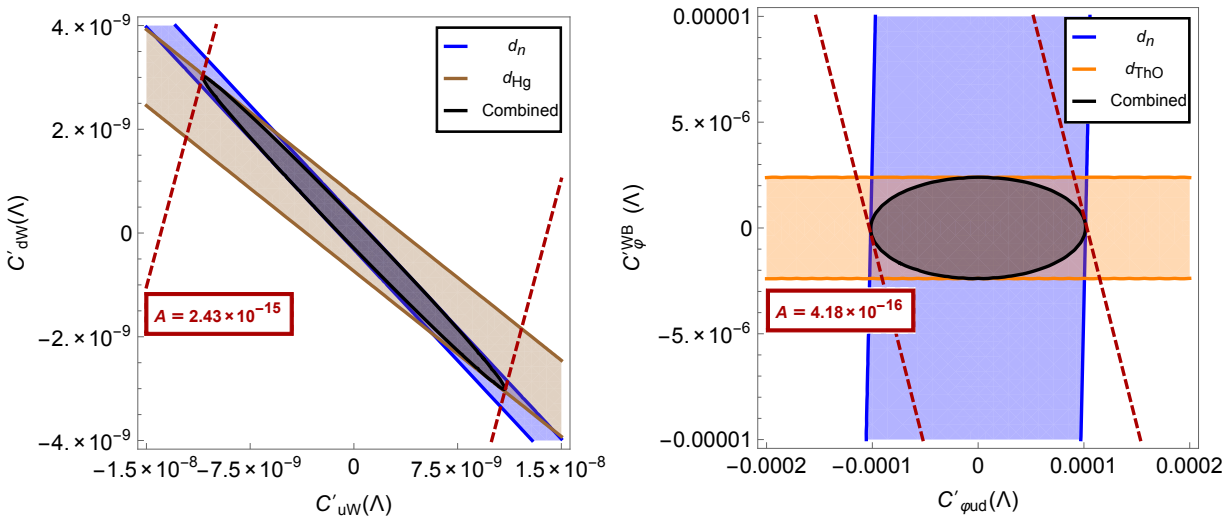

(a) (b)

Figure 3.3: Exclusion plots of the two-coupling analysis. The dotted line gives the bound on the radiative β-decay asymmetry defined in Eq. (3.5).

Schiff moment S [207]. For the Hg EDM, we have [208]

$$\begin{aligned} d_{\rm Hg} &= \mathcal{A}\Big[1.9(1)d_n + 0.20(6)d_p\Big]\,{\rm fm}^2\ , \\ d_p &= 0.74(7)d_u(M_{\rm QCD}) - 0.22(3)d_d(M_{\rm QCD})\ . \end{aligned} \tag{3.14}$$

where the range of the atomic screening is $\mathcal{A} = -2.8(6)\times 10^{-4}{\rm fm}^{-2}$ [209]. In principle the Hg EDM also depends on the isoscalar and isovector pion-nucleon couplings $\bar{g}_{0,1}$, however, these are not generated by the $C_{uW,dW}$ couplings. Using the smallest allowed absolute values of the matrix elements, and $|d_{\rm Hg}| < 2.6\times 10^{-29}$ (90% C.L.) [151] we then obtain Fig. 3.3a.

The second case we consider is that mainly $C_{\varphi WB}$ and $C_{\varphi ud}$ are generated. For the calculation of the nEDM in terms of $d_{u,d}$ we again use Eq. (3.13) with the smallest allowed absolute values for the matrix elements. For the contribution of $\Xi_{1,8}$ we use the NDA estimate in Eq. (3.13), and conservatively (and somewhat arbitrarily) assign an uncertainty of a factor of 10 to it. The Hg EDM also depends $\Xi_{1,8}$ via the isovector pion-nucleon coupling, $\bar{g}_1$, which is generated by $C_{\varphi ud}$. However, there is a large (NDA) uncertainty related to the size of the generated $\bar{g}_1$, as well as a large (nuclear) uncertainty related to the contribution of $\bar{g}_1$ to $d_{\rm Hg}$ [209]. Therefore, in this case, the best constraints come from d_n and d_e. These constraints are shown in Fig. 3.3b.

3.5 Conclusion

Radiative β decay offers the possibility to study a *spin-independent* T-violating triple-correlation coefficient K. We have considered T-violating new physics arising above the electroweak scale that contributes to this correlation. The leading effects of the new sources of T violation can then be described in terms of dimension-six operators in an

EFT framework. We show that the dimension-six operators that contribute to K also contribute to the spin-dependent EDMs. The EDM limits therefore stringently constrain these operators. In fact, comparing the EDM bounds in Table 3.2 to Eq. (3.9), we find that improving the EDM bounds would require a measurement of the neutron asymmetry better than 10^{-16}. This accuracy cannot be reached in present experiments. In deriving these constraints we have assumed that only one coupling at a time contributes. In principle, therefore, the bounds can be weakened in specific models by arranging cancellations in the EDMs between different contributions. To investigate this possibility we also performed a two-coupling analysis, taking the uncertainties related to the neutron and Hg EDMs into account. Figure 3.3 shows the constraints on the radiative β-decay asymmetry resulting from this analysis. Improving these constraints still requires a measurement of this asymmetry better than 10^{-15}. Therefore, significantly weakening or evading these constraints requires more complicated cancellations than those possible in the scenarios considered in Figure 3.3, which would imply large amounts of fine-tuning. We only consider new physics above the electroweak scale, such that in general our bounds do not apply for models involving new light degrees of freedom. In conclusion, barring very finely tuned scenarios of BSM physics, the T-odd correlation K is not "EDM safe" when considering CP-violating dimension-6 operators arising above the electroweak scale.

Chapter 4

Lorentz symmetry breaking in β decay

Lorentz violation can be parametrized by adding a general tensor $\chi^{\mu\nu}$ to the Minkowski metric. In this chapter we further discuss the possibilities to improve the current bounds on $\chi^{\mu\nu}$, discussed in Sec. 2.6. We focus on the possibilities for β decay and electron capture. Tests of Lorentz invariance in kaon and pion decay are discussed in Chapter 5.

4.1 Concurrent tests of Lorentz invariance in β-decay experiments

Modern experiments on neutron and allowed nuclear β decay search for new semileptonic interactions, beyond the "left-handed" electroweak force. We show that ongoing and planned β-decay experiments, with isotopes at rest and in flight, can be exploited as sensitive tests of Lorentz invariance. The variety of correlations that involve the nuclear spin, the direction of the emitted β particle, and the recoil direction of the daughter nucleus allow for relatively simple experiments that give direct bounds on Lorentz violation. The pertinent observables are decay-rate asymmetries and their dependence on sidereal time and the dependence of the lifetime on the speed and direction of the source's motion. We discuss the potential of several asymmetries that together cover a large part of the parameter space for Lorentz violation in the gauge sector. High counting statistics is required.

4.1.1 Motivation

β decay is a recognized probe of symmetry violation in the electroweak interaction. Because of the wide choice of β emitters and the various observables that can be measured with high precision, one can select isotopes that are tailored to specific searches for particle physics beyond the Standard Model (SM) [14, 22, 95, 192]. Over the years, strong limits were put on scalar, right-handed vector and axial vector, and tensor contributions to the

Published: K. K. Vos, H. W. Wilschut, and R. G. E. Timmermans, Phys. Rev. C **92**, 052501(R) (2015).

semileptonic process $d \to u + e^- + \overline{\nu}_e$. Recently, it was shown that β decay is moreover a unique laboratory for testing Lorentz invariance in the weak gauge [17, 21, 172, 192] and neutrino [39, 186] sectors. Such studies are strongly motivated by ideas how to unify the SM and general relativity in a theory of "quantum gravity" [27, 210]. We demonstrate here that ongoing and planned β-decay experiments can, with moderate modifications in the setup and data analysis, be exploited to improve the existing limits on Lorentz violation.

We base our studies on the theoretical framework for Lorentz and CPT violation developed in Refs. [17, 21] for β decay and in Ref. [172] for orbital electron capture. It covers effects from e.g. a modified low-energy W-boson propagator $\langle W^{\mu+} W^{\nu-} \rangle = -i(g^{\mu\nu}+\chi^{\mu\nu})/M_W^2$. The tensor components $\chi^{\mu\nu}$ were limited with data on allowed [173, 38, 180, 174] and forbidden [21] β decay, pion decay [175, 176], nonleptonic kaon decay [178], and muon decay [177]. The best upper bounds were derived from experiments on forbidden β decays [21], while a first experiment on allowed β decay with polarized nuclei gave additional, partly complementary information [38, 180]. These results were translated into bounds on Higgs- and W-boson parameters of the Standard Model Extension (SME) [29, 16, 37], the general effective field theory for Lorentz and CPT violation at low energies.

The allowed-β-decay rate with Lorentz violation was derived in Ref. [17] and given in Eq. (2.84). Compared to ordinary β decay, it contains additional, frame-dependent correlations between the momenta and spins of the nuclei and leptons and the tensor χ. The correlations involve linear combinations of the components $\chi^{\mu\nu}$, depending on the type of β decay, Fermi, Gamow-Teller, or mixed. While many of these correlations are hard to measure, a few appear relatively straightforward. We discuss a number of experiments on neutron and allowed nuclear β decay that can give competing bounds on Lorentz violation. The pertinent observables are all rather simple asymmetries recorded with sidereal-time stamps. We also consider the β decay of nuclei in flight, e.g. at proposed β-beam facilities, as a way to increase the sensitivity. We end with recommendations how to further explore Lorentz violation in weak decays.

4.1.2 Decay rate

We assume that Lorentz violation comes from propagator corrections and neglect momentum-dependent terms in χ, which are suppressed by powers of the W-boson mass. Hermiticity of the Lagrangian then implies that $\chi^{\mu\nu} = (\chi^*)^{\nu\mu}$. We also neglect here terms with only neutrino-momentum or neutrino-spin correlations, which are important in electron capture [172] (Sec. 4.2), but in β decay do not contain more information than the easier to measure β-particle correlations. In addition, we ignore for the moment terms proportional to the spin factor $\bar{\Lambda}_{J'J}$ [17], which is associated with higher-order spin correlations ($\bar{\Lambda}_{J'J} = 0$ for unpolarized and spin-1/2 nuclei).

With these simplifications the β-decay rate [17][1], in the rest frame of the parent nucleus, reduces to ($\hbar = c = 1$)

[1] In Eq. (18) in Ref. [17] it should read $w_3^l = -x\chi_r^{0l} + \breve{g}(\chi_r^{0l} + \tilde{\chi}_i^l)$. This also corrects Eq. (38) in Ref. [17].

X_r^{00}	X_r^{0l}	X_r^{kl}	X_i^{0l}	$\tilde{X}_i^k$
10^{-6}	10^{-8}	10^{-6}	–	10^{-8}

Table 4.1: Statistical precision for the components $X^{\mu\nu}$ required to compete with the existing upper bounds from forbidden β decay [21]. The components X_i^{0l} are unconstrained at present.

$$\begin{aligned} dW &= dW_0 \left\{ 1 + 2a\chi_r^{00} + 2\left(-a\chi_r^{0l} + \breve{g}\tilde{\chi}_i^l\right)\frac{p_e^l}{E_e} \right. \\ &\quad + \left(\left[a + 2\breve{a}\chi_r^{00}\right]\delta_{lm} - 4\breve{g}\chi_r^{lm}\right)\frac{p_e^l p_\nu^m}{E_e E_\nu} + 2a\chi_i^{0k}\frac{(\vec{p}_e \times \vec{p}_\nu)^k}{E_e E_\nu} \\ &\quad \left. + \frac{\langle J^k\rangle}{J}\left(-2\breve{L}\tilde{\chi}_i^k + \left[\left(A + B\chi_r^{00}\right)\delta_{kl} - B\chi_r^{kl}\right]\frac{p_e^l}{E_e}\right) - A\chi_i^{0k}\frac{(\langle\vec{J}\rangle \times \vec{p}_e)^k}{JE_e}\right\} \end{aligned} \quad (4.1)$$

where $dW_0 = |\vec{p}_e|E_e(E_e - E_0)^2 dE_e d\Omega_e d\Omega_\nu F(E_e, \pm Z)\bar{\xi}/(2\pi)^5$, $\vec{p}_{e(\nu)}, E_{e(\nu)}$ are the momentum and energy of the β particle (electron or positron) and neutrino, and $\langle\vec{J}\rangle$ is the expectation value of the spin of the parent nucleus. $F(E_e, \pm Z)$ is the usual Fermi function, with Z the atomic number of the daughter nucleus, and the upper (lower) sign holds for $\beta^{-(+)}$ decays; $\xi = 2g_V^2\langle 1\rangle^2 + 2g_A^2\langle\sigma\rangle^2$. The subscripts r and i denote the real and imaginary parts of $\chi = \chi_r + i\chi_i$, $\tilde{\chi}_i^k = \epsilon^{klm}\chi_i^{lm}$, and k, l, m are spatial directions. The coefficients a, A, and B are standard in β decay [24, 14], while $\breve{a}$, $\breve{g}$, and $\breve{L}$ multiply correlations that are Lorentz violating [17]. They are defined by

$$a = \left(1 - \tfrac{1}{3}\rho^2\right)/\left(1 + \rho^2\right) , \quad (4.2a)$$

$$A = \left(\mp\lambda_{JJ'}\rho^2 + 2\delta_{JJ'}\sqrt{J/(J+1)}\rho\right)/\left(1 + \rho^2\right) , \quad (4.2b)$$

$$B = \left(\pm\lambda_{JJ'}\rho^2 + 2\delta_{JJ'}\sqrt{J/(J+1)}\rho\right)/\left(1 + \rho^2\right) , \quad (4.2c)$$

$$\breve{a} = \left(1 + \tfrac{1}{3}\rho^2\right)/\left(1 + \rho^2\right) , \quad (4.2d)$$

$$\breve{g} = \tfrac{1}{3}\rho^2/\left(1 + \rho^2\right) , \quad (4.2e)$$

$$\breve{L} = \pm\tfrac{1}{2}\lambda_{JJ'}\rho^2/\left(1 + \rho^2\right) , \quad (4.2f)$$

where $\rho = |g_A||M_{GT}|/(g_V|M_F|)$ is the ratio between the Gamow-Teller and Fermi matrix elements. The value of the spin factor $\lambda_{JJ'}$, where $J\,(J')$ is the initial (final) nuclear spin, is $\lambda_{JJ'} = 1$ for $J' = J - 1$, $1/(J+1)$ for $J' = J$, and $-J/(J+1)$ for $J' = J + 1$.

4.1.3 Observables

There are 15 independent tensor components $\chi^{\mu\nu}$. It is standard to translate the tensor χ to the Sun-centered reference frame, in which it is denoted by X, and report limits for

the components $X^{\mu\nu}$ [37]. The best upper bounds on (linear combinations of) $X^{\mu\nu}$ are $\mathcal{O}(10^{-6})$-$\mathcal{O}(10^{-8})$, derived [21] from pioneering forbidden-β-decay experiments [181, 182] that used strong sources. In case there are accidental cancellations, the bounds on the individual components could be significantly weaker and range from $\mathcal{O}(10^{-4})$-$\mathcal{O}(10^{-6})$ [211]. The order-of-magnitude precision required to improve the existing bounds on the various components $X^{\mu\nu}$ is summarized in Table 4.1. A statistical precision of 10^{-n} requires at least $\mathcal{O}(10^{2n})$ events. This would require one year of data taking with a source of 1 Curie for an experiment of the type performed in Ref. [181]. An alternative option is electron capture, which allows experiments at high rates and low dose [172]. We focus here on the possibilities to improve the existing bounds in allowed β decay.

From Eq. (5.9) we derive asymmetries that are proportional to specific components $\chi^{\mu\nu}$. Asymmetries are practical to measure and ideal to control systematic errors. Expressed in terms of $X^{\mu\nu}$, they oscillate in time with the sidereal rotation frequency $\Omega = 2\pi/(23\text{h}\,56\text{m})$ of Earth and depend on the colatitude ζ of the site of the experiment. These sidereal-time variations of the observables are a unique feature of Lorentz violation, and help to separate the desired signal from systematic errors. They also distinguish Lorentz violation from effects due to *e.g.* scalar or tensor interactions, which would produce deviations from SM predictions that are independent of Earth's orientation.

(i) The simplest way to study Lorentz violation is to integrate over the neutrino direction and measure the dependence of the decay rate on the direction of the β particle. The highest sensitivity can be reached in pure Fermi or Gamow-Teller decays. For Fermi decays, the experimental observable is the asymmetry

$$A_F = \frac{W_F^+ - W_F^-}{W_F^+ + W_F^-} = -2\chi_r^{0l}\beta\hat{p}_e^l \,, \tag{4.3}$$

where $\beta = |\vec{p}_e|/E_e$ and $W_F^\pm$ is the rate of β particles measured in the $\pm\hat{p}_e$-direction. For Gamow-Teller decays of unpolarized nuclei, the analogous asymmetry is

$$A_{GT} = \frac{W_{GT}^+ - W_{GT}^-}{W_{GT}^+ + W_{GT}^-} = \tfrac{2}{3}\left(\chi_r^{0l} + \tilde{\chi}_i^l\right)\beta\hat{p}_e^l \,. \tag{4.4}$$

These two asymmetries are complementary and give direct bounds on χ_r^{0l} and $\tilde{\chi}_i^l$. Mixed decays are slightly less sensitive, e.g. for neutron β decay, with $\rho = \sqrt{3}\,|g_A|$, where $g_A \simeq -1.275$ [69, 68], the asymmetry is $A_n = (0.21\chi_r^{0l} + 0.55\tilde{\chi}_i^l)\beta\hat{p}_e^l$.

Figure 4.1 illustrates the sidereal-time dependence of the asymmetry A_F for three different observation directions. When the β particles are detected parallel to Earth's rotation axis, no oscillation is observed. Observation of the β particles perpendicular to the rotation axis, i.e. east-west, gives a sidereal-time variation. When the β particles are observed in the up-down ($\uparrow\downarrow$) direction, this oscillation has a constant offset. Systematic errors can result in a finite offset, and therefore observation in the direction perpendicular to the rotation axis is favored. The asymmetries should preferably be measured in a rotating setup [181] to reduce systematic errors. Alternatively, a multi-detector setup with appropriate symmetry can exploit the full polar and azimuthal dependence as shown in Fig. 4.1, while reducing the counting rates of the individual detectors. An experiment with a duration of one year can use diurnal variations to reduce systematic errors.

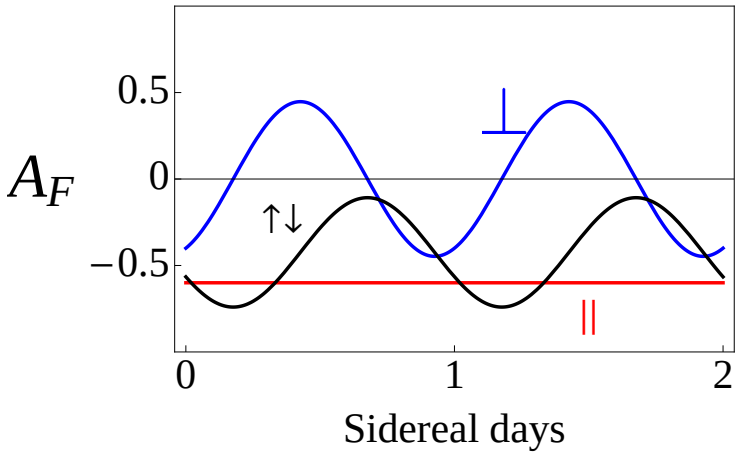

Figure 4.1: The sidereal time dependence of the asymmetry A_F in Eq. (4.3), for $X_r^{0x} = 0.1$, $X_r^{0y} = 0.2$, $X_r^{0z} = 0.3$, and colatitude $\zeta = 45°$. For β particles observed parallel ($\|$) to Earth's rotation axis A_F is constant. Observation in the $\uparrow\downarrow$ (up-down) direction or perpendicular ($\perp$) to the rotation axis results in an oscillation of A_F with sidereal time.

There are ongoing efforts to improve the bounds on tensor currents in β decay. A promising observable for this purpose is the energy spectrum of the β particles [111]. The Gamow-Teller decays of ^{6}He [106, 212] and ^{45}Ca [111] are currently under consideration. Such experiments require high statistics and accuracy. The ^{6}He facility promises to produce 10^{10} particles/s, but it remains to be seen how such a beam can be used for Lorentz-violation measurements [212]. Isotopes such as ^{32}P, ^{33}P, ^{35}S, and ^{63}Ni are also of interest, because they have clean ground-state-to-ground-state β^--transitions and low Q-values. For example, conveniently-shaped ^{63}Ni sources of 1GBq are commercially available. Such sources have minimal contributions of secondary radiation that can complicate the measurements. Moreover, strong sources can be produced in reactors. For the Fermi asymmetry A_F, any of the superallowed $0^+ \to 0^+$ decays [43, 213] can be considered. We recommend that in these experiments the asymmetries A_F of Eq. (4.3) and A_{GT} of Eq. (4.4) are measured concurrently, with sidereal-time stamps.

(*ii*) With polarized nuclei one can measure the correlations that involve the nuclear spin. The simplest of these is the spin asymmetry

$$A_J = \frac{W^\uparrow - W^\downarrow}{W^\uparrow + W^\downarrow} = -2\breve{L}\tilde{\chi}_i^k P \hat{J}^k \ , \tag{4.5}$$

where $\hat{J}$ is the unit vector in the direction of the parent spin, P is the degree of nuclear polarization, and $W^{\uparrow(\downarrow)}$ is the integrated decay rate in the $\pm\hat{J}$-directions. For pure Gamow-Teller decays, $\breve{L} = \frac{1}{2}B = -\frac{1}{2}A$. Isotopes for which $\lambda_{JJ'} = 1$ are optimal.

The first dedicated experiment to search for Lorentz violation in allowed β decay measured A_J in the β^+ decay of ^{20}Na [38]. The result of the most recent measurement is $|\tilde{\chi}_i^{x,y}| < 5\times10^{-4}$ with 90% confidence [180]. Data for polarized-neutron decay are currently being analyzed [174, 214]. When the sidereal-time dependence of A_J is measured, it is not necessary to know A and P with high precision. If the polarization is not exactly equal in the two directions, A_J will show an offset, which is independent of the sidereal frequency

as long as the polarization can be kept independent of Ω. Still, a measurement of the β asymmetry A_{GT}, as discussed above, is probably preferable for improving the bounds on $\tilde{\chi}_i^k$.

(*iii*) The components χ_i^{0k}, for which there are no bounds available yet, can be accessed through the correlations of $\hat{J}\times\hat{p}_e$ or $\hat{p}_e\times\hat{p}_\nu$ and a component of χ. The first correlation can be measured with the asymmetry

$$A_{\beta\nu}=\frac{W_L^\uparrow W_R^\downarrow-W_R^\uparrow W_L^\downarrow}{W_L^\uparrow W_R^\downarrow+W_R^\uparrow W_L^\downarrow}=4\left(a\chi_i^{0k}\epsilon^{klm}-2\breve{g}\chi_r^{lm}\right)\beta\hat{p}_e^l\hat{p}_\nu^m\ , \tag{4.6}$$

where $W_{L,R}$ is obtained by measuring the β particles in the opposite left (L) and right (R) $\hat{p}_e$-directions, while the recoiling nucleus is detected in the perpendicular $\uparrow$ ($\downarrow$) direction. For this asymmetry, pure Fermi decays, with $a=1$ and $\breve{g}=0$, are preferred. Experiments that measure both the β and the neutrino direction are thus of interest. Ref. [59] e.g. reports a search for a deviation from the SM prediction $a=1$ for the β-ν correlation in ^{38m}K, with an error on a of order $\mathcal{O}(10^{-3})$, which would be the corresponding limit for χ_i^{0k}.

With polarized nuclei, χ_i^{0k} can be measured from the asymmetry between the nuclear spin and the β particle,

$$A_{J\beta}=\frac{W_L^\uparrow W_R^\downarrow-W_R^\uparrow W_L^\downarrow}{W_L^\uparrow W_R^\downarrow+W_R^\uparrow W_L^\downarrow}=-2\left(A\chi_i^{0m}\epsilon^{mkl}+B\chi_r^{kl}\right)P\hat{J}^k\beta\hat{p}_e^l\ , \tag{4.7}$$

where now $W_{L,R}$ is the rate with the β particles in the opposite left (L) and right (R) $\hat{p}_e$-directions and the nuclei polarized in the perpendicular $\uparrow$ ($\downarrow$) $\hat{J}$-direction. Equation (4.7) holds for Gamow-Teller and mixed decays. Gamow-Teller decays with $\lambda_{JJ'}=1$ are preferred.

The bounds from forbidden β decay give $\left|\chi_r^{kl}\right|<\mathcal{O}(10^{-6})$ [21]. A measurement of $A_{J\beta}$ or $A_{\beta\nu}$ with a precision lower than 10^{-6}, therefore, translates to a bound on χ_i^{0k}. The sidereal-time variation of $A_{J\beta}$ and $A_{\beta\nu}$ is similar to that shown in Fig. 4.1. To reduce systematic errors $\hat{J}\times\hat{p}_e$ or $\hat{p}_e\times\hat{p}_\nu$ should point perpendicular to Earth's rotation axis. $A_{J\beta}$ can possibly be obtained in polarized-neutron decay by reanalyzing the data of Ref. [174]. Measuring the asymmetries better than 10^{-6} requires coincident event rates exceeding 3×10^4/s for a year, but will then also improve the bounds on χ_r^{kl}.

4.1.4 Exploiting Lorentz boosts

So far we discussed β decay of nuclei at rest. The required event rate in these measurements is a challenge. In forbidden β decays one can benefit from an enhancement of Lorentz violation of one order of magnitude [21]. A much larger enhancement can be obtained when the decaying particle is in flight. Consider specifically the total decay rate, which in the rest frame depends only on the isotropic term in Eq. (4.1),

$$W/W_0=1+2a\chi_r^{00}\ , \tag{4.8}$$

where W_0 is the SM decay rate and $a=1$ ($-1/3$) for Fermi (Gamow-Teller) decays. The component χ_r^{00} can *e.g.* be measured from the ratio between the longitudinal β

polarization, $P_\beta = (1 + 2a\chi_r^{00})\, G\beta$, for Fermi and Gamow-Teller decays, where $G = \mp 1$ [24, 14]. Comparing the best value $P_F/P_{GT} = 1.0010(27)$ [63, 64] to the SM prediction $P_F/P_{GT} = 1$ gives $-1.3 \cdot 10^{-3} < X_r^{00} < 2.0 \cdot 10^{-3}$ with 90% confidence, which is a much weaker bound than the one obtained for forbidden β decay [21], and hard to improve with nuclei at rest.

The decay rate in flight depends on the velocity $\vec{v} = v\hat{v}$ of the nucleus that results from a Lorentz boost. In terms of the components $X^{\mu\nu}$ in the Sun-centered frame one has $\chi_r^{00} = \gamma_r^2 \left(X_r^{00} - 2vX_r^{0l}\hat{v}_l + X_r^{kl} v^2 \hat{v}_k \hat{v}_l \right)$, where $\gamma_r = 1/\sqrt{1-v^2}$ is the Lorentz factor. When the velocity $\hat{v}$ is perpendicular to Earth's rotation axis (east-west) one finds

$$\begin{aligned} \chi_r^{00} &= \gamma_r^2 \Big(X_r^{00} + \tfrac{1}{2} v^2 \left[X_r^{xx} + X_r^{yy} \right] + 2vX_r^{0x} \sin\Omega t - 2vX_r^{0y} \cos\Omega t \\ &\quad - v^2 X_r^{xy} \sin 2\Omega t - \tfrac{1}{2} v^2 \left[X_r^{xx} - X_r^{yy} \right] \cos 2\Omega t \Big) \ , \end{aligned} \tag{4.9}$$

which is enhanced by a factor γ_r^2. The components $X_r^{\mu\nu}$ can be fitted to the sidereal-time dependence of the measured decay rate. Alternatively, one can measure the decay rate at time t and 12 hours later, and isolate X_r^{0l} via the "asymmetry"

$$A_t = \frac{W(\Omega t) - W(\Omega t + \pi)}{W(\Omega t) + W(\Omega t + \pi)} = 4a\, v \gamma_r^2 \left(X_r^{0x} \sin\Omega t - X_r^{0y} \cos\Omega t \right) \ , \tag{4.10}$$

while X_r^{kl} can be obtained by measuring at intervals of 6 hours, with

$$\begin{aligned} A_{2t} &= \frac{W(\Omega t) - W(\Omega t + \frac{1}{2}\pi) + W(\Omega t + \pi) - W(\Omega t + \frac{3}{2}\pi)}{W(\Omega t) + W(\Omega t + \frac{1}{2}\pi) + W(\Omega t + \pi) + W(\Omega t + \frac{3}{2}\pi)} \\ &= -a\, v^2 \gamma_r^2 \left(\left[X_r^{xx} - X_r^{yy} \right] \cos 2\Omega t + 2X_r^{xy} \sin 2\Omega t \right) \ , \end{aligned} \tag{4.11}$$

which oscillates only with the double frequency 2Ω.

The γ_r^2 enhancement in Eqs. (4.9), (4.10), and (4.11) can be exploited at a β-beam facility planned for neutrino physics [183]. A good nucleus for such a facility is ^{6}He, for which the production rates are estimated at 10^{12}/s with $\gamma_r = 100$ [215]. A possible setup for a β-beam facility that uses the proton synchrotrons at CERN is discussed in Refs. [215, 183].

Of course, any weakly-decaying particle in flight can be used, provided the coefficient a in Eq. (4.8) can be calculated reliably. Nonleptonic decays of strange hadrons such as kaons are problematic [178], but decays of heavy quarks do not have this drawback. Leptonic and semileptonic decays are clearly preferable. For fast-moving pions [216] bounds of $\mathcal{O}(10^{-4})$ on $\chi^{\mu\nu}$ were obtained [175]. Semileptonic kaon decays have been studied at the SPS at CERN [217] with $\gamma_r \simeq 150$ and will be part of the background in the NA62 experiment. LHCb, designed to observe decays at $\gamma_r \gtrsim 10$, is serendipitously oriented perpendicular to Earth's rotation axis. For all accelerator studies, the precise normalization of the decay rate as function of sidereal time is necessary for a concurrent test of Lorentz invariance.

4.1.5 β-γ correlations

We have only considered cases where the anisotropic decay rate is observed in the emission direction of the β particles and/or is associated with the polarization direction of

the parent nucleus. The anisotropy can also be observed from γ rays when an excited state in the daughter nucleus is populated. In Gamow-Teller transitions the daughter nucleus is left in a polarized state that reflects the degree of anisotropy of the emission. When measuring the γ-decay angular distribution this anisotropy can be observed as a residual alignment. Inspection of Eq. (5.9) shows that this will be the case for the term $-2\breve{L}\tilde{\chi}_i^k \hat{J}^k$. Clearly, such a measurement will have lower sensitivity compared with the direct measurements discussed above. The last line of Eq. (5.9) can also be accessed by measuring β-γ correlations. The last term is relevant because it contains the "missing" components χ_i^{0k}. In this case the lower sensitivity may be compensated by an efficient setup. To obtain the actual expressions and the corresponding asymmetries the terms proportional to $\bar{\Lambda}_{J'J}$ [17] have to be added to Eq. (5.9). The evaluation depends on the particular details of detection method and will be considered when the need arises.

4.1.6 Conclusion

The breaking of Lorentz invariance in the weak interaction can be probed in relatively simple allowed-β-decay experiments. We propose to measure a number of decay-rate asymmetries as function of sidereal time, which together can constrain all Lorentz-violating gauge components. Measurements of the β-decay asymmetry in Fermi and Gamow-Teller decays, Eq. (4.3) and Eq. (4.4), give direct bounds on χ_r^{0l} and $\tilde{\chi}_i^k$. The most complicated experiments require the measurement of a correlation between two observables, as in Eq. (4.6) or Eq. (4.7). The components χ_i^{0k} are still unconstrained and these measurements will give the first bounds. In addition, we point out the potential of β beams and LHCb for tests of Lorentz invariance. Ultimately, the experiments should aim to improve the existing forbidden-β-decay limits starting at $\mathcal{O}(10^{-6})$, which requires high-intensity sources and excellent control of systematic uncertainties. As we have shown, this can go hand-in-hand with high-precision allowed-β-decay experiments that search for new semileptonic physics. Such efforts are, therefore, of considerable general interest.

4.2 Testing Lorentz invariance in orbital electron capture

Searches for Lorentz violation were recently extended to the weak sector, in particular neutron and nuclear β decay [17]. From experiments on forbidden β-decay transitions strong limits in the range of 10^{-6}-10^{-8} were obtained on Lorentz-violating components of the W-boson propagator [21]. In order to improve on these limits strong sources have to be considered. In this section we study isotopes that undergo orbital electron capture and allow experiments at high decay rates and low dose. We derive the expressions for the Lorentz-violating differential decay rate and discuss the options for competitive experiments and their required precision.

4.2.1 Introduction

Motivated by insights that Lorentz and CPT invariance can be violated in unifying theories of particle physics and quantum gravity, a theoretical framework was developed in Refs. [17, 21] to study Lorentz violation in the weak gauge sector in neutron and (allowed and forbidden) nuclear β decay. This approach, which parametrizes Lorentz violation by adding a complex tensor $\chi^{\mu\nu}$ to the Minkowski metric, includes a wide class of Lorentz-violating effects, in particular contributions from a modified low-energy W-boson propagator $\langle W^{\mu+}W^{\nu-}\rangle = -i(g^{\mu\nu} + \chi^{\mu\nu})/M_W^2$ or from a modified vertex $\Gamma^\mu = (g^{\mu\nu} + \chi^{\mu\nu})\gamma_\nu$. Limits on Lorentz violation were subsequently extracted from experiments on allowed [38, 173, 174] and forbidden [21] β decay (see Sec. 2.6), pion [175, 176] (Sec. 5.2), kaon [178] (Sec. 5.1), and muon decay [177].

The strongest bounds on components $\chi^{\mu\nu}$ were obtained [21] from forbidden-β-decay experiments [181, 182] and range from 10^{-6}-10^{-8} on different linear combinations. We also discussed these bounds in Section 2.6. These bounds were translated in limits on parameters of the Standard Model Extension [16], which is the most general effective field theory for Lorentz and CPT violation at low energy. Specifically, $\chi^{\mu\nu} = -k^{\mu\nu}_{\phi\phi} - i\,k^{\mu\nu}_{\phi W}/2g$ in terms of parameters in the Higgs and W-boson sector, where g is the SU(2) electroweak coupling constant [17]. The resulting bounds on linear combinations of $k^{\mu\nu}_{\phi\phi}$ and $k^{\mu\nu}_{\phi W}$ can be found in Ref. [21] and in the 2014 Data Tables in Ref. [37]. The best bounds from allowed β decays are $\mathcal{O}(10^{-2})$ [38, 174] and from pion decay $\mathcal{O}(10^{-4})$ [175].

When seeking further improvement, one should realize that the bounds from forbidden β decay benefited from the use of high-intensity sources. Such strong β-decay sources, however, are hazardous because they have high disintegration rates (Bq) and high doses (Sv). In this section we consider orbital electron capture [218], because the pertinent sources can give high decay rates at a low dose. We first derive the theoretical expression for the differential decay rate including Lorentz violation. Next, we discuss the experimental possibilities to constrain the various components $\chi^{\mu\nu}$. Finally, we explore which isotopes are suitable for a competitive measurement. We end with our conclusions.

Published: K. K. Vos, H. W. Wilschut, and R. G. E. Timmermans, Phys. Rev. C **91**, 038501 (2015).

4.2.2 Decay rate

We consider allowed K-orbital electron capture [219] mediated by W-boson exchange with a propagator that includes $\chi^{\mu\nu}$. We follow the notation and conventions of Ref. [17] ($\hbar = c = 1$). The derivation of the two-body capture decay rate is similar to the calculation of allowed β decay [17], but with the electron in a bound state with binding energy $|E_K|$. Since Lorentz violation results in unique experimental signals, we restrict ourselves to the allowed approximation with a nonrelativistic electron wave function with $\psi_e(\vec{r}=0) = \sqrt{Z^3/(\pi a_0^3)}\,\chi_{s_e}$, where Z is the atomic number of the parent nucleus, $a_0 = 1/(\alpha m_e)$ is the Bohr radius, and χ_{s_e} is a Pauli spinor. The neutrino is emitted with momentum $\vec{p}_\nu$ with $|\vec{p}_\nu| = E_\nu$ and the recoiling daughter nucleus has momentum $\vec{p}_r = -\vec{p}_\nu$ and kinetic energy T_r. Because $E_\nu = Q - |E_K| - T_r \simeq Q$, the Q-value of the reaction, the recoil energy is $T_r \simeq Q^2/(2M_r)$, which is typically 1-10 eV.

The differential decay rate is given by

$$dW = \frac{\delta(E_\nu - Q)}{(2\pi)^2 2E_\nu} N_K \frac{1}{2} \sum_{s_e,s_\nu} |\mathcal{M}|^2 d^3p_\nu \ , \tag{4.12}$$

with $N_K = 2$ the number of K-shell electrons. We define $\xi = 2C_V^2\langle 1\rangle^2 + 2\,C_A^2\langle\sigma\rangle^2$, $x = 2C_V^2\langle 1\rangle^2/\xi$, $y = 2C_VC_A\langle 1\rangle\,\langle\sigma\rangle/\xi$, and $z = 1 - x = 2C_A^2\langle\sigma\rangle^2/\xi$, where $C_V = G_F\cos\theta_C/\sqrt{2}$ and $C_A \simeq -1.27\,C_V$ are the vector and axial-vector coupling constants; $M_F = \langle 1\rangle$ and $M_{GT} = \langle\sigma\rangle$ are the Fermi and Gamow-Teller reduced nuclear matrix elements. For a polarized source we find for the Lorentz-violating decay rate

$$\begin{aligned} dW &= dW^0\Big[\Big(1 + B\,\hat{p}_\nu\cdot\hat{J}\Big)/2 \\ &\quad + t + \vec{w}_1\cdot\hat{p}_\nu + \vec{w}_2\cdot\hat{J} + T_1^{km}\,\hat{J}^k\hat{J}^m + T_2^{kj}\,\hat{J}^k\hat{p}_\nu^j + S_1^{kmj}\,\hat{J}^k\hat{J}^m\hat{p}_\nu^j\Big] \ , \end{aligned} \tag{4.13}$$

where $dW^0 = (Z/a_0)^3E_\nu^2 d\Omega_\nu\,\xi/(2\pi^3)$, $\hat{p}_\nu = |\vec{p}_\nu|/E_\nu$, and $\hat{J}$ is the nuclear polarization axis. Latin indices run over the three spatial directions, with summation over repeated indices implied. The Lorentz-violating tensors for electron capture read, in terms of the components $\chi^{\mu\nu}$,

$$t = (a - c/2)\,\chi_r^{00} \ , \tag{4.14a}$$
$$w_1^j = -x\chi_r^{0j} - z(1 + 3\Lambda^{(2)}/2)(\tilde{\chi}_i^j - \chi_r^{j0})/3 \ , \tag{4.14b}$$
$$w_2^k = -y\Lambda_z(\chi_r^{k0} - \chi_r^{0k}) + z\Lambda^{(1)}\tilde{\chi}_i^k/2 \ , \tag{4.14c}$$
$$T_1^{km} = 3c\,\chi_r^{km}/2 \ , \tag{4.14d}$$
$$T_2^{kj} = A\chi_r^{00}\delta^{jk}/2 - z\Lambda^{(1)}(\chi_r^{jk} + \chi_i^{s0}\epsilon^{sjk})/2 + y\Lambda_z(\chi_r^{kj} + \chi_i^{0s}\epsilon^{sjk}) \ , \tag{4.14e}$$
$$S_1^{kmj} = -3c\,(\chi_r^{k0}\delta^{mj} - \chi_i^{ms}\epsilon^{sjk})/2 \ . \tag{4.14f}$$

The subscripts r and i denote the real and imaginary parts, respectively, of $\chi^{\mu\nu} = \chi_r^{\mu\nu} + i\chi_i^{\mu\nu}$, and $\tilde{\chi}^l = \epsilon^{lmk}\chi^{mk}$. The $V-A$ correlation coefficients [14, 24, 132] that appear are

$$a = (4x-1)/3 \ , \ c = z\Lambda^{(2)} \ , \ A = z\Lambda^{(1)} - 2y\Lambda_z \ , \ B = -z\Lambda^{(1)} - 2y\Lambda_z \ . \tag{4.15}$$

The angular-momentum coefficients $\Lambda^{(1)}$, $\Lambda^{(2)}$, and Λ_z are given in the Appendix 4.A. We absorbed a factor $\Lambda^{(2)}/3$ in c and a factor $\langle m\rangle/j$ in A and B [17].

Eq. (4.13) reduces to the simple $V-A$ expression for the electron-capture decay rate when the Lorentz-violating parameters are set to zero. In particular, the B term in the first line of Eq. (4.13) is the correlation between the spin of the parent nucleus and the recoil direction of the daughter nucleus discussed in Refs. [220, 221]. The second line of Eq. (4.13) gives Lorentz-violating, frame-dependent contributions to the decay rate.

4.2.3 Observables

From Eq. (4.13) we see that the possibilities to test Lorentz invariance in electron capture lie in measuring the decay rate as function of either the nuclear polarization or the recoil momentum, or both. We restrict ourselves to dimension-four propagator corrections, for which $\chi^{\mu\nu *}(p) = \chi^{\nu\mu}(-p)$ holds [17]. (The tensor $\chi^{\mu\nu}$ may contain higher-dimensional, momentum-dependent terms, but such terms are suppressed by at least one power of the W-boson mass.) Since χ is traceless, this gives a total of 15 independent parameters, of which at present only χ_i^{0l} are unconstrained. The χ_r^{00} term will not be considered, because it can only be accessed when comparing capture or β-decay rates between particles at rest and with a large Lorentz boost factor $\gamma \gg 1$. In addition, we specialize to the suitable isotopes (identified below), which decay by Gamow-Teller transitions, and for simplicity we assume that the source has vector polarization. This leaves

$$\begin{aligned} dW &= \frac{1}{2} dW^0 \Big[\Big(1 + B\, \hat{p}_\nu \cdot \hat{J} \Big) \\ &\quad - \left(\frac{2}{3} + \Lambda^{(2)} \right) (\tilde{\chi}_i^j - \chi_r^{j0}) \hat{p}_\nu^j + A \tilde{\chi}_i^k \, \hat{J}^k - A \chi_r^{jk} \hat{p}_\nu^j \hat{J}^k - A \chi_i^{s0} (\hat{p}_\nu \times \hat{J})^s \Big] \end{aligned} \tag{4.16}$$

where for pure Gamow-Teller decays $A = -B = \Lambda^{(1)}$. The different components $\chi^{\mu\nu}$ can be accessed by measuring asymmetries. We give three examples.

(*i*) χ_i^{jk} can be obtained from $\tilde{\chi}_i$, which can be measured from an asymmetry that depends on the nuclear polarization, *viz.*

$$\mathcal{A}_J = \frac{\tau^+ - \tau^-}{\tau^+ + \tau^-} = \frac{W^- - W^+}{W^+ + W^-} = -A \tilde{\chi}_i^k \, \hat{J}^k \ , \tag{4.17}$$

where A contains the degree of polarization of the source and $\tau^\pm$ and $W^\pm$ are the lifetime and decay rate, respectively, in two opposite polarization directions $\pm$. Such an experiment only requires to flip the spin of the sample and observe the change in decay rate. For a discussion on using the direction of polarization to reduce systematic errors, see Ref. [173]. In general, the observables must be expressed in a standard inertial frame, for example the Sun-centered frame [37]. In the laboratory frame $\mathcal{A}_J$ will vary with Ω, the angular rotation frequency of Earth, and the results depend on the colatitude ζ of the site of the experiment [17], *cf.* Fig. 4.2. In practice one searches for these variations as function of sidereal time in order to isolate the Lorentz-violating signal and to reduce systematical errors.

(*ii*) The asymmetry of the recoil emission direction in an unpolarized sample is given by

$$\mathcal{A}_r = \frac{W(-\hat{p}_\nu) - W(\hat{p}_\nu)}{W(-\hat{p}_\nu) + W(\hat{p}_\nu)} = \frac{2}{3} (\tilde{\chi}_i^j - \chi_r^{j0}) \hat{p}_\nu^j \ , \tag{4.18}$$

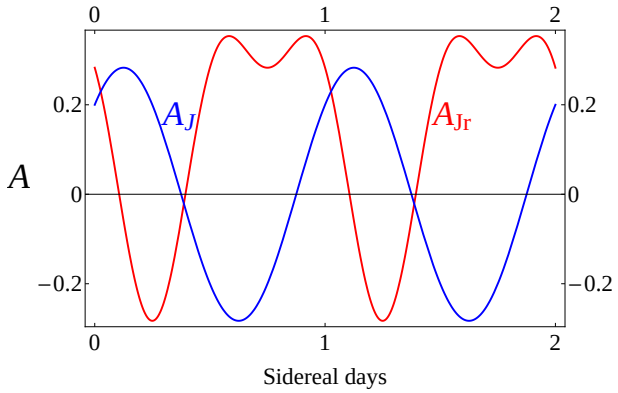

Figure 4.2: The oscillation of the asymmetries in Eqs. (4.17) and (4.19) as function of sidereal time, for $|\chi^{\mu\nu}| = 0.1$, $A = 1$, and colatitude $\zeta = 45°$. To avoid a constant offset of the signal, we assumed polarization in the east-west ($\hat{y}$) direction. For $\mathcal{A}_{Jr}$, $\hat{p}_\nu$ was taken in the laboratory $\hat{z}$ direction, *i.e.* perpendicular to Earth's surface.

which requires measuring the recoil direction $\hat{p}_r$ of the daughter nucleus. In this experiment it is necessary to rotate the setup as a whole to isolate the Lorentz-violating signal and reduce systematic errors, as was done in Refs. [181, 182]. $\mathcal{A}_J$ and $\mathcal{A}_r$ have the same sidereal frequency, but they can differ in phase.

(*iii*) When measurements of the recoil direction and polarization are combined, electron capture also offers the possibility to constrain the parameters χ_i^{s0}, for which no bounds have been set so far. Such an experiment should measure $\chi_i^{s0}(\hat{p}_\nu \times \hat{J})^s$, similar to a triple-correlation experiment to measure time-reversal violation in β decay. For example, the asymmetry

$$\mathcal{A}_{Jr} = \frac{W(-\hat{p}_\nu)^+ W(\hat{p}_\nu)^- - W(-\hat{p}_\nu)^- W(\hat{p}_\nu)^+}{W(-\hat{p}_\nu)^+ W(\hat{p}_\nu)^- + W(-\hat{p}_\nu)^- W(\hat{p}_\nu)^+} = 2A(\chi_r^{jk} + \chi_i^{s0}\epsilon^{sjk})\hat{p}_\nu^j \hat{J}^k \ , \tag{4.19}$$

where $\hat{p}_\nu$ is measured perpendicular to $\hat{J}$, contains both χ_r^{jk} and χ_i^{s0}. The first term also produces sidereal oscillations with frequency 2Ω. The difference for the asymmetries in Eqs. (4.17) and (4.19) is illustrated in Fig. 4.2.

4.2.4 Isotopes

The most stringent bounds found for a single component $\chi^{\mu\nu}$ so far are at a level of $\mathcal{O}(10^{-8})$, other components are at least as small as $\mathcal{O}(10^{-6})$ [21]. Most of the existing bounds concern linear combinations of several components $\chi^{\mu\nu}$, so that cancellations are in principle possible. Assuming maximal fine-tuning, the best bound for a real component is $\mathcal{O}(10^{-6})$ and for an imaginary term $\mathcal{O}(10^{-4})$ [211]. To achieve the highest statistical relevance very strong sources should be considered. In order to reach 10^{-9} statistical accuracy a source with a strength in the order of Curies (1 Curie-year $\simeq 10^{18}$ disintegrations) is required. For a high-statistics experiment a source that decays exclusively by electron capture is attractive, because the emission of ionizing radiation is strongly reduced: only X-ray emission and Auger electrons are involved. The most energetic radiation is due to internal bremsstrahlung, which is suppressed by at least the fine-structure constant.

Isotope	$t_{1/2}$ [s]	Q [keV]	$j^{\pi_i} \to j'^{\pi_f}$	
^{37}Ar	3.0×10^6	814	$\frac{3}{2}^+ \to \frac{3}{2}^+$	✓
^{49}V	2.9×10^7	602	$\frac{7}{2}^- \to \frac{7}{2}^-$	
^{55}Fe	8.6×10^7	231	$\frac{3}{2}^- \to \frac{5}{2}^-$	
^{71}Ge	9.9×10^5	232	$\frac{1}{2}^- \to \frac{3}{2}^-$	
^{131}Cs	8.4×10^5	355	$\frac{5}{2}^+ \to \frac{3}{2}^+$	✓
^{163}Ho	1.4×10^{11}	2.6	$\frac{7}{2}^- \to \frac{5}{2}^-$	✓
^{165}Er	3.7×10^4	376	$\frac{5}{2}^- \to \frac{3}{2}^-$	✓
^{179}Ta	5.7×10^7	106	$\frac{7}{2}^+ \to \frac{9}{2}^+$	
^{53}Mn	1.2×10^{14}	597	$\frac{7}{2}^- \to \frac{3}{2}^-$	
^{97}Tc	1.3×10^{14}	320	$\frac{9}{2}^+ \to \frac{3}{2}^+$	
^{137}La	1.9×10^{12}	621	$\frac{7}{2}^+ \to \frac{3}{2}^+$	
^{205}Pb	5.5×10^{14}	51	$\frac{5}{2}^- \to \frac{1}{2}^+$	

Table 4.2: Isotopes that decay exclusively by orbital electron capture to a stable ground state. The top eight are relatively short-lived species that decay via allowed transitions, the bottom four are long-lived isotopes that undergo forbidden transitions. ^{163}Ho is long-lived because of the very low Q-value. The isotopes check-marked in the last column can be polarized directly by optical pumping, or possibly also via an optically-pumped buffer gas.

A list of possible isotopes is given in Table 4.2. Which isotope is the most suitable depends on the detection and production method. The decay rate can be measured from the ionization current due to Auger processes and the shake-off of electrons that follows capture. This requires that the radioactive isotopes are available as atoms, possibly in a buffer gas. In this way one can polarize nuclei via optical pumping. The four isotopes for which this strategy is feasible are indicated in Table 4.2. To observe the nuclear polarization, internal bremsstrahlung can be used, which is anisotropic with respect to the spin direction [222, 223].

Because there are only four options we discuss the production of these isotopes separately:

- ^{37}Ar can be produced in a reactor via the reaction ^{40}Ca$(n,\alpha)^{37}$Ar. A source of 35 mCi was produced from 0.4 g of $CaCO_3$ for a transient NMR experiment [224] to test the linearity of quantum mechanics [225, 226]. An alternative method would be proton activation. A cyclotron beam of 25 MeV protons on ^{37}Cl allows for a production of 10^7 Bq/μAh [227], so that a source of one Curie can be produced well within a week.

- The production of ^{131}Cs was developed for brachytherapy. Neutron and proton activation are both options. Neutron activation is possible by using ^{130}Ba [228], and proton activation by using Xe or Ba isotopes, which gives a yield of $> 10^7$ Bq/μAh [229]. Commercial sources are available. Cs can be separated well from other radioactive by-products.

- ^{163}Ho is an isotope of interest for measuring the neutrino mass, and is studied by for instance the ECHo collaboration [230]. The production of Ho has been considered in detail [209]. The maximal production rate is projected to be about 10^4 Bq/h, which is insufficient for a competitive measurement to test Lorentz invariance.

- ^{165}Er can be produced with a proton beam on a Ho target [231] with a yield of 10^8 Bq/μAh. In view of its short half-life of 10 h, this is the only practical method. Although the production is sufficient, radioactive Ho is a by-product and Er cannot be separated effectively from Ho.

We conclude that ^{37}Ar and ^{131}Cs are the only viable isotopes to obtain competitive values for $\chi^{\mu\nu}$. ^{37}Ar has the lowest ionizing yield and in this respect may be preferred. It can be polarized via a buffer gas, or by first exciting the atom into the metastable state. In Ref. [224] the ^{37}Ar nuclei were polarized by spin exchange with optically-pumped K atoms and a nuclear polarization of 56% was achieved.

The experimental apparatus for a measurement of $\mathcal{A}_{Jr}$ in Eq. (4.19) could be based on that used to measure the recoil in electron capture of ^{37}Ar, first used to verify the existence of neutrinos [232]. In particular, the crossed-field spectrometer developed at that time [233] can be read with modern electronics and adapted to include polarization of ^{37}Ar. It is necessary to detect ionization currents instead of counting the recoils in order to accommodate the high event rate if one wants to aim for an accuracy of 10^{-9}. However, because there are no limits yet on χ_i^{s0}, such an experiment would immediately produce new results with a much more modest effort, while allowing to investigate the systematic errors that will limit the ultimate high-statistics and high-precision experiments.

4.2.5 Conclusions

We have explored the potential of orbital electron capture to put limits on Lorentz violation in β decay. The limits set in earlier work [21] are already so strong that high-intensity sources are required. A source with a strength of at least one Curie that decays solely by electron capture may allow such experiments. Our survey limits the choice to ^{37}Ar and possibly ^{131}Cs. The theoretical formalism for such experiments was developed, following Ref. [17], in a form applicable to any allowed electron-capture process. For one set of parameters quantifying Lorentz violation, no bound has been obtained as yet. These can be accessed in an experiment that measures the recoil from the neutrino emitted from a polarized nucleus, thus producing a new result while testing the viability of the suggested experimental program.

Appendix 4.A Angular-momentum coefficients

The angular-momentum coefficients in Eqs. (4.14b), (4.14c), (4.14e), and (4.15) are

$$\Lambda^{(1)} = \begin{cases} \frac{\langle m\rangle}{j} & (j' = j-1) \\ \frac{\langle m\rangle}{j(j+1)} & (j' = j) \\ \frac{-\langle m\rangle}{j+1} & (j' = j+1) \end{cases}, \; \Lambda^{(2)} = \begin{cases} \frac{\langle m^2\rangle - \frac{1}{3}j(j+1)}{j(2j-1)} & (j' = j-1) \\ \frac{-\langle m^2\rangle + \frac{1}{3}j(j+1)}{j(j+1)} & (j' = j) \\ \frac{\langle m^2\rangle - \frac{1}{3}j(j+1)}{(j+1)(2j+3)} & (j' = j+1) \end{cases} \tag{4.20}$$

$$\Lambda_z = \frac{\langle m\rangle}{j}\sqrt{\frac{j}{j+1}}\delta_{jj'} \; , \tag{4.21}$$

where j and j' denote the initial and final nuclear spin, respectively, and $\langle m\rangle$ and $\langle m^2\rangle$ denote the incoherent average of m and m^2 over the populations of the states $m = -j, \ldots, j$. $\Lambda^{(2)}$ vanishes for unpolarized sources and for decays with $j = j' = \frac{1}{2}$.

Chapter 5

Lorentz symmetry breaking in kaon and pion decay

In the previous chapter we discussed the possibilities to search for Lorentz symmetry breaking in β decay and electron capture. Here we discuss Lorentz symmetry breaking in nonleptonic decays, in particular kaon decay, and in pion decay. We consider for both Lorentz violation in the weak sector, as discussed previously in Section 2.6 and Chapter 4. Pion decay also offers the possibility to search for Lorentz violation in the muon sector and the quark sector, which we also address.

5.1 Exploration of Lorentz violation in neutral-kaon decay

The KLOE collaboration recently reported bounds on the directional dependence of the lifetime of the short-lived neutral kaon K_S^0 with respect to the dipole anisotropy of the cosmic microwave background. We interpret their results in an effective field theory framework developed to probe the violation of Lorentz invariance in the weak interaction and previously applied to semileptonic processes, in particular β decay. In this approach a general Lorentz-violating tensor $\chi^{\mu\nu}$ is added to the standard propagator of the W boson. We perform an exploratory study of the prospects to search for Lorentz violation in nonleptonic decays. For the kaon, we find that the sensitivity to Lorentz violation is limited by the velocity of the kaons and by the extent to which hadronic effects can be calculated. In a simple model we derive the K_S^0 decay rate and calculate the asymmetry for the lifetime. Using the KLOE data, limits on the values of $\chi^{\mu\nu}$ are determined.

5.1.1 Introduction

The KLOE collaboration recently reported a precision measurement of the lifetime of the short-lived neutral kaon K_S^0 [234, 235]. In addition, a search was made for the dependence of the lifetime on the direction of the K_S^0 with respect to the dipole anisotropy of the

Published: K. K. Vos, J. P. Noordmans, H. W. Wilschut, and R. G. E. Timmermans, Phys. Lett. B **729**, 112 (2014).

Cosmic Microwave Background (CMB). The asymmetry in the lifetime was measured to be less than about 10^{-3}. In this section we interpret the KLOE findings in a general effective field theory framework developed in Ref. [17] to study the possibility of Lorentz violation in the weak interaction, in particular in neutron and allowed nuclear β decay. A broad class of Lorentz-violating effects was considered, in which the standard low-energy propagator of the W-boson is modified to

$$\left\langle W^{\mu+}(q)W^{\nu-}(-q)\right\rangle = -i\,(g^{\mu\nu}+\chi^{\mu\nu})/M_W^2\ , \tag{5.1}$$

where the complex tensor $\chi^{\mu\nu}$ describes the effects of Lorentz violation in the weak interaction. In particular, such a tensor arises in the Standard Model Extension (SME) of Kostelecký and collaborators [16, 37], an effective field theory describing Lorentz violation at low energies. The new Lorentz-violating terms could originate from spontaneous Lorentz violation in, for instance, unifying theories of quantum gravity [26].

Taking the KLOE measurement as an example to study Lorentz violation of the form of Eq. (5.1) in nonleptonic decays, we explore to which extent nonleptonic decays can compete with the bounds from semileptonic decays, in particular forbidden β decay [21] (Sec. 2.6). The contributions of QCD (gluon) corrections in nonleptonic decays are not fully understood theoretically. It has been claimed that QCD effects cause an enhancement of the $\Delta I = 1/2$ decay modes and that this is at least partly due to so-called "penguin diagrams." On the other hand, recent lattice QCD results [236] shed doubt on the importance of penguin diagrams. Since in this work we aim to explore the generic features of Lorentz violation in nonleptonic decays, it is beyond our scope to derive the full effective weak Hamiltonian that includes Lorentz violation. We calculate the contribution of tree-level W exchange and show how this constrains $\chi^{\mu\nu}$. We find that the asymmetry is proportional to γ_r^2, where γ_r is the Lorentz boost factor, favoring experiments with high-velocity kaons. In Appendix 5.A, we demonstrate that the penguin diagram does not contribute to the Lorentz-violating part of the K_S^0 decay rate. Therefore, the sensitivity of the K_S^0 lifetime to Lorentz violation is further reduced by an amount which depends on the relative contribution of the penguin diagram.

5.1.2 Nonleptonic neutral-kaon decay

First, we briefly review the calculation of the K_S^0 decay rate into two pions in the SM [237] and we discuss the $\Delta I = 1/2$ rule. The neutral-kaon system is described not by the mass eigenstates, but by the CP eigenstates

$$K_1^0 \equiv \frac{K^0+\bar{K}^0}{\sqrt{2}} \sim K_S^0 \qquad \text{and} \qquad K_2^0 \equiv \frac{K^0-\bar{K}^0}{\sqrt{2}} \sim K_L^0\ . \tag{5.2}$$

The short-lived and long-lived kaons, K_S^0 and K_L^0, are approximately equal to the CP eigenstates K_1^0 and K_2^0. We neglect the small effect of CP violation and set $K_S^0 \equiv K_1^0$. The short-lived kaon decays into two pions, $K_S^0 \to \pi^+\pi^-$, $\pi^0\pi^0$, a strangeness-changing transition with $\Delta S = 1$. The two pions in the final state can have isospin $I = 0$, a $\Delta I = 1/2$ transition, and $I = 2$, a $\Delta I = 3/2$ transition. Experimentally it is found that the first transition is enhanced compared to the latter. The origin of this enhancement is

an open standing problem and is referred to as the $\Delta I = 1/2$ rule. If this were an exact rule only the $\Delta I = 1/2$ transition would be allowed in the SM, the ratio of the decay rates of the two final states would be

$$\frac{W(K_S^0 \to \pi^+\pi^-)}{W(K_S^0 \to \pi^0\pi^0)} = 2 \ . \tag{5.3}$$

From experiments this ratio is found to be 2.26, implying a small contribution from the $\Delta I = 3/2$ transition. To quantify the $\Delta I = 1/2$ enhancement, we can express the K_S^0 decay amplitudes in terms of A_0, the amplitude for the $I = 0$ final state, and A_2, the amplitude for the $I = 2$ final state. Using the experimental value for the ratio in Eq. (5.3), we find

$$\frac{\text{Re } A_2}{\text{Re } A_0} \simeq 4.4\% \ , \tag{5.4}$$

which shows the large enhancement of the $\Delta I = 1/2$ transition.

In the SM, nonleptonic $\Delta S = 1$ decays are usually described theoretically by an effective interaction, which is obtained by dressing the weak Hamiltonian with hard-gluon corrections. These corrections change the coefficients and the operator structure of the Hamiltonian. The hard-gluon corrections then also induce a $\Delta I = 3/2$ operator. Calculations with this effective Hamiltonian show an enhancement of the $\Delta I = 1/2$ transition, though insufficient to explain the experimental data. The effective Hamiltonian contains six operators and their Wilson coefficients [238]. Schematically,

$$\mathcal{H}_{\text{eff}} \sim \frac{4G_F}{2\sqrt{2}} \cos\theta_C \sin\theta_C \sum_{i=1}^{6} c_i \mathcal{O}_i \ , \tag{5.5}$$

where G_F is the Fermi constant, θ_C is the Cabibbo angle, and c_i are the Wilson coefficients of the operators $\mathcal{O}_i$. They can be found in Ref. [238]. The dominant contributions to the $\Delta I = 1/2$ transition are given by $\mathcal{O}_1$ and $\mathcal{O}_5$,

$$\mathcal{O}_1 = \bar{d}_L \gamma_\mu u_L \bar{u}_L \gamma^\mu s_L - \bar{u}_L \gamma_\mu u_L \bar{d}_L \gamma^\mu s_L \ , \tag{5.6a}$$

$$\mathcal{O}_5 = \bar{d}_L \gamma_\mu t^a s_L \, (\bar{q}_R \gamma^\mu t^a q_R) \ , \tag{5.6b}$$

where the subscript L, R denotes the chirality of the quark and t^a are the Gell-Mann matrices. Operator $\mathcal{O}_1$ arises from hard-gluon corrections to the tree-level diagram. The running of QCD logarithms gives a large coefficient c_1.

QCD enhancements also requires the inclusion of the so-called "penguin diagram". The penguin diagram can be written as an effective interaction that generates $\mathcal{O}_5$, where gluon exchange makes it possible to couple to right-handed quarks. This results in an enhancement of the hadronic matrix elements.

The combination of $\mathcal{O}_1$ and $\mathcal{O}_5$ gives the largest contribution to the decay rate, although even optimistic estimates of the matrix elements still find an amplitude that is a factor 5 too small compared to experimental data [239].

In the SM, all operators of the effective Hamiltonian can be related to the form of $\mathcal{O}_1$ by Fierz transformations and Dirac algebra. The amplitude for K^0 decay into $\pi^+\pi^-$ in

the SM can thus be written as

$$\begin{aligned}\left\langle \pi^+\pi^-|\mathcal{H}_{\rm eff}|K^0\right\rangle &= C_{\rm SM}\left\langle \pi^+|\bar{u}_L\gamma^\mu d_L|0\right\rangle\left\langle \pi^-|\bar{s}_L\gamma_\mu u_L|K^0\right\rangle \\ &= \frac{1}{4}C_{\rm SM}f_\pi(p_+\cdot p_K + p_+\cdot p_-) = \frac{1}{4}C_{\rm SM}f_\pi(m_K^2-m_\pi^2)\ , \end{aligned} \tag{5.7}$$

where p_K, p_+, and p_- are the K^0, π^+, and π^- momenta, respectively, and $f_\pi \simeq 0.95 m_\pi$ is the pion decay constant. To find the second equality we use that the $K^0-\pi^-$ matrix element is proportional to $f_+(p_K+p_-)^\mu + f_-(p_K-p_-)^\mu$, where the latter term can be neglected, since experiments give $f_- \ll f_+ \sim 1$. The coefficient $C_{\rm SM}$ contains factors from Fierz transformations and Dirac algebra. The matrix element for $\bar{K}^0$ decay is the complex conjugate of the matrix element for K^0 decay, with the same $C_{\rm SM}$.

When we include Lorentz violation, we can no longer separate the amplitude into two matrix elements, as in Eq. (5.7), which are contracted with the W boson propagator. Mixing between the different operators and new structures from Fierz transformations complicate the Lorentz-violating case even further. For a complete analysis the effective Hamiltonian with Lorentz violation should be calculated, this is however beyond the scope of our present work since we only wish to explore the possibilities for testing Lorentz-violation in nonleptonic decays. We shall instead use a theoretical model in which we consider tree-level W exchange. In Appendix 5.A we discuss the Lorentz-violating contribution to operator $\mathcal{O}_5$.

5.1.3 Theoretical model

We will derive the decay rate of K_S^0 into $\pi^+\pi^-$ in a tree-level W-exchange model. For the Lorentz-violating amplitude of K^0 decay the modified W-boson propagator from Eq. (5.1) is inserted between the matrix elements in Eq. (5.7),

$$\left\langle \pi^+\pi^-|\mathcal{H}|K^0\right\rangle = 2\sqrt{2}G_F\cos\theta_C\sin\theta_C\left\langle \pi^+|\bar{u}_L\gamma_\mu d_L|0\right\rangle(g^{\mu\nu}+\chi^{\mu\nu *})\left\langle \pi^-|\bar{s}_L\gamma_\nu u_L|K^0\right\rangle\ , \tag{5.8}$$

where the Hamiltonian only contains the tree-level operator. The differential decay rate of K_S^0 in the laboratory frame is given by

$$\begin{aligned}\frac{dW}{dE_+} &= \frac{8G_F^2\cos\theta_C^2\sin\theta_C^2 f_\pi^2}{128\pi|\vec{p}_K|E_K}(m_K^2-m_\pi^2)\Bigg[(m_K^2-m_\pi^2) \\ &\quad +\chi_r^{00}(E_K^2+2E_KE_+-2E_+^2) - (\chi_r^{i0}+\chi_r^{0i})p_K^i\,(E_K+E_+) + \chi_r^{ij}p_K^ip_K^j \\ &\quad +\left[-(\chi_r^{i0}+\chi_r^{0i})(E_K-2E_+)p_K^i + 2\chi_r^{ij}p_K^ip_K^j\right]\frac{2E_KE_+-m_K^2}{2|\vec{p}_K|^2} \\ &\quad -\left(\chi_r^{00}-\chi_r^{ij}\frac{p_K^ip_K^j}{|\vec{p}_K|^2}\right)(E_+^2-m_\pi^2) - \left(3\chi_r^{ij}\frac{p_K^ip_K^j}{|\vec{p}_K|^2}-\chi_r^{00}\right)\left(\frac{2E_KE_+-m_K^2}{2|\vec{p}_K|}\right)^2\Bigg]\ , \end{aligned} \tag{5.9}$$

where $\chi_r^{\mu\nu}$ is the real component of $\chi^{\mu\nu}$, we sum over repeated indices, and Latin indices run over $1,2,3$. The total decay rate is found by integrating over the pion energy between the boundaries

$$E_+ = \frac{1}{2}E_K \pm \frac{1}{2}|\vec{p}_K|\sqrt{1-\frac{4m_\pi^2}{m_K^2}}\ . \tag{5.10}$$

We find

$$W = \frac{8G_F^2 \cos\theta_C^2 \sin\theta_C^2 f_\pi^2}{128\pi E_K}(m_K^2 - m_\pi^2)\sqrt{1-\frac{4m_\pi^2}{m_K^2}} \times \left[(m_K^2 - m_\pi^2) + \frac{4}{3}\chi_r^{\mu\nu}(p_K)_\mu(p_K)_\nu\left(1+\frac{m_\pi^2}{2m_K^2}\right)\right] . \quad (5.11)$$

In general, the tensor $\chi^{\mu\nu}$ in Eq. (5.1) can depend on the W-boson momentum q, where for K^0 decay $q = p_+$ and for $\bar{K}^0$ decay $q = p_-$. A momentum-dependent $\chi^{\mu\nu}$ complicates the integrals over the angle between the directions of the K_S^0 and the π^+, as discussed in Appendix B of Ref. [17]. Here, we have restricted ourselves to a momentum-independent $\chi^{\mu\nu}$, because momentum-dependent parts are suppressed by powers of the W-boson mass. This can be shown explicitly in the minimal SME (mSME), the subset of the SME that is renormalizable and only contains terms up to mass dimension four [16]. In the mSME the W-boson propagator, in the unitarity gauge and to first order in Lorentz violation, reads [17]

$$\left\langle W^{\mu+}(q)W^{\nu-}(-q)\right\rangle = \frac{-i}{q^2-M_W^2}\left\{g^{\mu\nu} - \frac{q^\mu q^\nu}{M_W^2} + \frac{M_W^2}{q^2-M_W^2}(k_{\phi\phi}^{\mu\nu} + \frac{i}{2g}k_{\phi W}^{\mu\nu}) - \frac{1}{q^2-M_W^2}\left[2k_W^{\rho\mu\sigma\nu}q_\rho q_\sigma + q^\mu q_\rho(k_{\phi\phi}^{\rho\nu} + \frac{i}{2g}k_{\phi W}^{\rho\nu}) + q^\nu q_\rho(k_{\phi\phi}^{\rho\mu} + \frac{i}{2g}k_{\phi W}^{\rho\mu})\right] + \frac{k_{\phi\phi}^{\rho\sigma}q_\rho q_\sigma q^\mu q^\nu}{M_W^2(q^2-M_W^2)}\right\} , \quad (5.12)$$

where $k_{\phi\phi}$, $k_{\phi W}$ and k_W are SME parameters [16], and g is the SU(2) electroweak coupling constant. Comparing this to the low-energy propagator in Eq. (5.1) and neglecting momentum-dependent terms one finds [17]

$$\chi^{\mu\nu} = -(k_{\phi\phi})^{\mu\nu} - \frac{i}{2g}(k_{\phi W})^{\mu\nu} . \quad (5.13)$$

Following the discussion in Ref. [17] we remark that Eq. (5.13) agrees with the low-energy limit for the massive photon propagator [240] and with Ref. [161]. Furthermore, a Lorentz-violating correction to the quark-quark-W vertex gives the same structure for the effective interaction as Eq. (5.1) gives, but is more involved due to corrections to external quark states [17]. The tensor $\chi^{\mu\nu}$ can be both CPT-odd and CPT-even, but when considering only momentum-independent terms it is CPT-even. Since we only consider momentum-independent modifications to the W-boson propagator, hermiticity of the Lagrangian implies that $\chi^{\mu\nu *} = \chi^{\nu\mu}$ [17].

5.1.4 Constraints on Lorentz violation from the KLOE data

With the KLOE detector at DAΦNE, decay branching ratios of kaons [241] were measured to determine the value of the element V_{us} of the quark-mixing matrix. The K_S^0 mesons were created in the strong decay $\phi \to K_L^0 K_S^0$, where the long-lived K_L^0 is not detected. The K_S^0 lifetime was measured with high precision [234]. The collaboration also measured

$\{\ell, b\}$	$\mathcal{A}_{\rm cone} \times 10^3$
CMB0 = $\{264°, 48°\}$	-0.2 ± 1.0 [234]
CMB0 = $\{264°, 48°\}$	-0.13 ± 0.4 [235]
CMB1 = $\{174°, 0°\}$	0.2 ± 1.0 [234]
CMB2 = $\{264°, -42°\}$	0.0 ± 0.9 [234]

Table 5.1: Observed K_S^0 lifetime asymmetry [234, 235], where $\{\ell, b\}$ are the galactic coordinates. CMB0 is the direction of the dipole anisotropy in the CMB and CMB1 and CMB2 are two perpendicular directions. The errors are mainly statistical.

the difference in the K_S^0 lifetime parallel (τ^+) and lifetime antiparallel (τ^-) to a direction fixed in space, with the asymmetry defined as

$$\mathcal{A} = \frac{\tau^+ - \tau^-}{\tau^+ + \tau^-} \ . \tag{5.14}$$

The K_S^0 momenta in the laboratory frame were transformed event-by-event to galactic coordinates [242] specified by $\{\ell, b\}$, where ℓ is the galactic longitude and b is the galactic latitude.

The asymmetry was measured in three different directions in the CMB rest frame. The first direction, $\{264°, 48°\}$, is the direction of the CMB dipole anisotropy. The directions labeled CMB1 and CMB2 are two perpendicular directions. Only events inside a cone of 30° opening angle were used, resulting in a difference between the cone asymmetry and the asymmetry for one specific direction $\vec{n}$,

$$\mathcal{A}_{\rm cone} \simeq 0.93\, \mathcal{A}_{\vec{n}} \ . \tag{5.15}$$

The KLOE results for $\mathcal{A}_{\rm cone}$ for the different directions are listed in Table 5.1.

In our framework, the K_S^0 lifetime asymmetry can be constructed from the decay rate in Eq. (5.11). The KLOE collaboration measured charged pions coming from K_S^0 decay in different directions, and derived from this the total decay rate. In the quoted asymmetry we thus need the total K_S^0 lifetime, which includes the decay into two neutral pions. We found that the neutral decay does not acquire additional Lorentz-violating contributions, and the ratio between the two main decay modes in Eq. (5.3) is therefore not altered. We find

$$\begin{aligned} \mathcal{A}_{\vec{n}} &= \frac{\frac{4}{3} + \frac{2}{3}\frac{m_\pi^2}{m_K^2}}{m_K^2 - m_\pi^2} \left(\chi_r^{i0} + \chi_r^{0i}\right) E_K p_K^i \\ &= \frac{\frac{4}{3} + \frac{2}{3}\frac{m_\pi^2}{m_K^2}}{\left(1 - \frac{m_\pi^2}{m_K^2}\right)} \gamma_r^2\, \chi_S^{i0}\, \beta_K^i \ , \end{aligned} \tag{5.16}$$

where $\chi_S^{i0} \equiv \chi_r^{i0} + \chi_r^{0i}$, and β_K is the velocity of the K_S^0. Because the K_L^0 and K_S^0 originate from a ϕ-meson created nearly at rest in e^+e^- collisions, such that β_K=0.217

and $\gamma_r = 1.02$, this gives

$$\mathcal{A}_{\vec{n}} = 0.34\, \chi_S^{i0}\, \hat{\beta}_K^i \ , \tag{5.17}$$

where $\hat{\beta}_K$ is the direction of the K_S^0 velocity.

Several observations about this result should be made. The asymmetry in Eq. (5.16) shows a γ_r^2 enhancement, and a dependence on the real and symmetric part of $\chi^{\mu\nu}$ that transforms as a vector under rotations. This is a general result, i.e. the most advantageous way to measure Lorentz-violating effects in weak decays is from a fast-moving decaying particle. Only then can one compete with the results from forbidden β decay [21], which profited from the high statistics one can obtain with a high-intensity source. Considering the contribution of the $\mathcal{O}_5$ operator discussed in Appendix 5.A, we find no dependence on $\chi^{\mu\nu}$ when evaluating the dependence of the transition strength on the decay direction. Assuming that indeed the dominant contributions to the decay rate are from $\mathcal{O}_1$ and $\mathcal{O}_5$, the actual dependence on $\chi^{\mu\nu}$ in Eqs. (5.16) and (5.17) is reduced. The precise reduction depends on the relative amplitudes of the two operators and its evaluation is complicated by theoretical uncertainties in the hadronic effects. In this respect, semileptonic decays are at this moment theoretically favorable for Lorentz-violation tests.

To see what type of limits one may obtain, we ignore these caveats. From the KLOE data, we can then put a 95% confidence limit (C.L.) bound on χ_S^{i0} in the CMB direction of

$$|\chi_S^{\mathrm{CMB0,0}}| < 2.9 \times 10^{-3} \ . \tag{5.18a}$$

For the other two directions we find at 95% C.L.

$$|\chi_S^{\mathrm{CMB1,0}}| \ < \ 6.8 \times 10^{-3} \ , \tag{5.18b}$$

$$|\chi_S^{\mathrm{CMB2,0}}| \ < \ 5.5 \times 10^{-3} \ . \tag{5.18c}$$

For completeness and comparison between experiments, we transform the bounds from the KLOE asymmetries to the Sun-centered frame [37], in which $\hat{Z}$ is parallel to Earth's rotational axis, $\hat{X}$ points to the vernal equinox at time $t = 0$, and $\hat{Y}$ completes the right-handed coordinate system. To evaluate the bounds in the Sun-centered frame we first transform the galactic coordinates $\{\ell, b\}$ to equatorial coordinates (α, δ) via

$$\delta \ = \ \sin^{-1}\left[\cos b \cos(27.4^\circ)\sin(\ell - 33^\circ) + \sin b \sin(27.4^\circ)\right] \ , \tag{5.19a}$$

$$\alpha \ = \ \tan^{-1}\left[\frac{\cos b \cos(\ell - 33^\circ)}{\sin b \cos(27.4^\circ) - \cos b \sin(27.4^\circ)\sin(\ell - 33^\circ)}\right] + 192.25^\circ \ , \tag{5.19b}$$

where α is the right-ascension and δ is the declination. The equatorial coordinates can then be transformed to the Sun-centered frame $\{T, X, Y, Z\} \equiv \left\{T, \vec{I}\right\}$ by using $\vec{I} = (\cos\delta\cos\alpha, \cos\delta\sin\alpha, \sin\delta)$. For the CMB directions this gives

$$\chi_S^{\mathrm{CMB,0}} \ = \ -0.97 X_S^{XT} + 0.22 X_S^{YT} - 0.11 X_S^{ZT} \ , \tag{5.20a}$$

$$\chi_S^{\mathrm{CMB1,0}} \ = \ 0.12 X_S^{XT} + 0.82 X_S^{YT} + 0.56 X_S^{ZT} \ , \tag{5.20b}$$

$$\chi_S^{\mathrm{CMB2,0}} \ = \ 0.22 X_S^{XT} + 0.52 X_S^{YT} - 0.82 X_S^{ZT} \ , \tag{5.20c}$$

where $X_S^{\mu\nu} \equiv X_r^{\mu\nu} + X_r^{\nu\mu}$ are the Lorentz-violating quantities in the Sun-centered frame. For the values in the Sun-centered frame we then find at 95% C.L.

$$|X_S^{XT}| < 3.3 \times 10^{-3} , \tag{5.21a}$$
$$|X_S^{YT}| < 6.3 \times 10^{-3} , \tag{5.21b}$$
$$|X_S^{ZT}| < 6.0 \times 10^{-3} . \tag{5.21c}$$

5.1.5 Summary and outlook

In this section, we explored the possibilities to test Lorentz violation in nonleptonic decays, taking the KLOE K_S^0 lifetime asymmetry measurement as an example. We used the framework developed in Ref. [17], in which Lorentz violation in the weak interaction is studied by introducing a general Lorentz-violating tensor $\chi^{\mu\nu}$, which modifies the W-boson propagator. We discussed the difficulties concerning nonleptonic decays within the SM and restricted ourselves to a simplified model. We calculated the directional asymmetry of the K_S^0 lifetime, defined by the difference in lifetime between the K_S^0 decaying parallel and antiparallel to a specific direction in space. The KLOE collaboration measured this asymmetry with a precision of 10^{-3} in the direction defined by the CMB dipole. For this direction χ_S^{0i} is constrained to be less than 10^{-3}. Our results put constraints on the SME parameters, for example $k_{\phi\phi}$, by relating our $\chi^{\mu\nu}$ to Eq. (5.13) [17, 21]. We find at 95% C.L.

$$|(k_{\phi\phi})_S^{XT}| < 3.3 \times 10^{-3} , \tag{5.22a}$$
$$|(k_{\phi\phi})_S^{YT}| < 6.3 \times 10^{-3} , \tag{5.22b}$$
$$|(k_{\phi\phi})_S^{ZT}| < 6.0 \times 10^{-3} . \tag{5.22c}$$

The long-standing problem of the $\Delta I = 1/2$ rule shows the challenges of nonleptonic decays. In the usual effective Hamiltonian description the penguin diagram gives a large contribution, but we showed that the Lorentz-violating contribution to this penguin diagram vanishes. This would further reduce the sensitivity of the lifetime to Lorentz violation, which would worsen our bounds in Eq. (5.22). From a theoretical point of view, semileptonic and leptonic decays are at this point preferable for Lorentz-invariance tests. As far as the weak interaction is concerned bounds already exist from allowed [173, 38] and forbidden [21] β decay (Sec. 2.6) and from pion decay [175]. Possibilities to complement and/or compete with these bounds lie in exploiting the γ_r^2 enhancement that occurs in asymmetries in experiments with high-energy hadrons.

Appendix 5.A Penguin diagram

The penguin diagram generates $\mathcal{O}_5$ and can be written as an effective vertex by integrating out the W boson [243]. The Lorentz-violating (LV) operator is found by calculating this effective vertex with our modified W-boson propagator,

$$\begin{aligned} \mathcal{O}_5^{\text{LV}} = & -\frac{1}{2}\bar{d}_L t^a \left[\chi^{\mu\nu} + \chi^{\nu\mu} + i\epsilon^{\alpha\beta\mu\nu}\chi_{\alpha\beta}\right] \gamma_\nu s_L \left(\bar{q}_R t^a \gamma_\mu q_R\right) \\ & -\frac{1}{2}\bar{s}_L t^a \left[\chi^{\mu\nu *} + \chi^{\nu\mu *} + i\epsilon^{\alpha\beta\mu\nu}\chi^*_{\alpha\beta}\right] \gamma_\nu d_L \left(\bar{q}_R t^a \gamma_\mu q_R\right) . \end{aligned} \tag{5.23}$$

To calculate the matrix elements we use the vacuum-saturation method, in which we insert a complete set of states between the initial and final state. Using Fierz transformations and Gell-Mann matrix algebra we can write Eq. (5.23) in a more convenient form. For the Lorentz-violating case these transformations are more involved than in the SM, as the Dirac matrices are no longer contracted with $g^{\mu\nu}$. The Fierz transformations now give additional Lorentz scalar and tensor structures. Due to parity constraints some of these structures do not contribute. We find

$$\begin{aligned}\left\langle \pi^-\pi^+ \left|\mathcal{O}_5^{\rm LV}\right| \bar{K}^0\right\rangle &= -\frac{1}{2}\left[\chi^{\mu\nu}+\chi^{\nu\mu}+i\epsilon^{\alpha\beta\mu\nu}\chi_{\alpha\beta}\right]\left\langle \pi^-\pi^+\left|\bar{d}_L\gamma_\nu t^a s_L \bar{q}_R\gamma_\mu t^a q_R\right|\bar{K}^0\right\rangle \\ &= \frac{i}{8}B^{\mu\nu}\left\langle\pi^-\left|\bar{d}\gamma_5 u\right|0\right\rangle\left\langle\pi^+\left|\bar{u}\sigma_{\mu\nu}s\right|\bar{K}^0\right\rangle\ ,\end{aligned} \tag{5.24}$$

where

$$B^{\mu\nu}\equiv\chi^{\mu\nu}-\chi^{\nu\mu}-i\epsilon^{\alpha\beta\mu\nu}\chi_{\alpha\beta}\ , \tag{5.25}$$

and the matrix element $\left\langle\pi^-\left|\bar{d}\gamma_5 u\right|0\right\rangle = if_\pi m_\pi^2/(m_u+m_d)$ [239], $\left\langle\pi^+(p)\left|\bar{u}\sigma_{\mu\nu}s\right|\bar{K}^0(k)\right\rangle = (p_\mu k_\nu - k_\mu p_\nu)2f_T/(m_K+m_\pi)$, with $f_T=0.417$ [244]. We can now calculate the amplitude for K_S^0 decay with $\mathcal{O}_5^{\rm LV}$

$$\left\langle\pi^-\pi^+\left|\mathcal{O}_5^{\rm LV}\right|K_S^0\right\rangle = \frac{i}{\sqrt{2}}C_{\rm LV}\left(B_{\mu\nu}p_+^\mu p_K^\nu+\tilde{B}_{\mu\nu}p_-^\mu p_K^\nu\right)\ , \tag{5.26}$$

where $C_{\rm LV}$ contains numerical Fierz and matrix element factors and $\tilde{B}_{\mu\nu}\equiv B_{\mu\nu}(\chi_{\mu\nu}\to\chi^*_{\mu\nu})$. The interference of the amplitude in Eq. (5.26) and $\mathcal{M}_{\rm SM}\equiv\langle\pi^+\pi^-|\mathcal{H}_{\rm eff}|K_S^0\rangle = \sqrt{2}\,\langle\pi^+\pi^-|\mathcal{H}_{\rm eff}|K^0\rangle$, given in Eq. (5.7), gives for the LV contributions to the differential decay rate

$$\begin{aligned}\frac{dW_5^{\rm LV}}{dE_+} &= \frac{1}{16\pi|\vec{p}_K|E_K}\left\{\frac{iC_{\rm LV}}{\sqrt{2}}\mathcal{M}_{\rm SM}\left[(B_{0\nu}-B^*_{0\nu}-\tilde{B}_{0\nu}+\tilde{B}^*_{0\nu})E_+p_K^\nu\right.\right. \\ &\left.\left.+(B_{i\nu}-B^*_{i\nu}-\tilde{B}_{i\nu}+\tilde{B}^*_{i\nu})\hat{p}_K^i p_K^\nu\frac{2E_KE_+-m_K^2}{2|\vec{p}_K|}+(\tilde{B}_{\mu\nu}-\tilde{B}^*_{\mu\nu})p_K^\mu p_K^\nu\right]\right\}.\end{aligned} \tag{5.27}$$

Performing the integration over E_+, we find that the contribution to the total decay rate of $\mathcal{O}_5^{\rm LV}$ vanishes. This is anticipated since $B_{\mu\nu}$ is antisymmetric, while the K_S^0 four-momentum is the only non-LV variable the decay can depend on. The decay rate, which is observer Lorentz invariant, can thus only depend on $B_{\mu\nu}p_K^\mu p_K^\nu = 0$.

5.2 Limits on Lorentz violation from charged pion decay

Charged-pion decay offers many opportunities to study Lorentz violation. Using an effective field theory approach, we study Lorentz violation in the lepton, W-boson, and quark sectors and derive the differential pion-decay rate, including muon polarization. Using coordinate transformations we are able to relate the first-generation quark sector, in which no bounds were previously reported, to the lepton and W-boson sector. This facilitates a tractable calculation, enabling us to place bounds on the level of 10^{-4} on first-generation quark parameters. Our expression for the pion-decay rate can be used to constrain Lorentz violation in future experiments.

5.2.1 Motivation

Many quantum-gravity theories predict scenarios in which Lorentz symmetry is (spontaneously) broken [26, 27]. This breakdown of Lorentz symmetry is often studied in the context of the Standard-Model Extension (SME) [16]. The SME is an effective field theory containing all possible Lorentz-violating terms that are singlets under the gauge group of the Standard Model (SM) of particle physics. These terms are built out of SM fields contracted with tensor coefficients that parametrize Lorentz violation. Many of these SME coefficients have been constrained with high precision [37], but weak decays still offer interesting possibilities to obtain new bounds, or to improve existing bounds [17, 21, 216, 39].

In this section we investigate Lorentz violation in the charged-pion decay $\pi \to \mu + \nu_\mu$. In our analysis we consider Lorentz violation in the lepton sector, the quark sector, and in the W-boson propagator. Lorentz violation in the lepton and quark sector is described by the SME [16], which we discussed in Sec. 2.2.2. The SME is an EFT which contains all possible Lorentz-violating terms that are singlets under the gauge group of the SM. We treat the quark-sector parameters by using coordinate redefinitions, while we study the effects of Lorentz violation on the W-boson propagator as in Eq. (5.1). We derive the Lorentz-violating differential decay rate, including the dependence on the direction of the outgoing muon and its polarization, which extends previous work [245, 175]. Our results lead to many possibilities to constrain Lorentz-violating effects in future pion experiments. Using existing data we obtain bounds on first-generation quark coefficients in the SME.

5.2.2 Lepton parameters

We start from the Lorentz-violating Lagrangian density for second-generation leptons, which contains the dimensionless and traceless coefficient $c^{\mu\nu}$,

$$\mathcal{L}^{\rm LV}_{\rm leptons} = c_{\mu\nu}\left[i\bar{\ell}\gamma^\mu\partial^\nu\ell + i\bar{\nu}\gamma^\mu\partial^\nu\nu + \bar{\ell}_L W^{\nu-}\gamma^\mu\nu_L + \bar{\nu}_L W^{\nu+}\gamma^\mu\ell_L\right] , \tag{5.28}$$

where ℓ is the charged-lepton field, ν is the neutrino field of the corresponding flavor, and $\psi_L = \frac{1}{2}(1-\gamma^5)\psi$. We assume for simplicity that the coefficients for the left-handed and

Published: J. P. Noordmans and K. K. Vos, Phys. Rev. D **89**, 101702(R) (2014).

right-handed fields are equal. Gauge invariance then dictates the equality of the neutrino and charged-lepton coefficients. To calculate the pion-decay rate from Eq. (5.28) we follow the procedure developed in Ref. [246].

The Lagrangian density in Eq. (5.28) contains additional, unconventional, time-derivative terms, which cause the Hamiltonian to be non-Hermitian in general. To remove these terms, we apply a field redefinition for both the neutrino and the charged lepton. This field redefinition is, to first order in Lorentz violation, given by [247]

$$\psi = A\chi = \left(1 - \tfrac{1}{2} c_{\mu 0}\gamma^0\gamma^\mu\right)\chi \ , \tag{5.29}$$

where χ is the new physical field. Written in terms of χ the time-derivative term is conventional and the Hamiltonian is Hermitian. In terms of the redefined fields, which we will write again as ℓ_L and ν_L, the interaction term becomes

$$\mathcal{L} = W^-_\nu \bar{\ell}_L (g_{\mu\nu} + \mathcal{C}_{\mu\nu})\gamma^\mu \nu_L = W^-_\nu \bar{\ell}_L \breve{\gamma}^\nu \nu_L \ , \tag{5.30}$$

with

$$\breve{\gamma}^\mu = (g^{\mu\nu} + \mathcal{C}^{\nu\mu})\gamma_\nu \ , \tag{5.31a}$$

$$\mathcal{C}^{\mu\nu} = c^{\mu\nu} - c^{\mu 0} g^{0\nu} + c^{\nu 0} g^{0\mu} - c^{00} g^{\mu\nu} \ . \tag{5.31b}$$

Hence, $\mathcal{C}^{\mu 0} = 0$, which shows that the extra
time-derivative terms have been removed by the field redefinition. From Eq. (5.30) we see that the vertex is now proportional to $\breve{\gamma}^\mu$, while it was proportional to $\gamma^\mu + c^{\nu\mu}\gamma_\nu$ before the redefinition.

From the Dirac equation, the dispersion relation and the spinor solutions can be obtained. When $c^{\mu\nu}$ is the only nonzero Lorentz-violating coefficient, the dispersion relation can be written as $\tilde{p}^2 - \tilde{m}_l^2 = 0$, with $\tilde{p}^\mu = p^\mu + \mathcal{C}^{\mu\nu}p_\nu$, $\tilde{m}_l = m_l(1 - c^{00})$ and m_l is the lepton mass. The energy of both the particle and the antiparticle of either spin state is, to first order in Lorentz violation, given by $E(\vec{p}) = \bar{p}^0 - c_{\mu\nu}\bar{p}^\mu\bar{p}^\nu/\bar{p}^0$, where we introduced the convenient notation $\bar{p} = (\bar{p}^0, \vec{p})$ with $\bar{p}^0 = \sqrt{\vec{p}^2 + m_l^2}$. From the Dirac equation we determine that

$$\begin{aligned} u^s(\vec{p})\bar{u}^s(\vec{p}) &= (\not{\tilde{p}} + \tilde{m}_l)(1 + \gamma^5 \not{\tilde{s}})/4\tilde{p}^0 \ , \\ v^s(\vec{p})\bar{v}^s(\vec{p}) &= (\not{\tilde{p}} - \tilde{m}_l)(1 + \gamma^5 \not{\tilde{s}})/4\tilde{p}^0 \ , \end{aligned} \tag{5.32}$$

with

$$\tilde{s} = \left(\frac{\vec{\tilde{p}}\cdot\hat{s}}{\tilde{m}_l}, \hat{s} + \frac{(\vec{\tilde{p}}\cdot\hat{s})\vec{\tilde{p}}}{\tilde{m}_l(\tilde{m}_l + \tilde{p}^0)}\right) \ , \tag{5.33}$$

where $\hat{s}$ the muon spin in its restframe, and the spinors are normalized to unity [211]. This results from explicit calculation or can be understood because $(\not{\tilde{p}} - \tilde{m}_l)\chi = 0$, which is just the normal Dirac equation with $p \to \tilde{p}$ and $m_l \to \tilde{m}_l$. We can now determine the squared matrix element for pion decay. After summing over neutrino spin and using momentum conservation, it is given by

$$\sum_{\nu \text{ spin}} |\mathcal{M}|^2 = \frac{\tilde{m}_l^2 G_F^2 f_\pi^2}{\tilde{k}^0\tilde{p}^0}(\tilde{p} \pm \tilde{m}_l\tilde{s})\cdot\tilde{k} \ , \tag{5.34}$$

where p and k are the muon and neutrino momentum, respectively, G_F is the Fermi coupling constant, $f_\pi \simeq 92$ MeV is the pion decay constant, and the upper (lower) sign applies for π^- (π^+) decay. The matrix element is proportional to the muon mass. This can be understood by the usual spin-balance argument for pion decay, which shows that, in the pion restframe, the outgoing leptons should have the same helicity, while the weak interaction only couples to the chiral component of the charged-lepton field that is of the opposite handedness. Interestingly, the Lorentz-violating spinors are eigenvectors of the operator $\vec{\Sigma}\cdot\vec{\tilde{p}}$ instead of the usual helicity operator. Also, in the pion restframe, $\sum_{\nu\ \mathrm{spin}}|\mathcal{M}|^2 \propto (1 \pm \hat{\tilde{p}}\cdot\hat{s})$, with $\hat{\tilde{p}} = \vec{\tilde{p}}/|\vec{\tilde{p}}|$. This shows that the muons are polarized in the $\pm\vec{\tilde{p}}$-direction, instead of in the normal $\pm\vec{p}$-direction. This influences experiments that depend on pion decay for their polarized muons, such as $g-2$ [248] or TWIST [249]. The first could detect the discussed effect, for example in the phase of the muon polarization, varying over the course of a sidereal day. Based on the current precision of the experiment a statistical precision of 10^{-6} seems attainable.

The differential decay rate is given by

$$d\Gamma = \frac{1}{2m_\pi}\frac{d^3p}{(2\pi)^3}\frac{d^3k}{(2\pi)^3}\sum_{\nu\ \mathrm{spin}}|\mathcal{M}|^2(2\pi)^4\delta^4(q-p-k)\ , \tag{5.35}$$

where q is the pion momentum. By using the dispersion relations and momentum conservation repeatedly, we find for the differential pion decay rate in the pion restframe

$$\frac{d\Gamma}{d\Omega} = \frac{G_F^2 f_\pi^2}{8\pi^2}\widetilde{M}_-^2\left(\widetilde{M}_+ - \widetilde{M}_-\right)\left(1+3c^{00}+3c^{ij}\hat{p}_i\hat{p}_j\right)\left(1\pm\hat{\tilde{p}}\cdot\hat{s}\right)\ , \tag{5.36}$$

where $\hat{\tilde{p}}^i = \tilde{p}^i/|\vec{\tilde{p}}| = \hat{p}^i(1+c^{jk}\hat{p}_j\hat{p}_k)+c^{ij}\hat{p}_j$, $\widetilde{M}_+ = (m_\pi^2+\tilde{m}_l^2)/2m_\pi$, $\widetilde{M}_- = (m_\pi^2-\tilde{m}_l^2)/2m_\pi$, and Latin indices run over space indices only. We see that indeed the π^- (π^+) decay rate vanishes if the muon spin is antiparallel (parallel) to $\hat{\tilde{p}}$. We can write Eq. (5.36) more explicitly as

$$\begin{aligned}\frac{d\Gamma}{d\Omega} &= \frac{G_F^2 f_\pi^2}{8\pi^2}M_-^2(M_+-M_-)\Bigg[1+c^{00}\frac{2M_+-M_-}{M_-}+3c^{ij}\hat{p}_i\hat{p}_j \\ &\quad \pm(\hat{p}\cdot\hat{s})\left(1+c^{00}\frac{2M_+-M_-}{M_-}+4c^{ij}\hat{p}_i\hat{p}_j\right)\mp c^{ij}\hat{s}_i\hat{p}_j\Bigg]\ ,\end{aligned} \tag{5.37}$$

where $M_+ = (m_\pi^2+m_l^2)/2m_\pi$ and $M_- = (m_\pi^2-m_l^2)/2m_\pi$. This formula corrects the decay rate in Ref. [245], which misses a factor $(1-c_{00})^2$. This factor can be traced to the field redefinition in Eq. (5.29) and the corresponding normalization of the fields. There are no terms proportional to $c^{0j}\hat{p}_j$ or $c^{j0}\hat{p}_j$ in Eq. (5.37). This implies that there will be no difference in rate for muons going in opposite directions, when the polarization of the muons is not detected. Notice also that the decay rate, integrated over muon direction, does not depend on the muon spin, *i.e.* $\Gamma(\uparrow)-\Gamma(\downarrow)=0$. We expect this to be no longer the case when the coefficients for left-handed and right-handed fields are taken to be different. The energies of the two spin states are then no longer degenerate, and the form of the operators $u^s(\vec{p})\bar{u}^s(\vec{p})$ and $v^s(\vec{p})\bar{v}^s(\vec{p})$ is considerably more involved [211, 250].

5.2.3 W-boson parameters

Lorentz violation in pion decay can also result from the modified W-boson propagator

$$\left\langle W^{\mu+}W^{\nu-}\right\rangle = -i(g^{\mu\nu}+\chi^{\mu\nu})/M_W^2 \ , \tag{5.38}$$

where $\chi^{\mu\nu}$ parametrizes a broad class of Lorentz-violating effects in the SME [17]. The difference with the conventional Lorentz-invariant calculation resides only in the matrix element, because there are no external W bosons present. To first order in Lorentz violation

$$\sum_{\nu \text{ spin}} |\mathcal{M}| = \frac{G_F^2 f_\pi^2}{2p^0k^0}(g_{\mu\nu}g_{\rho\sigma}+\chi_{\mu\nu}g_{\rho\sigma}+g_{\mu\nu}\chi^*_{\rho\sigma})q^\mu q^\rho \,\mathrm{Tr}\left[(\not{p}\mp m_l\not{s})\gamma^\nu \not{k}\gamma^\sigma(1-\gamma^5)\right] \ , \tag{5.39}$$

where s is defined as $\tilde{s}$ with the replacements $\tilde{m}_l \to m_l$ and $\tilde{\hat{p}} \to \hat{p}$. Using Eq. (5.35) and performing the integrals over $\vec{k}$ and $|\vec{p}|$ results in

$$\begin{aligned}\frac{d\Gamma}{d\Omega} &= \frac{G_F^2 f_\pi^2}{8\pi^2}M_-^2(M_+-M_-)\Bigg[(1\pm\hat{p}\cdot\hat{s})(1+2\chi_r^{00}-2\chi_r^{0j}\hat{p}_j) \\ &\quad \mp\frac{m_\pi}{m_l}\left[2\chi_r^{0j}\left(\hat{s}_j-(\hat{p}\cdot\hat{s})\,\hat{p}_j\right)+2\chi_i^{0j}\left(\hat{p}\times\hat{s}\right)_j\right]\Bigg] \ ,\end{aligned} \tag{5.40}$$

where $\chi_r^{\mu\nu}$ and $\chi_i^{\mu\nu}$ denote the real and imaginary parts of $\chi^{\mu\nu}$, respectively.

The differential decay rate with polarized muons in terms of $c^{\mu\nu}$ and $\chi^{\mu\nu}$ is now given in Eqs. (5.37) and (5.40), respectively. For $c^{\mu\nu}$ there are no terms proportional to $c^{0j}\hat{p}_j$, while for $\chi^{\mu\nu}$ there are no terms proportional to $\chi^{ij}\hat{p}_i\hat{p}_j$. For $c^{\mu\nu}$ one has to search for a higher-order multipole asymmetry, while for $\chi^{\mu\nu}$ there will be a nonzero dipole asymmetry in the muon direction. Another difference between $c^{\mu\nu}$ and $\chi^{\mu\nu}$ is the enhancement factor m_π/m_l for the spin-dependent terms in Eq. (5.40), which is not present in Eq. (5.37). For the dominant branching fraction $\pi \to \mu + \nu_\mu$ this is of order unity. However, if one would measure the electron spin in $\pi \to e + \nu_e$ decay, this gives a sizable enhancement. We point out that $\chi^{\mu\nu}$, in contrast with $c^{\mu\nu}$, produces a nonzero asymmetry in the spin of the muon:

$$\frac{\Gamma(\uparrow)-\Gamma(\downarrow)}{\Gamma(\uparrow)+\Gamma(\downarrow)} = \pm\frac{2}{3}\left(\frac{2m_\pi+m_l}{m_l}\right)\chi_r^{0z} \ , \tag{5.41}$$

where we chose the quantization axis in the z-direction. Finally, we notice that the decay rate in Eq. (5.37) has its maximum if $\hat{s} = \pm\hat{\vec{p}}$. To first order in Lorentz violation Eq. (5.40) is proportional to $1\pm\vec{V}_\ell\cdot\hat{s}$, with $\vec{V}_\ell$ given by $V_\ell^l = \hat{p}^l + 2m_\pi\left[\chi_r^{0l}+\hat{p}^l(\chi_r^{0j}\hat{p}_j)-\epsilon^{ljk}\hat{p}_j(\chi_i)_{0k}\right]/m_l$. Both $c^{\mu\nu}$ and $\chi^{\mu\nu}$ thus influence the polarization of the outgoing muons.

5.2.4 Coordinate choices

It is known [251, 252, 253], that some (combinations of) SME coefficients are physically unobservable. At the level of the Lagrangian, this can be shown by using field or coordinate redefinitions to bring the Lagrangian with the apparent Lorentz violation to a

conventional Lorentz-symmetric form. Since the physics does not depend on a choice of coordinates or fields, the coefficients that can be removed are unobservable in experiments. In many cases interactions between different sectors of the SME prevent the full removal of the Lorentz-violating coefficients.

As an example of this, we look at a $c^{\mu\nu}$ parameter for a fermion field of a particular species, such as in Eq. (5.28). According to Refs. [251, 252], a Lagrangian with a nonzero $c^{\mu\nu}$ parameter is equivalent to a conventional Lagrangian in a skewed coordinate system. The $c^{\mu\nu}$ can be removed by a coordinate transformation $x^\mu \to x'^\mu = x^\mu + c^{\mu\nu}x_\nu$. However, this transformation introduces $-c^{\mu\nu}$ in the other fermion sectors, while for the gauge field sector $W^{\mu\nu}W_{\mu\nu} \to W^{\mu\nu}W^{\rho\sigma}\,(\eta_{\mu\rho}\eta_{\nu\sigma} + 2\eta_{\mu\rho}c_{\nu\sigma} + 2\eta_{\nu\sigma}c_{\mu\rho})$. The latter has the same form as a partly nonzero $k_W^{\mu\nu\rho\sigma}$ parameter in the gauge field sector.

If we only consider $c^{\mu\nu}$ coefficients for fermions and the relevant parts of the $k_W^{\mu\nu\rho\sigma}$ coefficients for gauge fields, we can always make one sector of the SME conventional by means of a coordinate transformation. Notice that this is not a general coordinate transformation, in the usual sense. This is because we do not transform the metric, but reinterpret the coordinates with respect to the metric. This means that we make a choice which sector of the Lagrangian defines the clocks and measuring rods, and is therefore the conventional sector. The choice as to which sector is conventional depends on the experimental setup.

5.2.5 Quark parameters

We now turn to the quark sector of the SME. Although there are strict bounds for effective parameters from meson oscillations and measurements on the neutron and the proton [37], the best bounds on actual quark parameters are in the top quark sector and they are at the 10^{-1}-10^{-2} level [254]. Bounds on parameters for the other generations are lacking[1]. Using coordinate transformations, we calculate the effects of quark parameters in leptonic pion decay.

The SM first-generation quark Lagrangian is given by

$$\mathcal{L}_{\text{quark}} = \bar{u}(i\partial\!\!\!/ - m_u)u + \bar{d}(i\partial\!\!\!/ - m_d)d + \frac{g}{\sqrt{2}}V_{ud}\left[\bar{u}_L W\!\!\!/^+ d_L + \bar{d}_L W\!\!\!/^- u_L\right] , \tag{5.42}$$

where g is the $SU(2)$ coupling constant and V_{ud} is the relevant entry of the CKM matrix. The corresponding Lorentz-violating part of the SME Lagrangian is

$$\mathcal{L}^{\text{LV}}_{\text{quark}} = ic_{\mu\nu}\bar{u}\gamma^\mu\partial^\nu u + ic_{\mu\nu}\bar{d}\gamma^\mu\partial^\nu d + \frac{g}{\sqrt{2}}V_{ud}\left[c_{\mu\nu}\bar{u}_L\gamma^\mu W^{\nu+} d_L + c_{\mu\nu}\bar{d}_L\gamma^\mu W^{\nu-} u_L\right] , \tag{5.43}$$

where we assume that Lorentz violation is equal for left-handed and right-handed quarks and that $c_{\mu\nu}$ is diagonal in flavor space. Gauge invariance then forces the parameters to be equal for up and down quarks.

As mentioned above, a coordinate transformation $x^\mu \to x'^\mu = x^\mu + c^{\mu\nu}x_\nu$ brings the quark Lagrangian to its conventional, Lorentz-symmetric, form. The coordinate transformation results in a low-energy W-boson propagator of the form in Eq. (5.38) with

[1] Indirect limits have been reported in Ref. [255]

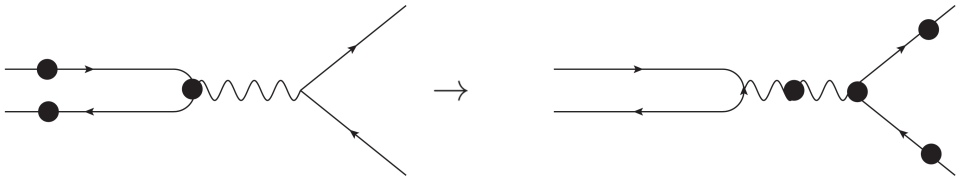

Figure 5.1: The effect of the coordinate transformations on pion decay. Blobs represent Lorentz violation.

$\chi^{\mu\nu} = 2c^{\mu\nu}$ and a $-c^{\mu\nu}$ coefficient for the second generation leptons. The effect of the coordinate transformations is depicted in the diagrams in Fig. 5.1. Notice that the transformation also changes the other sectors of the SME. It depends on the experimental conditions if this is relevant. In practice observables always depend on differences between Lorentz-violating parameters of the involved particles. Pion decay thus actually depends on differences between quark, lepton, and W-boson parameters. We will focus on the quark parameters the remainder of this section.

The calculation of the decay rate in terms of quark parameters can now be split in two parts, one dealing with Lorentz violation in the lepton kinetic terms and interaction vertex and one dealing with the Lorentz violation in the W-boson propagator. The former part of the calculation exactly parallels the calculation above, with the substitution $c^{\mu\nu} \to -c^{\mu\nu}$. The latter part, with a modified W-boson propagator, is treated by putting $\chi^{\mu\nu} = 2c^{\mu\nu}$. Since we treat Lorentz violation to first order, we can simply combine the results in Eqs. (5.37) and (5.40), resulting in

$$\begin{aligned}\frac{d\Gamma}{d\Omega} &= \frac{G_F^2 f_\pi^2}{8\pi^2} M_-^2 (M_+ - M_-)\Bigg[1 + c^{00}\frac{5M_- - 2M_+}{M_-} - 3c^{ij}\hat{p}_i\hat{p}_j - 4c^{0j}\hat{p}_j \\ &\quad \pm(\hat{p}\cdot\hat{s})\left[1 + c^{00}\frac{5M_- - 2M_+}{M_-} - 4c^{ij}\hat{p}_i\hat{p}_j + 4\left(\frac{m_\pi}{m_l} - 1\right)c^{0j}\hat{p}_j\right] \\ &\quad \mp\frac{4m_\pi}{m_l}c^{0j}\hat{s}_j \pm c^{ij}\hat{s}_i\hat{p}_j\Bigg] . \end{aligned} \tag{5.44}$$

To first order in Lorentz violating parameters, this decay rate is proportional to $1 \pm \vec{V}_q \cdot \hat{s}$, with $V_q^l = \hat{p}^l\left(1 - c^{jk}\hat{p}_j\hat{p}_k\right) - c^{lk}\hat{p}_k + 4m_\pi\left[c^{0l} + \hat{p}^l(c^{0j}\hat{p}_j)\right]/m_l$, which summarizes the way the quark parameters will influence the polarization of the outgoing muons. The expression in Eq. (5.44) offers many opportunities for future experiments to constrain the $c^{\mu\nu}$ quark coefficient, by observing the muon direction or spin in pion decay.

Integrating Eq. (5.44) over muon directions and summing over spin gives the total decay rate

$$\Gamma/\Gamma_0 = 1 + (4M_- - 2M_+)c^{00}/M_- \simeq (1 - 3.4c^{00}) . \tag{5.45}$$

Since this expression holds in the restframe of the pion, the sensitivity to Lorentz-violating effects in the decay rate is enhanced by a γ_π^2 dependence for pions in flight. Our result can be compared with the result in Refs. [245] and the bounds in Refs. [216, 175], derived from MINOS data [256, 257]. The translation of these bounds is complicated by possible Lorentz-violating effects in the detection system. As noted in Ref. [175], we expect from

Coefficient	Bound
$\lvert c_{(TX)}\rvert$, $\lvert c_{(TY)}\rvert$	4×10^{-5}
$\lvert c_{XX} - c_{YY}\rvert$, $\lvert c_{(XY)}\rvert$	9×10^{-5}
$\lvert c_{(XZ)}\rvert$, $\lvert c_{(YZ)}\rvert$	7×10^{-5}

Table 5.2: $3\,\sigma$ bounds on u, d quark parameters from the analysis in Ref. [216], which uses MINOS data [256, 257]; $c_{(TJ)} \equiv c_{TJ} + c_{JT}$.

energy conservation that the processes in the detector are at least 4 times less sensitive to Lorentz violation. Neglecting the effects of these processes and using the analysis in Ref. [216] together with Eq. (5.45), we derive order-of-magnitude bounds on quark coefficients. These are listed in Table 5.2. The capital indices on *e.g.* c^{TJ} denote time and space components in the standard Sun-centered inertial reference frame [37].

From Eq. (5.45) bounds on the isotropic components of the quark tensor $c^{\mu\nu}$ can also be found, by using the ratio of the decay rates for $\pi \to e + \nu_e$ and $\pi \to \mu + \nu_\mu$. For the $\pi \to e + \nu_e$ rate, we need to remember that the electron sector is also modified by the coordinate transformations. This results in a decay rate as in Eq. (5.45) with the electron mass replacing the muon mass. The ratio then becomes

$$R_\pi \equiv \frac{\Gamma(\pi^- \to e^- \bar{\nu}_e)}{\Gamma(\pi^- \to \mu^- \bar{\nu}_\mu)} = (1 + 5.4 c^{TT}) R_\pi^{\rm SM} \ , \tag{5.46}$$

where $R_\pi^{\rm SM} = 1.2352(1) \times 10^{-4}$ is the theoretical SM value [83] and $R_\pi = 1.230(4) \times 10^{-4}$ is the experimental value [56]. By attributing the deviation from the SM value to c^{TT} we find

$$c^{TT} = -8(6) \times 10^{-4} \ . \tag{5.47}$$

For the muon c^{TT} coefficient the method gives a value of $c^{TT} = 6(4) \times 10^{-4}$, which, to our knowledge, is the first bound on this parameter.

5.2.6 Discussion

In this section we obtained bounds on first-generation quark parameters, summarized in Table 5.2 and Eq. (5.47). We calculated the Lorentz-violating differential pion decay rate with polarized muons. The results for Lorentz violation in the lepton sector, the W-boson propagator, and the quark sector are given in Eqs. (5.37), (5.40), and (5.44), respectively. These offer many experimental opportunities to improve bounds on Lorentz violation. We also noted some qualitative differences between the influence of the different parameters on the pion decay rate. These pertain to asymmetries in muon and muon-spin directions, enhancements of spin effects for $\pi \to e + \nu_e$, and unusual polarization directions of the outgoing muons.

Weak decays have been used in the past to obtain direct bounds on Lorentz violation in the lepton and gauge sector. Bounds on $\chi^{\mu\nu}$, derived from forbidden β decay, are at

the 10^{-6} level on χ^{TT} and χ^{TJ}, and are on the order of 10^{-8} for χ^{JK} [21]. The analysis of pion decay using MINOS data [256, 257] limits c^{TJ} and c^{JK} to the level of 10^{-5} [216].

A dedicated experiment for pion decay that measures the muon direction can provide improved bounds, in particular on χ^{TJ} and $c^{\mu\nu}$ for both the lepton and the quark sector. Such an experiment should preferably benefit from the γ_π^2 dependence, as this increases the sensitivity of the measurement to Lorentz-violating effects and reduces uncertainties arising from possible Lorentz violation in the detection mechanism. We can estimate the reachable precision of such an experiment. Pion beams with an intensity of 10^{10}/s are available at modern facilities, suggesting a reachable precision on muon flux asymmetries of $10^{-4}\sqrt{\text{s}}$ or better. A statistical precision of the order of 10^{-6} on various lifetime asymmetries thus seems attainable, enabling a dedicated experiment to put competitive or new bounds on the Lorentz-violating parameters in lepton, quark, and gauge sectors of the SME.

Chapter 6

Summary and outlook

In this thesis we focused on symmetry violations in the weak interaction. Our understanding of particle physics is to a large extent based on symmetries. Discrete symmetries played a crucial role in the development of the Standard Model of particle physics (SM), as did Lorentz symmetry for general relativity (GR). Although successful on their own, the unification of these two theories in a theory of quantum gravity is an outstanding problem. In addition, there are important observations that are left unexplained by the SM, which require "new" physics, i.e. physics beyond the SM (BSM). In the quest for the ultimate theory of nature, symmetries and symmetry violations serve as a guiding tool.

The weak interaction violates the discrete symmetries parity (P), charge-conjugation (C), and time reversal (T). Part of the success of the SM is that it correctly describes the observed breaking of these symmetries. The precision of current experiments, therefore, limits deviations from the mechanisms of symmetry breaking described in the SM, and thus limits the possibilities for BSM physics. Roughly speaking, we can divide our study into two sorts of symmetry breaking. First, we studied the breaking of the discrete symmetries P, C, and T, while assuming, as in the SM, that the combined CPT symmetry is conserved. In this case, T violation is equivalent to CP violation. Second, we considered the breaking of Lorentz and CPT symmetry. Searches for Lorentz violation are motivated by theories of quantum gravity that allow the breakdown of this fundamental symmetry. Relatively new are searches in the weak interaction, and the bounds in this sector are significantly weaker than in, for example, the electromagnetic sector. We studied the breaking of the discrete symmetries and Lorentz symmetry in an effective-field-theory (EFT) approach, which allowed us to set limits on BSM physics that are model independent. In this way, many different experiments, both at low and at high energies, could be compared.

In Chapter 2 we discussed the search for symmetry violations in neutron and nuclear β decay. In the era of the LHC it is of increasing importance to compare bounds on new physics from different experiments. We first discussed the search for deviations from the standard vector$-$axial-vector ($V-A$) structure of the weak interaction, in the form of scalar (S), tensor (T), and right-handed vector ($V+A$) interactions. These exotic interactions modify the differential β-decay rate, which can be observed by measuring the decay correlations. By using the β decay of nuclei pure Fermi and Gamow-Teller decays can be selected, which are sensitive only to V, S or to A, T interactions, respec-

tively. Alternatively, neutron β decay, for which the relative contributions of the Fermi and Gamow-Teller transitions is precisely known, can be studied. In the various studies also the SM parameters, the *ud*-entry of the CKM matrix V_{ud} and the neutron axial-vector charge g_A, can be determined. In an EFT approach, the BSM interactions are parametrized by dimension-6 operators, which are suppressed by the scale of new physics (Sec. 2.2.1). These operators add all possible S, V, A, and T interactions with left- and right-handed fields to the effective Lagrangian (Eq. (2.11)). Vector and axial-vector interactions were denoted by $a_{LR,RR,RL}$, where the first L, R represent the chirality of the neutrino and the second the chirality of the down quark, scalar interactions were denoted with an $A_{L,(R)}$ couplings and tensor interactions by $\alpha_{L,(R)}$, where the index denotes the chirality of the neutrino. This EFT approach allows for the comparison between searches for BSM physics in different fields. If present, exotic interactions would leave a small signature in β-decay experiments, but would also affect experiments at the LHC (Sec. 2.4.2) and contribute to the neutrino mass (Sec. 2.4.3).

We first discussed the most precise correlation measurements in β decay. Many correlation coefficients depend linearly on left-handed scalar or tensor couplings, where left-handed refers the the chirality of the neutrino, via the Fierz interference term b (Sec. 2.4). In superallowed Fermi decays, it is possible to combine the measurements of the ft-values of several isotopes, which leads to the most precise determination of both V_{ud} and the Fermi part of the Fierz interference term, b_F. Unfortunately, such a combination of measurements is not possible for Gamow-Teller decays. The best bounds on left-handed tensor interactions come from combined fits of neutron and nuclear data. The limits on right-handed couplings are more than an order of magnitude weaker, because the observables only depend quadratically on these couplings. We compared the best current β-decay experiments with limits from the LHC experiments and the neutrino mass, summarized in Fig. 2.6 and Fig. 2.7 for scalar and tensor interactions, respectively. In these cases, the β-decay experiments give the best current bounds $A_L < 2.5 \times 10^{-3}$ and $\alpha_L < 3 \times 10^{-3}$ (at 90% C.L.). However, for right-handed interactions the limits from β-decay experiments are superseded by the current bounds derived from LHC experiments, namely $A_R < 6 \times 10^{-3}$ and $\alpha_R < 2 \times 10^{-3}$ (at 90% C.L.).

In Sec. 2.5 we discussed the limits on T violation. In β decay, T violation can be probed by the T-odd triple-correlations $\vec{J} \cdot (\vec{p}_e \times \vec{p}_\nu)$ and $\vec{\sigma}_e \cdot (\vec{J} \times \vec{p}_e)$, where $\vec{J}$ is the nuclear spin and $\vec{\sigma}_e$ is the spin vector of β particle. The expectation value depends on the coefficients D and R, respectively. The coefficient D is determined by the imaginary part of the interference between V and A interactions, while R is determined by the imaginary parts of interferences between S and T interactions. We showed that the D and R coefficient can result from the same exotic interactions as the P- and T-odd electric dipole moments (EDMs). In this way, the strong limits on EDMs put also strong limits on D and R. Therefore, they leave little room for β-decay experiments to contribute to the current bounds (Table 2.7). Even for specific models, such as leptoquark models, which were previously considered "EDM safe", these EDM constraints are stronger than the bounds derived from β decay.

Besides these more traditional searches for new physics, we discussed the status of tests of Lorentz invariance in allowed and forbidden β decay (Sec. 2.6). The effects of the breaking of Lorentz symmetry at low energies can also be parametrized in an EFT ap-

proach and are described by the Standard Model Extension (SME). In the SME, Lorentz violation is introduced as tensor coefficients that couple to the SM fields. These coefficients can be seen as constant tensor background fields. For experiments on Earth, which moves through space and rotates, this means that the value of observables can change with the rotation of Earth. In β decay, it is possible to search for Lorentz violation in two relatively unexplored sectors of the SME, the W-boson sector and the counter-shaded neutrino sector. In the W-boson sector, Lorentz violation can be parametrized by adding a general Lorentz-violating tensor $\chi^{\mu\nu}$ to the W-boson propagator. The tensor $\chi^{\mu\nu}$ includes all possible modifications to the W-boson propagator, including higher-dimensional interactions, which depend on the momentum of the W boson. These momentum-dependent terms are always suppressed by at least the W-boson mass, and can therefore be neglected given the current experimental precision. We discussed the consequences for the β-decay rate and how these can be measured by β-decay experiments. Strong bounds of $\chi^{\mu\nu} < 10^{-6}$ - 10^{-8} were derived from forbidden-β-decay experiments, while the only dedicated experiment in allowed β decay reaches a sensitivity of $\mathcal{O}(10^{-4})$. Improving the bounds on $\chi^{\mu\nu}$ using allowed β decay can be done in parallel with the searches for scalar and tensor interactions, although the required statistical precision remains challenging. We further elaborated on such experiments in Chapter 4.

Chapter 2 was concluded with a roadmap for future symmetry tests in β decay. We emphasized that β-decay experiments should focus on left-handed couplings. It is important to improve the measurement of the Gamow-Teller part of the Fierz interference term, b_{GT}, which would improve the bound on α_L. This can be done by precisely measuring the Fierz-interference term in Gamow-Teller decays via either the β-ν correlation a or via the β-energy spectrum. These searches for left-handed couplings can go hand-in-hand with measurements of V_{ud} in superallowed Fermi decays and decays of mirror nuclei and of g_A in neutron decay. Other future experiments, such as measurements of right-handed interactions or of the R or D coefficients, should consider the bounds of the LHC experiments and the neutrino mass for complementarity.

In addition to searches for T violation in β decay, we discussed T violation in radiative β decay in Chapter 3. In radiative β decay, T violation can be measured by considering the triple-correlation $\vec{k} \cdot (\vec{p}_e \times \vec{p}_\nu)$, where k is the photon momentum. The expectation value is given by the coefficient K. This correlation is analogous to the triple correlations in β decay, although it does not contain spin observables. Therefore, the coefficient K was claimed to be free from EDM constraints, but we showed that this is not generally the case. In an EFT approach, we calculated that the current EDM measurements constrain the K coefficient in radiative β decay to be immeasurably small.

The last two chapters of this thesis focused on the search for Lorentz violation in the weak interaction by expanding and elaborating on the $\chi^{\mu\nu}$ parametrization introduced in Chapter 2. In Chapter 4 we elaborated on Lorentz symmetry breaking in allowed β decay and electron capture. In general, it is challenging to obtain the necessary statistics to improve the strong constraints on $\chi^{\mu\nu}$ from forbidden β decay. In Sec. 4.1, we discussed how to further test Lorentz violation in β decay. The real coefficients χ_r^{0l} and the imaginary coefficients $\tilde{\chi}_i$ can be constrained by measuring the direction-dependent decay rate in pure Fermi and Gamow-Teller decays, respectively. More complicated experiments can limit the, so far, unconstrained coefficients χ_i^{s0}. These require the measurement of the

correlation between two observables [Eqs. (4.6) and (4.7)]. We showed that such studies can go hand-in-hand with β-decay experiments that search for new physics beyond the SM. It would be also interesting to exploit the Lorentz boosts at future β-beam facilities or in (semi)leptonic decays at LHCb.

In Sec. 4.2, we expanded our formalism to orbital electron capture. Here the neutrino correlations become important, unlike in β decay where they lead to unnecessarily complicated experiments. The required statistical precision to improve the forbidden-β-decay bounds makes it interesting to consider electron capture, as this allows for experiments with high statistics but low dose. We identified ^{37}Ar and possibly ^{131}Cs as good isotopes for tests of Lorentz invariance. To obtain bounds on the unconstrained coefficients χ_i^{0l} a measurement of both the neutrino direction and the nuclear polarization is required [Eq. (4.19)].

Lorentz invariance in the weak interaction can be tested in any weak decay. In Sec. 5.1 we explored the possibilities for nonleptonic decays to improve the current bounds on $\chi^{\mu\nu}$. Recent KLOE data, in which the directional dependence of neutral-kaon lifetime was studied, served as an example for such tests. The nonpertubative QCD effects involved with nonleptonic decays make it preferable for future experiments to use (semi)leptonic decays. To reach the statistical precision necessary to improve current bounds on $\chi^{\mu\nu}$ the Lorentz-boost enhancement should be exploited. This enhancement gives rise to excellent opportunities for searches at accelerators, for example at LHCb or NA62 at CERN. Section 5.2 describes how both the coefficients $\chi^{\mu\nu}$ and the muon and quark coefficients $c^{\mu\nu}$ can be bounded in pion decay. We obtained the first direct bounds on quark parameters, which are $\mathcal{O}(10^{-3})$. With $\chi^{\mu\nu}$ and the muon coefficients $c^{\mu\nu}$ we calculated the polarized-pion decay rate, and showed the relation between these two sectors. Our calculations suggest that new experiments using highly-boosted pions, and that measure the direction of the muons can obtain improved limits on both $c^{\mu\nu}$ and $\chi^{\mu\nu}$.

In this thesis, we studied the bounds on new physics in the weak interaction. In neutron and nuclear β decay, symmetry tests will remain relevant, provided they are complementary to constraints from other low-energy and high-energy experiments. The testing of Lorentz invariance in the weak interaction has just begun, and many theoretical and experimental opportunities still exist. This thesis suggests measuring the unconstrained coefficients χ_i^{0l} in either highly-boosted (semi)leptonic decays or in electron capture, and shows how this can be done. These measurements would produce new results, while exploring the viability of improving the strong forbidden-β-decay constraints. Ultimately, improving the existing constraints on Lorentz violation in the weak interaction should be possible by using the decay of highly-boosted particles. On the theoretical side, it would be interesting to further study the effects of higher-dimensional Lorentz-violating interactions. For the searches for new Lorentz-symmetric physics, this thesis showed the power of EFT and how different experiments sometimes probe similar dimension-6 coefficients. It will be interesting to explore if a similar analysis could be performed in other fields of particle physics, thereby linking a wide variety of experimental probes.

Nederlandse Samenvatting

Symmetrieschending in zwak verval

Het standaardmodel beschrijft onze kennis van de deeltjesfysica. Sinds de ontwikkeling van het standaardmodel zijn er vele experimenten geweest die haar voorspellingen testen, zowel bij hele hoge als bij lage energie. Met uitzondering van de ontdekking van neutrino oscillaties, waaruit blijkt dat neutrino's, anders dan in het standaardmodel, een massa hebben, zijn deze experimenten, tot nu toe, allemaal in overeenstemming met het standaardmodel.

Het standaardmodel beschrijft de elementaire deeltjes: quarks, leptonen, de ijkbosonen en het Higgs boson. Verder beschrijft ze de elektromagnetische kracht en de zwakke en sterke kernkrachten[1]. De up en down quarks zijn de bouwstenen van de protonen en neutronen, die op hun beurt atoomkernen vormen. Het standaardmodel beschrijft dus de zichtbare materie in het heelal, maar kan bijvoorbeeld het bestaan van donkere materie niet verklaren[2]. Een andere onopgeloste puzzel is de overheersing van materie over antimaterie in het universum. Cosmologie voorspelt dat materie en antimaterie in ongeveer gelijke hoeveelheden moeten voorkomen, dus waar is alle antimaterie gebleven?

Deze openstaande vragen zouden kunnen worden beantwoord door nieuwe deeltjes en interacties. Wereldwijd zijn en worden er vele experimenten gedaan die zoeken naar tekenen en bewijs voor deze nieuwe deeltjes en interacties, maar toe nu toe zonder succes. In plaats daarvan beperken de resultaten van deze metingen de mogelijkheden nieuwe modellen en zetten ze een limiet op de massa van de nieuwe deeltjes. In dit proefschrift onderzoeken we deze limieten en bekijken we hoe verschillende experimenten bijdragen aan deze zoektocht. Daarbij hebben symmetrieën en symmetriebreking een sturende rol.

Symmetrieën en symmetriebreking

Bij het beschrijven van macroscopische en microscopische natuurkundige processen spelen symmetrieën een belangrijke rol. Voorbeelden van symmetrieën zijn bekend uit de natuur, aangezien er ontelbare organismen en structuren zijn die één of meerdere symmetrieën bezitten. Veel belangrijke natuurkundige wetten en vergelijkingen bevatten ook één of meerdere symmetrieën, of anders gezegd: ze zijn invariant onder een symmetrieoperatie.

[1] Zwaartekracht wordt dus niet door het standaardmodel beschreven en de vereniging van het standaardmodel en zwaartekracht is één van de openstaande problemen in de natuurkunde.

[2] Het heelal bestaat voor slechts 5% uit zichtbare baryonische (protonen en neutronen) materie. Het overgrote deel van het heelal bestaat uit donkere materie (27%) en donkere energie (68%). De aard van donkere materie en donkere energie is nog onbekend en één van de openstaande uitdagingen in de natuurkunde.

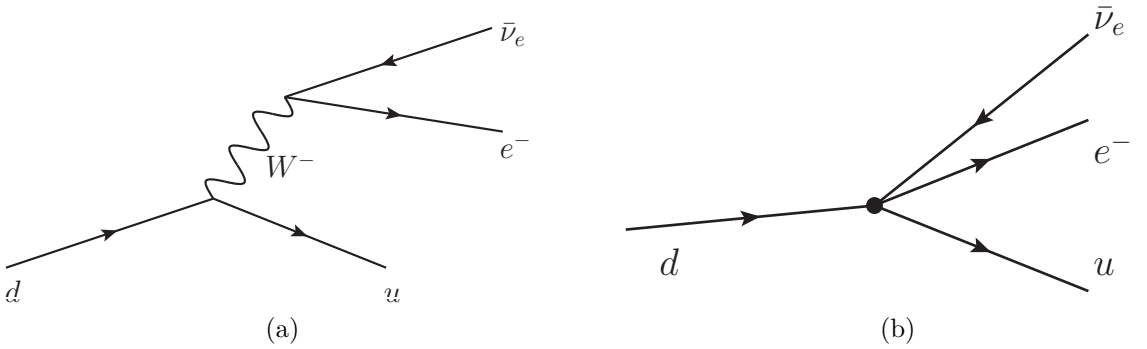

Figuur 6.1: Figuur (a) beschrijft β verval op quarkniveau. Hierbij transformeert een down quark in een up quark, een elektron en een antineutrino, door de uitwisseling van een W boson. Figuur (b) is de effectieve beschrijving van dit proces bij lage energie, waarbij het zware W boson "uitgeïntegreerd" is. Wat overblijft is een vierpuntsinteractie. Op dezelfde manier kunnen we bij lage energie de effecten van nieuwe deeltjes beschrijven.

Emmy Noether toonde aan dat als een systeem invariant is onder een bepaalde symmetrie, er altijd een grootheid is die behouden blijft. Zo volgen energie- en impulsbehoud, cruciaal in de mechanica voor het opschrijven van bewegingsvergelijkingen, uit de invariantie van de wetten van mechanica onder ruimte-tijdtranslaties.

Deze ruimte-tijdtranslaties, samen met Lorentztransformaties beschrijven de symmetrie van onze vier-dimensionale ruimte-tijd. Voor relativistische theorieën, die deeltjes beschrijven met snelheden in de buurt van de lichtsnelheid, wordt invariantie onder Lorentztransformaties altijd aangenomen. De bijbehorende Lorentzsymmetrie zorgt ervoor dat alle wetten van de natuurkunde aan het relativiteitsprincipe voldoen, namelijk dat de wetten van de natuur gelijk zijn voor alle waarnemers die stilstaan of met constante snelheid bewegen. Dit betekent automatisch dat de snelheid van het licht, 2.98×10^8 meter per seconde, hetzelfde is voor alle waarnemers[3]. Dat de snelheid van het licht gelijk is voor alle waarnemers is het fundament voor Einstein's speciale en algemene relativiteitstheorie. De speciale relativiteitstheorie en quantummechanica vormen de onderliggende structuur van het standaardmodel van de deeltjesfysica (SM). Daarmee is Lorentzsymmetrie dus één van de fundamenten van de deeltjesfysica.

Behalve Lorentzsymmetrie zijn ook de discrete symmetrieën pariteit (P), ladingsconjugatie (C) en tijdsomkering (T) belangrijk in het SM. Pariteit keert de ruimtelijke coördinaten om, C verwisselt deeltjes en antideeltjes en T keert de tijd om. De gecombineerde CPT symmetrie moet behouden zijn in elke Lorentz-symmetrische quantumveldentheorie. Sterker nog, CPT kan alleen gebroken worden als Lorentzsymmetrie ook gebroken is. In dit proefschrift onderzoeken we de mogelijke schending van Lorentzsymmetrie en van de discrete symmetrieën in de zwakke wisselwerking van het SM.

[3]De snelheid van het licht kan worden afgeleid uit Maxwell's vergelijkingen voor elektromagnetisme en deze vergelijkingen zijn invariant onder Lorentztransformaties.

De zwakke interactie Voor 1957 werd gedacht dat alle natuurwetten en interacties symmetrisch waren onder pariteit, maar in dat jaar werd de verassende ontdekking gedaan van pariteitsschending in β verval. Dit verval is afgebeeld in figuur 6.1a op quarkniveau, waarin een down quark transformeert in een up quark, onder het uitzenden van een elektron en een anti-elektronneutrino. De zwakke interactie, die verantwoordelijk is voor dit verval, vindt plaatst door de uitwisseling van een W boson. In werkelijkheid zijn de quarks gebonden in een neutron of een proton, dat op hun beurt weer gebonden kan zijn in een kern. Als deze kern instabiel is, omdat ze, bijvoorbeeld, te veel neutronen bevat, kan een neutron vervallen naar een proton onder uitzending van radioactieve β straling (de elektronen). De ontdekking van pariteitsschending had grote gevolgen voor de kijk op de zwakke wisselwerking en staat aan het begin van de ontwikkeling van het SM.

De ontdekking van P schending in de zwakke interactie, en daaropvolgende studies van β verval gaven inzicht in de structuur van de zwakke kernkracht, namelijk dat deze met een vector$-$axial-vector ($V-A$) structuur kan worden beschreven. Pariteit is niet de enige symmetrie die door de zwakke interactie wordt gebroken. In hetzelfde jaar werd namelijk ook C schending ontdekt. Iets later werd ook CP schending ontdekt, terwijl directe T schending pas veel later werd ontdekt. Het SM is deels zo succesvol omdat het deze symmetriebreking precies beschrijft. Een mogelijke manier om nieuwe fysica te vinden is daarom het nauwkeurig bestuderen van de in het SM beschreven symmetriebreking. Wanneer experimenten afwijkingen van dit patroon vinden, betekent dit dat er nieuwe interacties meespelen. Doordat zulke afwijkingen tot nu toe niet zijn gevonden legt de nauwkeurigheid van huidige experimenten beperkingen op aan hoe zulke nieuwe interacties en deeltjes zich kunnen manifesteren. In dit proefschrift bestuderen we in hoeverre op dit moment nieuwe interacties kunnen worden uitgesloten.

Nieuwe fysica en effectieve veldentheorie

Ondanks het succes van het SM blijven belangrijke observaties onverklaard. Zoals genoemd biedt het SM geen donkere-materiekandidaat en kan het de overheersing van materie over antimaterie niet verklaren. Daarnaast blijkt uit experimenten dat neutrinos (de elementaire deeltjes die vrijkomen bij β verval) een massa hebben, terwijl ze in het SM massaloos zijn. Om deze onopgeloste vragen te beantwoorden is er een tot nu toe onbekende vorm van nieuwe fysica nodig. Experimenten proberen deze nieuwe fysica te zoeken bij hoge energie in deeltjesversnellers, zoals bij de Large Hadron Collider (LHC) op CERN, maar ook bij lage energie, zoals bijvoorbeeld in β verval.

De experimenten die plaatsvinden bij lage energie dragen bij aan de zoektocht naar nieuwe fysica door heel nauwkeurige metingen te doen. Als nieuwe fysica bestaat zou dit namelijk minieme verschillen met het SM veroorzaken, die in extreem precieze experimenten kan worden gedetecteerd. Daarmee zijn ze complementair aan de experimenten op hoge energie die direct zoeken naar de nieuwe deeltjes. Hoe de nieuwe fysica bepaalde lage-energie processen precies beïnvloedt verschilt per nieuwe theorie. Daarom is het nuttig om de effecten van nieuwe fysica te beschouwen zonder aannames te maken over de volledige nieuwe theorie. Dit kan door gebruik te maken van effectieve-veldentheorie (afgekort tot EVT) technieken.

Deze methode is geillustreerd in Figuur 6.1b voor β verval. Bij lage energie is er geen enkele afhankelijkheid van de dynamiek van het W boson, omdat dat zwaar is vergeleken

met de andere deeltjes in het proces. Hierdoor kunnen we het W boson "uitintegreren", waardoor er een vierpuntsinteractie overblijft. Bij lage energie kunnen we β verval dus beschrijven zonder het W boson door EVT te gebruiken[4]. Bij hoge energieën is het wel nodig om het W boson expliciet te beschrijven.

Voor nieuwe fysica geldt hetzelfde principe. Omdat het SM vele experimenten verklaart en beschrijft nemen we aan dat deze theorie goed werkt tot op een bepaalde energie. Bij hogere energie zouden andere deeltjes en interacties een rol kunnen spelen. Als deze nieuwe deeltjes en interacties bestaan, dan zou het kunnen dat ze ook een klein effect hebben bij lage energie. Met behulp van EVT kunnen we deze effecten omschrijven op een modelonafhankelijke manier.

Discrete en Lorentzsymmetriebreking

Dit proefschrift kan globaal worden opgedeeld in twee delen. Als eerste bestuderen we de breking van de discrete symmetrieën P, C en T. In dit geval is, omdat CPT symmetrie behouden is, T schending gelijk aan CP schending. Ten tweede bestuderen we Lorentzsymmetriebreking. Deze symmetrie is van fundamenteel belang voor zowel het SM als in de algemene relativiteitstheorie. Toch zijn er nieuwe theorieën, die het SM en de zwaartekracht proberen te verenigen, die Lorentzsymmetriebreking toestaan. Er is veel onderzoek gedaan naar Lorentzsymmetrie en haar mogelijke breking, maar opmerkelijk minder vaak in de zwakke interactie. In dit proefschrift bestuderen we daarom de breking van zowel de discrete symmetrieën als van Lorentzsymmetrie in de zwakke wisselwerking in een EVT benadering.

In hoofdstuk 2 bestuderen we symmetriebreking in β verval. In β verval is het mogelijk om het verband tussen de richtingen waarin het electron, antineutrino en de dochterkern worden uitgezonden te onderzoeken. Het SM geeft een nauwkeurige voorspelling voor deze onderlinge richtingen (de vervalscorrelaties), maar nieuwe fysica zou deze kunnen veranderen. Nauwkeurige metingen in β verval kunnen daarom een limiet zetten op nieuwe fysica. Wij interpreteren deze limieten, en richten ons voornamelijk op de limieten op nieuwe scalar- en tensorinteracties. Deze limieten vergelijken we met de limieten die komen van LHC-experimenten en met de limieten die volgen uit metingen van de neutrinomassa. Hiervoor gebruiken we EVT. Het grote voordeel hiervan is dat we deze verschillende experimenten met elkaar kunnen vergelijken op een modelonafhankelijke manier. Uit deze vergelijking blijkt dat alleen bepaalde experimenten in β verval nog bijdragen aan de zoektocht naar nieuwe fysica.

In sectie 2.5 en in hoofdstuk 3 bestuderen we T schending in β verval en β verval waarbij een extra foton wordt uitgezonden. Experimenten die zoeken naar extra T schending (in dit geval hetzelfde als CP schending) zijn interessant omdat er extra CP schending nodig is om de materie overheersing in het heelal te verklaren. Het oplossen van deze puzzel is van groot belang en daarom zijn er veel onderzoeken die proberen nieuwe CP schending te vinden. Veel interesse is er voor het meten van elektrische dipoolmomenten (afgekort: EDMs) van het neutron, atomen en moleculen. Tot nu toen zijn er nog geen EDMs gemeten (in het SM zijn EDMs extreem klein), maar er zijn wel sterke limieten op hun grootte. Daarom geven deze experimenten ook hele sterke limieten op de mogelijk-

[4]Voor de ontdekking van het W boson werd β verval op deze manier beschreven.

heden voor nieuwe fysica. De vraag is daarom of andere experimenten, zoals bijvoorbeeld experimenten in β verval, nog iets kunnen toevoegen aan de zoektocht naar nieuwe CP-schendende fysica. Met behulp van EVT laten we zien dat β verval en EDMs gevoelig zijn voor dezelfde soorten nieuwe fysica. De sterke limieten op nieuwe fysica van EDM metingen zijn dus ook van toepassing op β verval. Het verbeteren van deze limieten met behulp van β verval vraagt daarom om ongekend hoge precisie[5].

In sectie 2.6, hoofdstuk 4 en 5 onderzoeken we Lorentzsymmetriebreking in de zwakke wisselwerking. Lorentzsymmetrie zorgt ervoor dat de wetten van de natuurkunde gelijk zijn voor alle waarnemers, zodat het geen verschil maakt waar of wanneer een experiment gedaan wordt. Dit is anders als Lorentzsymmetrie gebroken is. In dat geval kan het uitmaken waar op aarde een experiment plaatsvindt en op welk tijdstip. Doordat Lorentzsymmetrie gebroken is, is er als het ware een soort constant achtergrondveld in het heelal. Dit achtergrondveld kan, bijvoorbeeld, de elektronen in β verval beïnvloeden waardoor ze een voorkeur hebben voor een bepaalde richting. Ook kan het zijn dat de vervaltijd (levensduur) van een kern langer of korter is wanneer het in een bepaalde richting beweegt. Als dit soort effecten bestaan dan moeten ze heel klein zijn, en daarom is het nodig om extreem precieze experimenten te doen. Wij onderzoeken Lorentzsymmetriebreking in de zwakke wisselwerking door het effect hiervan op het W boson te bestuderen. Dit doen we door een tensor χ toe te voegen aan de bewegingsvergelijking van het W boson (de propagator) en vervolgens te berekenen wat het effect hiervan is op een aantal zwakke vervallen.

In sectie 2.6 en sectie 4.1 bestuderen we precies hoe Lorentzsymmetriebreking β verval beïnvloedt. We bespreken kort de beste limieten op χ, een maat voor hoe sterk het achtergrondveld kan zijn en we bespreken hoe deze limieten verbeterd kunnen worden. In hoofdstuk 5 bestuderen we pionverval en niet-leptonisch kaonverval. Pionen en kaonen zijn mesonen, ze bestaan uit een quark en een antiquark, die door de zwakke wisselwerking vervallen. In sectie 5.1 bekijken we een experiment waarin de richtingsafhankelijkheid van de kaonlevensduur werd onderzocht. Wij onderzochten de bijbehorende limiet op χ. In sectie 5.2 bestuderen we hoe pionverval afhangt van de richting waarin het pion en de vervalproducten bewegen.

In dit proefschrift bestudeerden we de limieten op nieuwe fysica. β verval zal een belangrijke rol blijven spelen in de zoektocht naar nieuwe fysica, als deze experimenten een aanvulling blijven op andere zoektochten zowel bij hoge als bij lage energie. Het testen van Lorentzinvariantie in de zwakke wisselwerking is nog vrij nieuw en er bestaan nog veel theoretische en experimentele mogelijkheden om verder te verkennen. In dit proefschrift laten we zien hoe nuttig het is om EVT technieken te gebruiken, omdat dit duidelijk maakt hoe verschillende experimenten soms dezelfde vorm van nieuwe fysica bestuderen. Het zou nuttig zijn om dit onderzoek uit te breiden naar andere velden van de deeltjesfysica, zodat de relatie tussen een groter aantal experimenten duidelijk wordt.

[5]Met onze EVT benadering kijken we alleen naar de effecten van nieuwe zware deeltjes en interacties die een rol spelen op hoge energie.

Acknowledgments

Let me start by saying that I extremely enjoyed the years that led to this dissertation. I learned many things and I am grateful to many people for their help and suggestions which allowed me to finish my PhD project.

I would like to thank my promotores, Rob Timmermans and Hans Wilschut. Rob, bedankt voor de begeleiding van mijn bachelor, master en promotie onderzoek. Bedankt voor de vrijheid die je me hebt gegeven, voor de uitdagende projecten, de vele suggesties, de vele conferenties die ik mocht bijwonen en voor het perfectioneren van de artikelen. Hans, bedankt voor alle aanmoedigingen en de vele discussies over experimenten. Zonder jou had dit proefschrift er heel anders uitgezien.

I am grateful to the members of the reading committee, Bret Altschul, Daniël Boer and Albert Young. Thank you for carefully reading my thesis and for your valuable suggestions and feedback.

I would like to thank Elisabetta Pallante, Lex Dieperink, Olaf Scholten and Daniël Boer for the discussions in the theory lunch meetings and their help and suggestions. I would also like to thank Eric Laenen, Robert Fleischer and Piet Mulders at Nikhef for organising interesting seminars and for always making me feel welcome at Nikhef. Robert, thank you for your help in my search for a postdoc and your recommendation letters. I would also like to thank the people at the LHCb group for a great Bfys outing and many discussions.

I would also like to thank my theory friends for the all the fun and discussions at the Van Swinderen Institute, CTN, Nikhef, Veldhoven, Corfu, the DPG meetings, Trends in Theory, the DRSTP schools, the PhD Days and of course after working hours. Thank you; Andrea, Daniel, Dries, Domenico, Giuseppe, Jacob, Jan, Jan-Willem, Jordy, Jules, Kristof, Luca, Maarten, Marco, Marija, Natasja, Niels, Olena, Paddie, Reinier, Remco, Rob, Robbert, Roel, Sander, Satish, Sophie, Susi, Tiago, Thomas, Tom, Wouter, and Wilco. Wouter, ik vond het leuk om een kantoor met je te delen en om samen te werken. Bedankt voor de vele discussies, de tequila en de lol. Jacob, bedankt voor de fijne samenwerking en de vele discussies over Lorentzsymmetriebreking. Jordy en Corien, heel erg bedankt voor jullie vele waardevolle adviezen en oplossingen voor mijn problemen en de cocktails.

Thanks to all my (former) colleagues and friends at the Van Swinderen Institute, the KVI, in the PV and at the CTN for making my time much more enjoyable. I would like to thank Eric Bergshoeff, Diederik Roest, Klaus Jungmann, Steven Hoekstra, Ronnie Hoekstra and Gerco Onderwater for their support. I would like to thank Hilde, Amarins, Marjan, Annelien, Robert, Miranda, Harry, Eveline and Iris for their help. Especially, I

would like to thank Joost, Corine, Elwin, Tom, Leon, Geert, Roel, Niels, Wouter, Jacob, Steven, Leo, Sophie, Mayerlin, Aernout, Gerco, Janko, Auke and Olivier. Bedankt voor alle theepauzes, het cubben, de wijn, de risotto, de spelletjes en het klaverjassen. Gerco bedankt voor je hulp bij het programmeren, de aanmoediging and voor je nooit aflatende enthousiasme. Geert bedankt voor alle discussies en je tips en suggesties. Corien en Olivier bedankt dat jullie mijn paranimfen zijn.

I really enjoyed organizing the PhD Day 2014, and would like to thank my fellow organizers; Brenda, Maarten, Linda, Naomi, Nicky and Anne, for the awesome time we had with the preparations, the day and afterward. Thanks for the fun, the gin tonics, the wine, the awesome food, our time in Londen, the pictures and for your support. I would like to thank my colleagues in the Gopher board for all the (necessary) distractions from my PhD thesis. I enjoyed it a lot; Simon, Els, Christel, Linda, Brenda, Wouter and Ni! Thanks to my colleagues in the PhD Council of the Graduate School of Science; Zsofia, Maryam, Marijke, Marija, Stefano, Daniel and Olivier. I would also like to thank the Graduate School of Science, especially Anke and Marco, for listening to our advice and for all their work.

Anne, Marjon, Maria, Dagmar, Lieneke, Linda, Marloes en Petra, bedankt voor jullie vriendschap en de soms nodige afleiding van mijn werk. Kim, Jelle, Monique en Gerco, bedankt dat we nog steeds (af en toe) een Cookiesdiner hebben. Papa en mama, Nikki en Amber bedankt dat jullie er altijd voor mij zijn en voor jullie oneindige steun.

Keri

List of Publications

K. K. Vos, J. P. Noordmans, H. W. Wilschut, and R. G. E. Timmermans,
Exploration of Lorentz violation in neutral-kaon decay,
Phys. Lett. B **729**, 112 (2014).

J. P. Noordmans and K. K. Vos,
Limits on Lorentz violation from charged pion decay,
Phys. Rev. D **89**, 101702(R) (2014).

K. K. Vos, H. W. Wilschut, and R. G. E. Timmermans,
Testing Lorentz invariance in orbital electron capture,
Phys. Rev. C **91**, 038501 (2015).

W. Dekens and K. K. Vos,
T violation in radiative β decay and electric dipole moments,
Phys. Lett. B **751**, 500 (2015).

K. K. Vos, H. W. Wilschut, and R. G. E. Timmermans,
Symmetry violations in nuclear and neutron β decay,
accepted for publication in Rev. Mod. Phys. (2015).

K. K. Vos, H. W. Wilschut, and R. G. E. Timmermans,
Concurrent tests of Lorentz invariance in β-decay experiments,
Phys. Rev. C **92**, 052501(R)(2015).

H. W. Wilschut *et al.*,
A new approach to test Lorentz invariance,
Ann. Phys. **525**, 653 (2013).

K. K. Vos, H. W. Wilschut, and R. G. E. Timmermans,
Limits on Lorentz violation in neutral-kaon decay,
Conference proceedings of the 6th meeting on CPT and Lorentz Symmetry,
Bloomington, Indiana, June 17-21 2013. ArXiv:hep-ph/1308.6468.

K. K. Vos, H. W. Wilschut, and R. G. E. Timmermans,
Possibilities for Lorentz violation in nonleptonic decays,
PoS **CORFU2014**, 054 (2015).

Bibliography

[1] O. W. Greenberg, Phys. Rev. Lett. **89**, 231602 (2002).

[2] C. S. Wu, E. Ambler, R. W. Hayward, D. D. Hoppes, and R. P. Hudson, Phys. Rev. **105**, 1413 (1957).

[3] R. L. Garwin, L. M. Lederman, and M. Weinrich, Phys. Rev. **105**, 1415 (1957).

[4] J. H. Christenson, J. W. Cronin, V. L. Fitch, and R. Turlay, Phys. Rev. Lett. **13**, 138 (1964).

[5] A. Angelopoulos *et al.*, Phys. Lett. B **444**, 43 (1998).

[6] S. Weinberg, Phys. Rev. Lett. **43**, 1566 (1979).

[7] B. Grzadkowski, M. Iskrzyński, M. Misiak, and J. Rosiek, J. High Energ. Phys. **1010**, 085 (2010).

[8] V. Cirigliano, J. P. Jenkins, and M. González-Alonso, Nucl. Phys. B **830**, 95 (2010).

[9] J. A. Behr and G. Gwinner, J. Phys. G **36**, 033101 (2009).

[10] G. Sprouse and L. Orozco, Ann. Rev. Nucl. Part. Sci. **47**, 429 (1997).

[11] H. Abele, Prog. Part. Nucl. Phys. **60**, 1 (2008).

[12] J. S. Nico, J. Phys. G **36**, 104001 (2009).

[13] D. Dubbers and M. G. Schmidt, Rev. Mod. Phys. **83**, 1111 (2011).

[14] N. Severijns, M. Beck, and O. Naviliat-Cuncic, Rev. Mod. Phys. **78**, 991 (2006).

[15] B. R. Holstein, J. Phys. G **41**, 110301 (2014).

[16] D. Colladay and V. A. Kostelecký, Phys. Rev. D **58**, 116002 (1998).

[17] J. P. Noordmans, H. W. Wilschut, and R. G. E. Timmermans, Phys. Rev. C **87**, 055502 (2013).

[18] S. Weinberg, Phys. Rev. **112**, 1375 (1958).

[19] Particle Data Group, K. A. Olive *et al.*, Chin. Phys. C **38**, 090001 (2014).

[20] A. N. Ivanov, M. Pitschmann, and N. I. Troitskaya, Phys. Rev. D **88**, 073002 (2013).

[21] J. P. Noordmans, H. W. Wilschut, and R. G. E. Timmermans, Phys. Rev. Lett. **111**, 171601 (2013).

[22] V. Cirigliano, M. González-Alonso, and M. L. Graesser, J. High Energ. Phys. **1302**, 046 (2013).

[23] T. D. Lee and C. N. Yang, Phys. Rev. **104**, 254 (1956).

[24] P. Herczeg, Prog. Part. Nucl. Phys. **46**, 413 (2001).

[25] V. A. Kostelecký and S. Samuel, Phys. Rev. D **39**, 683 (1989).

[26] S. Liberati and L. Maccione, Ann. Rev. Nucl. Part. Sci. **59**, 245 (2009).

[27] S. Liberati, Class. Quant. Grav. **30**, 133001 (2013).

[28] D. Mattingly, Living Rev. Rel. **8**, 5 (2005).

[29] D. Colladay and V. A. Kostelecký, Phys. Rev. D **55**, 6760 (1997).

[30] V. A. Kostelecký and M. Mewes, Phys. Rev. D **88**, 096006 (2013).

[31] V. A. Kostelecký and M. Mewes, Phys. Rev. D **85**, 096005 (2012).

[32] V. A. Kostelecký and M. Mewes, Phys. Rev. D **80**, 015020 (2009).

[33] P. A. Bolokhov and M. Pospelov, Phys. Rev. D **77**, 025022 (2008).

[34] D. Mattingly, (2008), ArXiv:0802.1561[gr-qc].

[35] P. A. Bolokhov, S. Groot Nibbelink, and M. Pospelov, Phys. Rev. D **72**, 015013 (2005).

[36] S. Groot Nibbelink and M. Pospelov, Phys. Rev. Lett. **94**, 081601 (2005).

[37] V. A. Kostelecký and N. Russell, Rev. Mod. Phys. **83**, 11 (2011), ArXiv:0801.0287[hep-ph].

[38] S. Müller *et al.*, Phys. Rev. D **88**, 071901(R) (2013).

[39] J. S. Díaz, V. A. Kostelecký, and R. Lehnert, Phys. Rev. D **88**, 071902 (2013).

[40] J. D. Jackson, S. B. Treiman, and H. W. Wyld Jr., Nucl. Phys. **4**, 206 (1957).

[41] P. Herczeg and I. B. Khriplovich, Phys. Rev. D **56**, 80 (1997).

[42] MuLan, D. M. Webber *et al.*, Phys. Rev. Lett. **106**, 041803 (2011).

[43] J. C. Hardy and I. S. Towner, Phys. Rev. C **79**, 055502 (2009).

[44] F. E. Wietfeldt and G. L. Greene, Rev. Mod. Phys. **83**, 1173 (2011).

[45] N. Severijns, M. Tandecki, T. Phalet, and I. S. Towner, Phys. Rev. C **78**, 055501 (2008).

[46] O. Naviliat-Cuncic and N. Severijns, Phys. Rev. Lett. **102**, 142302 (2009).

[47] P. D. Shidling *et al.*, Phys. Rev. C **90**, 032501 (2014).

[48] L. J. Broussard *et al.*, Phys. Rev. Lett. **112**, 212301 (2014).

[49] S. Triambak *et al.*, Phys. Rev. Lett. **109**, 042301 (2012).

[50] N. Severijns and O. Naviliat-Cuncic, Ann. Rev. Nucl. Part. Sci. **61**, 23 (2011).

[51] J. R. Green *et al.*, Phys. Rev. D **86**, 114509 (2012).

[52] T. Bhattacharya *et al.*, Phys. Rev. D **89**, 094502 (2014).

[53] M. González-Alonso and J. M. Camalich, Phys. Rev. Lett. **112**, 042501 (2014).

[54] G. Colangelo *et al.*, Eur. Phys. J. C **71** (2011).

[55] T. Bhattacharya *et al.*, Phys. Rev. D **85**, 054512 (2012).

[56] Particle Data Group, J. Beringer *et al.*, Phys. Rev. D **86**, 010001 (2012).

[57] R. W. Pattie, K. P. Hickerson, and A. R. Young, Phys. Rev. C **88**, 048501 (2013).

[58] F. Wauters, A. García, and R. Hong, Phys. Rev. C **89**, 025501 (2014).

[59] A. Gorelov *et al.*, Phys. Rev. Lett. **94**, 142501 (2005).

[60] ISOLDE Collaboration, E. G. Adelberger *et al.*, Phys. Rev. Lett. **83**, 1299 (1999).

[61] P. A. Vetter, J. R. Abo-Shaeer, S. J. Freedman, and R. Maruyama, Phys. Rev. C **77**, 035502 (2008).

[62] J. C. Hardy and I. S. Towner, Phys. Rev. C **71**, 055501 (2005).

[63] V. A. Wichers, T. R. Hageman, J. van Klinken, H. W. Wilschut, and D. Atkinson, Phys. Rev. Lett. **58**, 1821 (1987).

[64] A. S. Carnoy, J. Deutsch, T. A. Girard, and R. Prieels, Phys. Rev. C **43**, 2825 (1991).

[65] F. Glück, Nucl. Phys. A **628**, 493 (1998).

[66] C. H. Johnson, F. Pleasonton, and T. A. Carlson, Phys. Rev. **132**, 1149 (1963).

[67] F. Wauters *et al.*, Phys. Rev. C **82**, 055502 (2010).

[68] D. Mund *et al.*, Phys. Rev. Lett. **110**, 172502 (2013).

[69] UCNA Collaboration, M. P. Mendenhall *et al.*, Phys. Rev. C **87**, 032501 (2013).

[70] J. Hardy and I. Towner, J. Phys. G **41**, 114004 (2014), 1312.3587.

[71] X.-G. He and B. McKellar, Phys. Rev. D **47**, 4055 (1993).

[72] P. Liaud *et al.*, Nucl. Phys. A **612**, 53 (1997).

[73] B. Yerozolimsky, I. Kuznetsov, Y. Mostovoy, and I. Stepanenko, Phys. Lett. B **412**, 240 (1997).

[74] B. Erozolimskii, I. Kuznetsov, I. Stepanenko, I. Kuida, and Y. Mostovoi, Phys. Lett. B **263**, 33 (1991).

[75] P. Bopp *et al.*, Phys. Rev. Lett. **56**, 919 (1986).

[76] A. P. Serebrov *et al.*, J. Exp. Theor. Phys. **86**, 1074 (1998).

[77] M. Schumann *et al.*, Phys. Rev. Lett. **99**, 191803 (2007).

[78] J. Byrne *et al.*, J. Phys. G **28**, 1325 (2002).

[79] F. P. Calaprice, S. J. Freedman, W. C. Mead, and H. C. Vantine, Phys. Rev. Lett. **35**, 1566 (1975).

[80] M. Bychkov *et al.*, Phys. Rev. Lett. **103**, 051802 (2009).

[81] V. Mateu and J. Portolés, Eur. Phys. J. C **52**, 325 (2007).

[82] P. Herczeg, Phys. Rev. D **49**, 247 (1994).

[83] V. Cirigliano and I. Rosell, J. High Energ. Phys. **0710**, 005 (2007).

[84] B. A. Campbell and D. W. Maybury, Nucl. Phys. B **709**, 419 (2005).

[85] V. Cirigliano, S. Gardner, and B. Holstein, Prog. Part. Nucl. Phys. **71**, 93 (2013).

[86] G. Konrad, W. Heil, S. Baessler, D. Pocanic, and F. Glück, (2010), ArXiv:1007.3027.

[87] W. Dekens and D. Boer, Nucl. Phys. B **889**, 727 (2014).

[88] CMS Collaboration, S. Chatrchyan *et al.*, J. High Energ. Phys. **1405**, 108 (2014).

[89] S. Bertolini, A. Maiezza, and F. Nesti, Phys. Rev. D **89**, 095028 (2014).

[90] M. Moulson, (2013), ArXiv:1301.3046.

[91] E. Thomas *et al.*, Nuclear Physics A **694**, 559 (2001).

[92] A. Maiezza and M. Nemevšek, Phys. Rev. D **90**, 095002 (2014).

[93] ATLAS Collaboration, G. Aad *et al.*, Eur. Phys. J. C **72**, 2241 (2012).

[94] CMS Collaboration, S. Chatrchyan *et al.*, J. High Energ. Phys. **1208**, 023 (2012).

[95] O. Naviliat-Cuncic and M. González-Alonso, Annalen Phys. **525**, 600 (2013).

[96] CMS Collaboration, V. Khachatryan *et al.*, (2014), 1408.2745.

[97] T. M. Ito and G. Prezeau, Phys. Rev. Lett. **94**, 161802 (2005).

[98] Troitsk Collaboration, V. Aseev *et al.*, Phys. Rev. D **84**, 112003 (2011).

[99] C. Kraus *et al.*, Eur. Phys. J. C , 447 (2005).

[100] KATRIN Collaboration, A. Osipowicz *et al.*, (2001), ArXiv:0109033[hep-ex].

[101] WMAP, G. Hinshaw *et al.*, Astrophys. J. Suppl. **208**, 19 (2013).

[102] Planck Collaboration, P. A. R. Ade *et al.*, Astron. Astrophys. A **571**, 16 (2014).

[103] G. Prezeau and A. Kurylov, Phys. Rev. Lett. **95**, 101802 (2005).

[104] P. Wang, PhD thesis, Caltech, 2007.

[105] G. Ban, D. Durand, X. Fléchard, E. Lièn ard, and O. Naviliat-Cuncic, Annalen Phys. **525**, 576 (2013).

[106] A. Knecht *et al.*, Phys. Rev. Lett. **108**, 122502 (2012).

[107] X. Fléchard *et al.*, Phys. Rev. Lett. **101**, 212504 (2008).

[108] X. Fléchard *et al.*, J. Phys. G **38**, 055101 (2011).

[109] A. Knecht *et al.*, Nucl. Instrum. Meth. A **660**, 43 (2011).

[110] O. Naviliat-Cuncic, in *33rd Solvay Workshop on Beta Decay Weak Interaction Studies in the Era of the LHC*, Bruxelles, Belgium, 2014.

[111] N. Severijns, J. Phys. G **41**, 114006 (2014).

[112] O. Aviv *et al.*, J. Phys.: Conf. Ser. **337**, 012020 (2012).

[113] B. Märkisch *et al.*, Nucl. Instrum. Meth. A **611**, 216 (2009).

[114] Perc Collaboration, G. Konrad *et al.*, J. Phys.: Conf. Ser. **340**, 012048 (2012).

[115] S. Baessler *et al.*, Eur. Phys. J. A **38**, 17 (2008).

[116] F. E. Wietfeldt *et al.*, Nucl. Instrum. Meth. A **611**, 207 (2009).

[117] Nab Collaboration, D. Počanić *et al.*, Nucl. Instrum. Meth. A **611**, 211 (2009).

[118] S. Baessler, J. D. Bowman, S. Penttilä, and D. Počanić, J. Phys. G **41**, 114003 (2014).

[119] C. Couratin *et al.*, Phys. Rev. Lett. **108**, 243201 (2012).

[120] G. Li *et al.*, Phys. Rev. Lett. **110**, 092502 (2013).

[121] A. D. Sakharov, Pisma Zh. Eksp. Teor. Fiz. **5**, 32 (1967).

[122] T. Ibrahim and P. Nath, Rev. Mod. Phys. **80**, 577 (2008).

[123] G. C. Branco, R. González Felipe, and F. R. Joaquim, Rev. Mod. Phys. **84**, 515 (2012).

[124] W. Dekens *et al.*, J. High Energ. Phys. **07**, 069 (2014).

[125] M. Pospelov and A. Ritz, Annals of Physics **318**, 119 (2005).

[126] J. de Vries *et al.*, Phys. Rev. C **84**, 065501 (2011).

[127] J. de Vries, E. Mereghetti, R. G. E. Timmermans, and U. van Kolck, Phys. Rev. Lett. **107**, 091804 (2011).

[128] J. de Vries, R. G. E. Timmermans, E. Mereghetti, and U. van Kolck, Phys. Lett. B **695**, 268 (2011).

[129] J. de Vries, E. Mereghetti, R. G. E. Timmermans, and U. van Kolck, Annals of Physics **338**, 50 (2013).

[130] J. Bsaisou, U.-G. Meissner, A. Nogga, and A. Wirzba, Annals Phys. **359**, 317 (2015).

[131] P. Herczeg, J. Res. Natl. Inst. Stand. Tech. **110**, 453 (2005).

[132] J. D. Jackson, S. B. Treiman, and H. W. Wyld, Phys. Rev. **106**, 517 (1957).

[133] A. L. Hallin *et al.*, Phys. Rev. Lett. **52**, 337 (1984).

[134] T. E. Chupp *et al.*, Phys. Rev. C **86**, 035505 (2012).

[135] H. P. Mumm *et al.*, Phys. Rev. Lett. **107**, 102301 (2011).

[136] C. G. Callan and S. B. Treiman, Phys. Rev. **162**, 1494 (1967).

[137] S.-i. Ando, J. A. McGovern, and T. Sato, Phys. Lett. B **677**, 109 (2009).

[138] R. Huber *et al.*, Phys. Rev. Lett. **90**, 202301 (2003).

[139] nTRV Collaboration, A. Kozela *et al.*, Phys. Rev. C **85**, 045501 (2012).

[140] M. Morita and R. S. Morita, Phys. Rev. **107**, 1316 (1957).

[141] R. B. Curtis and R. R. Lewis, Phys. Rev . **107**, 1381 (1957).

[142] A. Young *et al.*, Phys. Rev. C **52**, R464 (1995).

[143] M. E. Ebel and G. Feldman, Nucl. Phys. **4**, 213 (1957).

[144] V. V. Braguta, A. A. Likhoded, and A. E. Chalov, Phys. Rev. D **65**, 054038. [Phys. Atom. Nucl. **65**, 1868.] [Yad. Fiz. **65**, 1920.] (2002).

[145] S. Gardner and D. He, Phys. Rev. D **86**, 016003 (2012).

[146] S. Gardner and D. He, Phys. Rev. D **87**, 116012 (2013).

[147] W. Dekens and K. K. Vos, Phys. Lett. B **751**, 500 (2015).

[148] J. Ng and S. Tulin, Phys. Rev. D **85**, 033001 (2012).

[149] I. B. Khriplovich, Nucl. Phys. B **352**, 385 (1991).

[150] C. A. Baker *et al.*, Phys. Rev. Lett. **97**, 131801 (2006).

[151] W. C. Griffith *et al.*, Phys. Rev. Lett. **102**, 101601 (2009).

[152] B. C. Regan, E. D. Commins, C. J. Schmidt, and D. DeMille, Phys. Rev. Lett. **88**, 071805 (2002).

[153] J. J. Hudson *et al.*, Nature **473**, 493 (2011).

[154] ACME Collaboration, J. Baron *et al.*, Science **343**, 269 (2014).

[155] W. Dekens and J. de Vries, J. High Energ. Phys. **1305**, 149 (2013).

[156] C.-Y. Seng, J. de Vries, E. Mereghetti, H. H. Patel, and M. Ramsey-Musolf, Phys. Lett. B **736**, 147 (2014).

[157] H. An, X. Ji, and F. Xu, J. High Energ. Phys. **1002**, 043 (2010).

[158] T. M. Ito, J. Phys.: Conf. Ser. **69**, 012037 (2007).

[159] CryoEDM Collaboration, M. G. D. van der Grinten *et al.*, Nucl. Instrum. Meth. A **611**, 129 (2009).

[160] I. Altarev *et al.*, Nucl. Instrum. Meth. A **611**, 133 (2009).

[161] I. Altarev *et al.*, Nuovo Cim. **C35**, 122 (2012).

[162] C. A. Baker *et al.*, Physics Procedia **17**, 159 (2011).

[163] A. P. Serebrov *et al.*, Nucl. Instr. Meth. A **611**, 276 (2009).

[164] I. B. Khriplovich and S. K. Lamoreaux, *CP violation without strangeness: Electric dipole moments of particles, atoms, and molecules* (Springer Berlin / Heidelberg, 1997).

[165] J. S. M. Ginges and V. V. Flambaum, Phys. Rept. **397**, 63 (2004).

[166] P. Herczeg, Phys. Rev. D **68**, 116004 (2003).

[167] K. Bodek *et al.*, Physics Procedia **17**, 30 (2011).

[168] J. A. Behr *et al.*, Hyperfine Int. **225**, 115 (2014).

[169] E. Liénard, in *33rd Solvay Workshop on Beta-Decay Weak Interaction Studies in the Era of the LHC*, Bruxelles, Belgium, 2014.

[170] Y. Totsuka *et al.*, Physics of Particles and Nuclei **45**, 244 (2014).

[171] P. Herczeg, Phys. Rev. D **52**, 3949 (1995).

[172] K. K. Vos, H. W. Wilschut, and R. G. E. Timmermans, Phys. Rev. C **91**, 038501 (2015).

[173] H. W. Wilschut *et al.*, Annalen Phys. (Berlin) **525**, 653 (2013).

[174] K. Bodek *et al.*, PoS **XLASNPA**, 029 (2014).

[175] B. Altschul, Phys. Rev. D **88**, 076015 (2013).

[176] J. P. Noordmans and K. K. Vos, Phys. Rev. D **89**, 101702(R) (2014).

[177] J. P. Noordmans, H. W. Wilschut, C. J. G. Onderwater, and R. G. E. Timmermans, in preparation (2015).

[178] K. K. Vos, J. P. Noordmans, H. W. Wilschut, and R. G. E. Timmermans, Phys. Lett. B **729**, 112 (2014).

[179] K. K. Vos, H. W. Wilschut, and R. G. E. Timmermans, Phys. Rev. C **92**, 052501(R) (2015).

[180] A. Sytema *et al.*, in preparation (2015).

[181] R. Newman and S. Wiesner, Phys. Rev. D **14**, 1 (1976).

[182] J. D. Ullman, Phys. Rev. D **17**, 1750 (1978).

[183] M. Lindroos and M. Mezzetto, Ann. Rev. Nucl. Part. Sci. **60**, 299 (2010).

[184] V. A. Kostelecký and M. Mewes, Phys. Rev. D **69**, 016005 (2004).

[185] V. A. Kostelecký and J. D. Tasson, Phys. Rev. Lett. **102**, 010402 (2009).

[186] J. S. Díaz, Adv. High Energy Phys. **2014**, 305298 (2014).

[187] I. S. Towner and J. C. Hardy, Rept. Prog. Phys. **73**, 046301 (2010).

[188] A. Czarnecki, W. J. Marciano, and A. Sirlin, Phys. Rev. D **70**, 093006 (2004).

[189] A. Riotto and M. Trodden, Ann. Rev. Nucl. Part. Sci. **49**, 35 (1999).

[190] V. A. Kuzmin, M. E. Shaposhnikov, and I. I. Tkachev, Phys. Rev. D **45**, 446 (1992).

[191] P. Huet and E. Sather, Phys. Rev. D **51**, 379 (1995).

[192] K. K. Vos, H. W. Wilschut, and R. G. E. Timmermans, accepted for publication in Rev. Mod. Phys. (2015).

[193] A. Kozela *et al.*, Phys. Rev. Lett. **102**, 172301 (2009).

[194] S. Gardner and D. He, Hyperfine Int. **214**, 71 (2013).

[195] W. Buchmuller and D. Wyler, Nucl. Phys. B **268**, 621 (1986).

[196] M. Ciuchini, E. Franco, L. Reina, and L. Silvestrini, Nucl. Phys. B **421**, 41 (1994).

[197] G. Degrassi, E. Franco, S. Marchetti, and L. Silvestrini, J. High Energ. Phys. **0511**, 044 (2005).

[198] V. Bernard, S. Gardner, U.-G. Meissner, and C. Zhang, Phys. Lett. B **593**, 105 (2004).

[199] J. Behr, private communication.

[200] A. D. Rújula, M. B. Gavela, O. Pène, and F. J. Vegas, Nucl. Phys. B **357**, 311 (1991).

[201] K. T. J. Hisano and M. J. S. Yang, Phys. Lett. B **713**, 473 (2012).

[202] T. Bhattacharya, V. Cirigliano, R. Gupta, H.-W. Lin, and B. Yoon, (2015), ArXiv:1506.04196.

[203] T. Bhattacharya *et al.*, (2015), ArXiv:1506.06411.

[204] A. Manohar and H. Georgi, Nucl. Phys. B **234**, 189 (1984).

[205] S. Weinberg, Phys. Rev. Lett. **63**, 2333 (1989).

[206] M. Pospelov and A. Ritz, Phys. Rev. D **63**, 073015 (2001).

[207] V. A. Dzuba and V. V. Flambaum, Int. J. Mod. Phys. E **21**, 1230010 (2012).

[208] V. F. Dmitriev and R. A. Sen'kov, Phys. Rev. Lett. **91**, 212302 (2003).

[209] J. Engle *et al.*, Nucl. Instr. Meth. Phys. Res. B. **311**, 131 (2013).

[210] J. D. Tasson, Rept. Prog. Phys. **77**, 062901 (2014).

[211] J. P. Noordmans, PhD thesis, University of Groningen, 2014.

[212] O. Naviliat-Cuncic and F. Wauters, in *33rd Solvay Workshop on Beta Decay Weak Interaction Studies in the Era of the LHC*, Bruxelles, Belgium, 2014.

[213] J. C. Hardy and I. S. Towner, Phys. Rev. C **91**, 025501 (2015).

[214] A. Kozela *et al.*, CPT and Lorentz Symmetry **V**, 174 (2011).

[215] B. Autin *et al.*, J. Phys. G **29**, 1785 (2003).

[216] B. Altschul, Phys. Rev. D **87**, 096004 (2013).

[217] J. R. Batley *et al.*, Eur. Phys. J. C , 329 (2007).

[218] W. Bambynek *et al.*, Rev. Mod. Phys. **49**, 77 (1977).

[219] E. J. Konopinski, *The theory of beta radioactivity* (Oxford Univerity Press, 1966).

[220] S. B. Treiman, Phys. Rev. **110**, 448 (1958).

[221] H. Frauenfelder, J. D. Jackson, and H. W. Wyld, Phys. Rev. **110**, 451 (1958).

[222] R. L. Intemann, Phys. Rev. C **3**, 1 (1971).

[223] J. Vanhaverbeke *et al.*, Hyperfine Int. **43**, 373 (1988).

[224] M. L. Pitt, PhD thesis, Princeton University, 1992.

[225] S. Weinberg, Phys. Rev. Lett. **62**, 485 (1989).

[226] S. Weinberg, Ann. Phys. **194**, 336 (1989).

[227] R. Kishore, R. Colle, S. Katcoff, and J. B. Cumming, Phys. Rev. C **12**, 21 (1975).

[228] N. Otuka *et al.*, Nuclear Data Sheets **120**, 272 (2014).

[229] F. Tarkanyi *et al.*, Appl. Radiat. Isot. **68**, 1869 (2010).

[230] L. Gastaldo *et al.*, J. Low Temp. Phys. **176**, 876 (2014).

[231] N. Zandi, M. Sadeghi, and H. Afarideh, J. Radioanal. Nucl. Chem. **295**, 923 (2013).

[232] G. W. Rodeback and J. S. Allen, Phys. Rev. **86**, 446 (1952).

[233] O. Kofoed-Hansen, Phys. Rev. **96**, 1045 (1954).

[234] KLOE Collaboration, F. Ambrosino *et al.*, Eur. Phys. J. **71**, 1 (2011).

[235] A. De Angelis, M. De Maria, M. Antonelli, and M. Dreucci, Nuovo Cim. **C034N3**, 323 (2011).

[236] P. A. Boyle *et al.*, Phys. Rev. Lett. **110**, 152001 (2013).

[237] L. B. Okun, *Leptons and Quarks* (North-Holland, 1985).

[238] M. Shifman, A. Vainshtein, and V. Zakharov, Nucl. Phys. B **120**, 316 (1977).

[239] J. F. Donoghue, Phys. Rev. D **30**, 1499 (1984).

[240] M. Cambiaso, R. Lehnert, and R. Potting, Phys. Rev. D **85**, 085023 (2012).

[241] KLOE Collaboration, F. Ambrosino *et al.*, J. High Energ. Phys. **0804**, 059 (2008).

[242] M. De Maria, PhD thesis, University of Udine, 2010.

[243] M. B. Wise and E. Witten, Phys. Rev. D **20**, 1216 (1979).

[244] I. Baum *et al.*, Phys. Rev. D **84**, 074503 (2011).

[245] B. Altschul, Phys. Rev. D **84**, 091902 (2011).

[246] D. Colladay and V. A. Kostelecký, Phys. Lett. B **511**, 209 (2001).

[247] R. Bluhm, V. A. Kostelecký, and N. Russell, Phys. Rev. D **57**, 3932 (1998).

[248] Muon g-2 Collaboration, G. W. Bennett *et al.*, Phys. Rev. D **73**, 072003 (2006).

[249] TWIST Collaboration, J. F. Bueno *et al.*, Phys. Rev. D **84**, 032005 (2011).

[250] B. Altschul, Phys. Rev. D **70**, 101701 (2004).

[251] D. Colladay and P. McDonald, J. Math. Phys. **43**, 3554 (2002).

[252] V. A. Kostelecký and J. D. Tasson, Phys. Rev. D **83**, 016013 (2011).

[253] B. Altschul, J. Phys. A **39**, 13757 (2006).

[254] V. M. Abazov *et al.*, Phys. Rev. Lett. **108**, 261603 (2012).

[255] C. D. Carone, M. Sher, and M. Vanderhaeghen, Phys. Rev. D **74**, 077901 (2006).

[256] P. Adamson *et al.*, Phys. Rev. Lett. **101**, 151601 (2008).

[257] P. Adamson *et al.*, Phys. Rev. D **85**, 031101 (2012).